Delft University of Technology

Master of Science Thesis

Disentangling Sea Level, and Sediment Supply Signals From The Panther Tongue Parasequence.

Author:
L.E Nonnekes

Supervisors:
Dr. J.E.A. Storms
Drs. A. Forzoni

TU Delft Delft University of Technology

Title:	Disentangling Sea Level, and Sediment Supply Signals From The Panther Tongue Parasequence.
Author:	L.E. Nonnekes
Date:	November 2014
Supervisors:	Dr. J.E.A. Storms, Drs. A. Forzoni

Postal address:	Section for Petroleum Engineering Department of Geoscience & Engineering Faculty of Civil Engineering & Geosciences Delft University of Technology P.O. Box 5028 The Netherlands
Telephone:	(31)152781328 (secretary)
Fax:	(31)152781189

Abstract

To assess, and validate the most recent interpretations on the Panther Tongue's depositional history we use the conceptual process-response model, 2Dstratsim. The focus of this study is on the Ksp040 parasequence which reflects the wave-dominated shoreface along the southern Wasatch Plateau. The associated Panther Tongue delta to the north is considered as the dominant sediment source for the Ksp040 parasequence. As a result of the complex 3D nature of the individual Panther Tongue delta lobes it is infeasible to correlate it to a 2D simulated profile of 2Dstratsim. Before field data is used in the 2Dstratsim model, the model is first brought to a workable level through debugging, and rewriting of the C++ source code. Then the model uses parameterised equations together with user implemented input signals in a forward routine to generate a cross-sectional profile of a shoreface on a linear decreasing initial surface. This forward routine is used through inversion techniques to automatically correlate measured, and simulated logs with the data format average grain-size to depth. By generating a best match between these logs, the forcing signals of the geologic environment are disentangled. To disentangle the forcing signals of the Panther Tongue first the cross-sectional diagram of the Panther Tongue's shoreface is modified to prepare it for a visual correlation to the simulated cross-sections based on observed bedset characteristics. Then, the measured average grain-size log data is digitised to enable a detailed correlation calculation between the measured, and simulated logs. New tools are added to examine the model's output graphically, in addition existing ones are enhanced. Four forward scenarios are created based on the bedset characteristics of the shoreface to set preliminary parameters, and constrain the statistical functions of the inversion routine. This improves the automated correlation procedure between the measured logs and the simulated logs. The forward scenarios use two different geologic settings, with, and without back-barrier formation on the shoreface profile. These settings are again subdivided into a scenario where solely the sea level is changed to match the simulated profile to the measured cross-sectional diagram. The other scenario primarily uses fluctuations in the sediment supply to match the cross-sections, and uses the sea level to a minimal extent. In the inversion scenario the model is matched to the simulated logs of the forward scenario, that was created without back-barrier formation, and only changes in sea level. Because the model requires additional work to generate a profile from the field measured logs. This issue is related to the stability and sensitivity of the 2Dstratsim model, the difference in average grain-size classification between the model and the field, and the gaps in the individual measured logs. Thus, 2Dstratsim can be used to create sedimentary environments using the forward routine. The model is also able to use its inversion routine to automatically recreate sedimentary environments to a limited extent as no geologic constraints are considered in this routine. Therefore, there is no assurance that the final result is geologically plausible. Additionally, extensive preliminary work is required to use the inversion routine.

Contents

1. Introduction

Fluctuations in sea level are no new concept in the earth's history. In coastal sedimentary systems that are supplied with sediment, these sea level fluctuations, and sediment supply signals are preserved in the stratigraphy. The sea level, and sediment supply signals form the major controls in shaping delta, and shoreface environments. However, their individual contributions to the formation of these environments is hard to quantify. To improve our understanding of their individual contribution resent day modelling techniques are developed to imitate the underlying physical processes using parametrised equations. These equations are established on in-depth knowledge of said processes, and are able to recreate the stratigraphy. Recreating the stratigraphy using parametrised equations supplemented with field data helps to disentangle these sedimentary systems. Modelling of sedimentary systems thereby enhances our the understanding of their causative controls.

We attempt to disentangle sea level, and sediment supply signals from the Panther Tongue deposit using modelling techniques, and measured stratigraphic record. To achieve this goal, geologic field data is prepared, and the modelling tool, 2Dstratsim, is repaired, and improved.

Disentangling the controls of a geologic system will grant valuable information to test or challenge current theories on its formation. Geologic data from the Panther Tongue is used in the model to quantify the resemblance of the simulated model data to the reality. The Panther Tongue system encompasses a shallow marine sedimentary system that was active in late-Cretaceous time, it is located on the Wasatch Plateau, Utah, U.S.A.. The system encompasses a coupling of environments including a delta, and a shoreface. These are deposited in the same parasequence but show distinct records in stratigraphy to similar signals. Field data, and interpretations on the Panther Tongue deposition are presented in Forzoni et al. (in prep.), Hampson et al. (2011), Hwang and Heller (2002). Cross-sections of the deposition are made by correlating logs, and field observations. The recent interpretations have yet to be tested by models with realistic parameters.
The model used, 2Dstratsim, is build to simulate a coupled environment of a delta to a shoreface. These environments are substituted to a common input signal per event, while the stratigraphic response is recorded in both of the environments. Therefore, it chosen as a tool to disentangle the deposition history of the Panther Tongue system. 2Dstratsim is a so-called process-response model, which uses parameterised equations to generate a simulated stratigraphy per environment. It is described in detail, and tested by de Jager et al. (in prep.). The model generates stratigraphic output on a 2D-profile along the dip direction of an environment, and is therefore considered a 2D model. It is used to validate the simulated stratigraphy to measured grain-size to depth distribution logs or interpreted cross-sectional diagrams.
In 2Dstratsim two different routines are implemented. The first one is the forward rou-

tine. The forward routine uses user-implemented sea level, and sediment input signals. Together with adjustable parameters the model is able to generate a simulated stratigraphy. The second routine is the inversion. In the inversion routine the model adjusts the input signals automatically to optimise the correlation between the field data, and the simulated data by using a statistical approach.

The goal is to obtain a simulated cross-sectional profile from 2Dstratsim that resembles the cross-sections from recent interpretations found in literature. This goal can be acquired by means of visual correlation or automated through the inversion routine. By establishing a sufficient correlation the sea level, and sediment supply signals contributing to the formation of the Panther Tongue system will be disentangled.

1.1 Problem definition

The Delta profile is well covered by logs, however most of them are not in the format required by the 2Dstratsim model, and do not cover a cross-section perpendicular to the river mouth. This poses a problem when correlating it to a simulated cross-section that does. New data does offer a cross-section perpendicular to the paleo-shore of the shoreface. Consequently this environment should be recreated first, then a rough match should follow for the delta section. To match the cross-section of the shoreface to a simulated cross section, the measured logs of the shoreface are digitised.

2Dstratsim generates erratic output, indicating the presence of buggs this ought to be repaired. Additionally the implementation of an inversion routine is scheduled, and should automate the correlation of the simulated data to field data using a Markov chain Bayesian approach to make it unbiased. This routine is first developed by Charvin (2008), the implementation of this routine in 2Dstratsim is handled by an external expert.
The available scripts used to visualise this inversion data are not generic, and have overly long run times. On the other hand the visualisation of the forward data, is generic but can be improved in order to use it more efficiently as an evaluation tool by both making it more clear as well as plotting more of the generated data.

1.2 Approach

To disentangle the signals from the Panther Tongue the data needs to be digitised, and 2Dstratsim improved. Then we can use the model to test recent interpretations of the Panther Tongue deposit. To achieve a correlation the following steps are preformed.

Firstly, the available logs need to be digitised in order to implement them in the model. The logs are crucial for correlating the model, without these the only way to correlate your simulated profile, is by more general means of generating similar trends.

Secondly, the samples, taken by Forzoni et al. (in prep.) require evaluation. This is accomplished via image analysis of photographs of thin sections, and CT-scans taken from cores.

Thirdly, the 2Dstratsim model needs to be improved, and repaired. Buggs are found and fixed by testing the model to basic scenarios and observing its behaviour. Mass balance calculations are preformed to confirm mass conservation in the model.

Fourthly, the visualisation of the data is optimised. Overall the application of these scripts is now more generic.

Lastly, a correlation between the digitised field data, and the model's simulated data, is established. This is done by manually adjusting the boundary conditions, and input signals of forward runs to generate a visually similar scenario. Thereby disentangling the sea level, and sediment supply signals from the Panther Tongue. To stress the non-uniqueness of a scenario, the input signals are shaped to generate two boundary scenarios. In the first scenario the sediment supply is unchanged, while the sea level fluctuates. In the second scenario a single rise and fall of sea level takes place, and sediment supply fluctuates. Then, when possible, an inversion routine is initiated to automatically create a most-likely scenario.

2. Literature review

Disentangling geology grants insight in how the formation of a geologic environment depends on various factors. Remaining stratigraphy will serve as a geologic record of sea level fluctuation, sediment supply changes, and wave activity. Therefore it contains valuable information to test or challenge current theories on the formation. The Panther Tongue stratigraphic unit records a shallow marine deposition originating from late-Cretaceous time, it encompasses a fluvial dominated deltaic system coupled to a wave dominated shoreface. The deposition records coarsening-upward sequences as a result of different progradation events into the west side of the Western Interior Seaway, (Hwang and Heller, 2002). The relevance to disentangle, and better understand the formation factors originates from the growing need in the petroleum industry for new hydrocarbon reservoirs. The search for new reservoirs is an ongoing quest as oil, and gas globally remain the main source of energy, (Petroleum, 2011). However, these reservoirs become increasingly hard to find, resulting in an increased demand for efficient methods to asses potential geologic sites with limited data.

In a delta-shoreface environment, upstream factors can influence the delta or shoreface as much as changes proximal to the coastline. The fluvial system supplying the delta, and shoreface with sediment is strongly influenced by climatic, and tectonic in the catchment. A fluvial system consists of three main components, firstly; a drainage basin, sediment, and a water source area. Secondly transfer of sediments, and water from source to sink, and thirdly a sedimentary basin to deposit the sediment, which can be a coastal zone, as in the delta-shoreface environment, (Schumm, 1981). The first component is especially important for the model as it sets the amount of sediment influx to the delta. The water source area, and the drainage basin set a limit to the amount of discharge. Because sediment concentration in water is limited the discharge therefore sets restrictions to the total amount, and type of sediment that can be transported by the river, (Bates, 1953). The discharge of the river can change over time. These fluctuations can be seasonal, or over longer periods of time responding to climate or geological setting changes at the source. At the coast a delta forms. Here sea level fluctuations, and wave activity dictates the depositional behaviour of the sediment. This behaviour is illustrated with an analogue. To suppress influence from external factors imagine a bathtub filled by a proportionally equivalent river transporting sediment, to represent river-sea interaction. Because of the absence of external factors only the discharge will directly influence deposition, sediment will disperse radially where the "river" flows into the "sea". Zooming in, the heavy grains will deposit more proximal to the "coast" when compared to the lighter sediment fractions. This forms the basis of clinoform formation. Patterns of clinoforms are as described in (Helland-Hansen and Hampson, 2009, Mitchum Jr et al., 1977, Storms, 2003). Clinoform formation is important because the clinoform's geometry is subject to our three main components. Therefore it will record their influence in the stratigraphy.

The shoreface is supplied with sediment from the delta. The sediment is transported along the shore mostly via tidally, and wave induced currents. Here also the three main factors influence the deposition of the sediment, and thereby the resulting stratigraphy.

In the field, stratigraphic data is directly observed from outcrops, more close up from samples. Indirect observations come from geophysical methods, literature, log data, and possibly in detail from thin sections. Together the data is fundamental to evaluations done either by hand or a model. Integration of data in a model greatly reduces the time to understand stratigraphic architecture, and how natural processes work. Many modelling methods are available to reconstruct geologic scenarios.
Numerical modelling allows one to evaluate, and reconstruct complex systems by reducing them to a skeleton of the most important processes. This concept is especially interesting in geology, where systems are formed by an interplay of variables (Hansen and Rasmussen, 2008, Jerolmack and Paola, 2010, Overeem et al., 2003, Storms, 2003, Storms et al., 2002). Hence a reduction in these variables is often required to mitigate computational times, input parameters, and numerical complexity.
Depending on what kind of model one uses it will require some sort of data as input. Stratigraphic data, parameters from observed processes, or empirical formulas can serve as input.

In statistical models, routines are developed to interpolate between data, based on a given statistical method. These generally work well with data, e.g. log data, but the scenarios they generate are not bound to physics, and therefore have a hard time generating realistic geometries (Pyrcz and Deutsch, 2014). To obtain a more realistic geologic geometry a more deterministic approach is required, and found in object based models. However in these models one should closely observe the placement, and the dimensions of the object. A balanced but more complex approach is found in process-response modelling, where output is generated via formulas describing geologic, processes. The output is later compared to measured geologic data. "Process-response modelling is a rapidly expanding tool to investigate controls on formation of the stratigraphic record", after (Storms et al., 2002).
In process-response modelling, geologic events, and processes are described in formulas and parameters. This allows the models to simulate geologic settings in 3D with a detailed stratigraphy, (de Jager et al., in prep., Roelvink and Van Banning, 1995, Syvitski and Hutton, 2001, Tetzlaff and Harbaugh, 1989). An example is DELFT3D, (Hydraulics, 1999), it can accurately simulate delta morphology and stratigraphy in 3D under the influence of fluvial, tidal, and wave processes. However if one is interested in simulations of long geologic times, a long computational time or compensation in numerical resolution is required. In 2DH models, like simClast (Dalman and Weltje, 2012), geologic time scales are no issue, consequently the processes are highly parameterised to reduce computational time. Additional consideration is required in significant amount of input these models need, as every event is based on several parameters, can hard to quantify. 2D models like DELTASIM, by (Hoogendoorn et al., 2008), and BARSIM, by (Storms, 2003) fulfill a more conceptual role in the evaluation of stratigraphic response to changes in sediment supply and sea level. They simulate accumulation, and erosion on a cross-shore longitudinal profile. The coupling of these inspired 2Dstratsim, (de Jager et al., in prep.). Like its predecessors this model distinguishes different grain-size classes, and has a separate routine for sedimentation, and erosion. This allows for the simulation of coastal and

clinoform evolution, stratigraphy, erosion surfaces, and transport of the grain-size classes. 2Dstratsim is a 2D model that includes geometric constraints on the delta shape, (de Jager et al., in prep.) it can simulate the deposition in different environments along a longitudinal profile. Volumes are not considered directly but is compensated by the use of pseudo volumes to mitigate long computational time, and avoid numerical complexity. Additionally, to reduce the complexity of the input parameters the model allows to implement rough estimates of relevant parameters with a limited amount of data. This makes it a powerful tool to evaluate a geologic setting. In addition the model has a new numerical inversion technique based on Monte Carlo-Markov chain Bayesian approach, that was developed by Charvin (2008) to disentangle the boundary conditions signal based on stratigraphic data.

To test the 2Dstratsim model the data set of, the Panther Tongue delta-shoreface system on the eastern Wasatch Plateau, Utah, U.S.A., is chosen as a test case. This system is described in (Hampson et al., 2011), where crop data, log data, well correlations, and cross sections of the Wasatch Plateau are presented. The system is composed of a coupled delta-shoreface environment, with the delta sub-parallel to the shore. The delta deposits are coeval with the shoreface deposits, and are found in the same parasequence. Current theory on the formation of the Panther Tongue ksp040 parasequence states a sequence of four vertically, and laterally stacked units both progradational and aggradational. However a contradiction is observed in the stratigraphic records. These records indicate strong variance in wave regime, and sea level signals between the two systems along depositional strike, (Forzoni et al., in prep.). The shoreface to the south is supplied with sediment from the delta via currents flowing alongshore, its stratigraphy indicates significant wave action. This contradicts the observations at the delta to the north, that suggest a fluvial-dominated system with only minor of wave reworking. This is presumably related to its sub-parallel orientation to the shore sheltering it from wave activity, (Hampson et al., 2011). Additionally a discrepancy in the sea level signal is observed leading from the observations made at the shoreface, which shows normal regression. This is inconsistent with the delta records that show evidence of long distance forced regression, (Forzoni et al., in prep., Hwang and Heller, 2002). This discrepancy makes this coupled system an excellent environment for 2Dstratsim, for it is able to conceptually investigate the relevance of the sea level fluctuations, and changes in sediment supply. Data from Forzoni et al. (in prep.), Hampson et al. (2011) will act as a reference, and validation when compared to the simulated logs generated by the 2Dstratsim model.

3. Data

The Panther Tongue area, figure 3.1, is chosen as 2Dstratsim's test case. Since it has been thoroughly studied in the past by (Dubiel et al., 2000, Forzoni et al., in prep., Hampson et al., 2011, Hwang and Heller, 2002).
Their data revealed that the system consists of a fluvial dominated delta in the northern Wasatch Plateau, and a wave dominated shoreface environment down in the southern Wasatch Plateau, figure 3.2. This coupled sedimentary system provides a suitable configuration for 2Dstratsim which is build to conceptually analyse coupled geologic environments, (de Jager et al., in prep.).

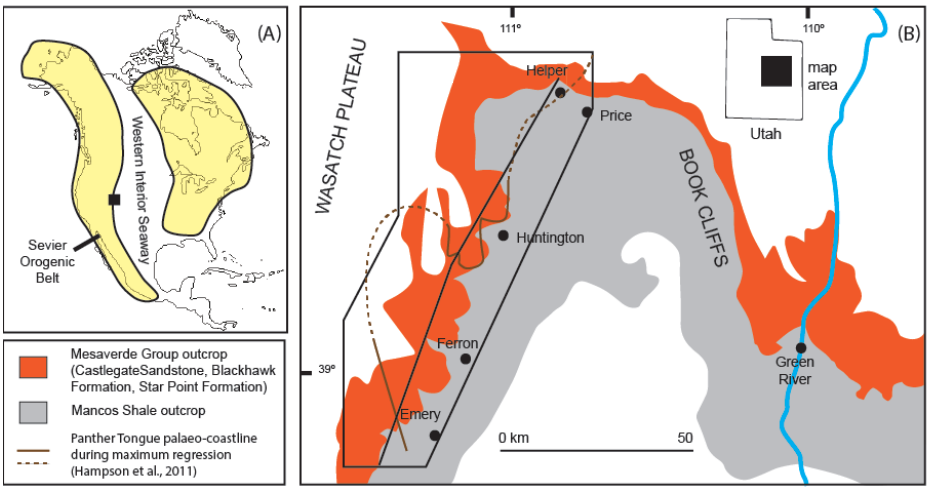

Figure 3.1: Location of the studied area, the Panther Tongue on the Wasatch plateau, Utah, U.S.A..(A) Western Interior Seaway, transposed on a map showing the current shape of the North American continent, after (Kauffman and Caldwell, 1993) in (Forzoni et al., in prep.). The black square indicates the study area, located on the western margin of the paleo continent. (B) Location of the Mesaverde Group (Star Point Sandstone, Blackhawk Formation, Castlegate Sandstone) and Mancos Shale outcrop belt in the Wasatch Plateau and western Book Cliffs, modified after (Forzoni et al., in prep.).

.

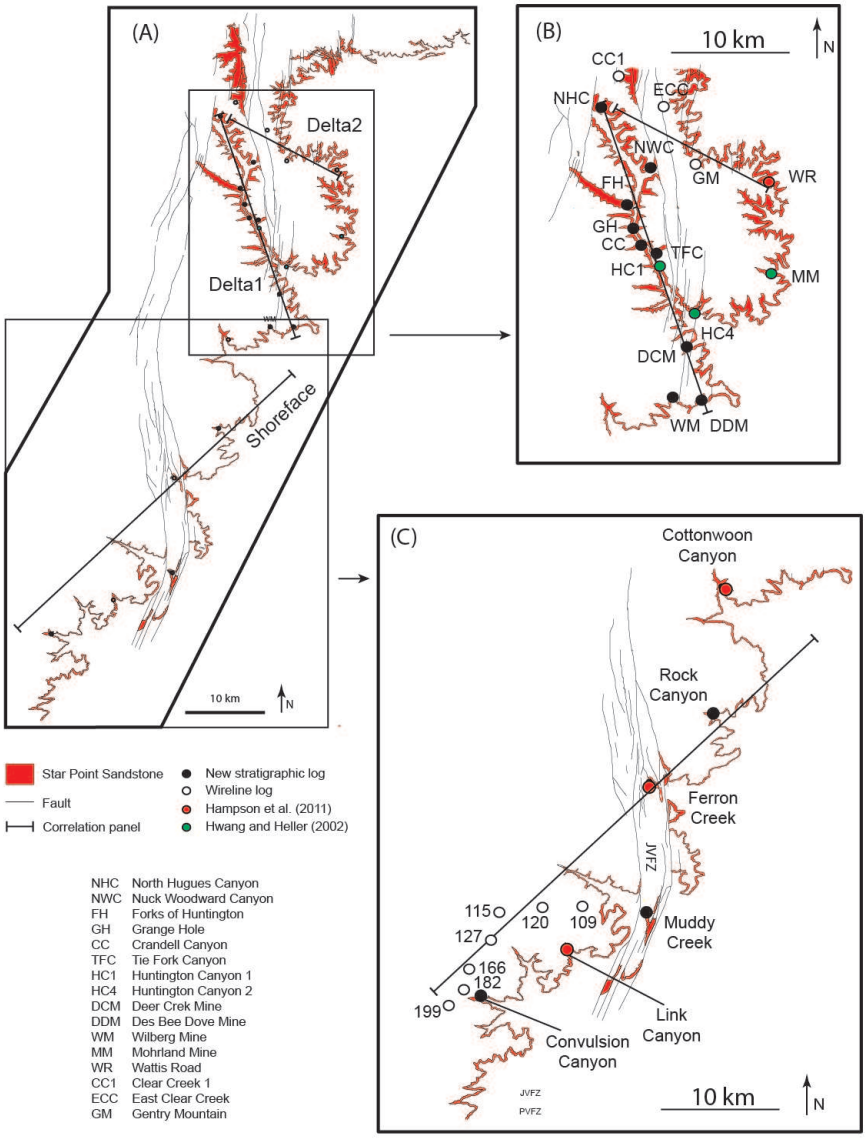

Figure 3.2: (A) Magnified area of the eastern Wasatch Plateau, shown in figure 3.1 B, indicating the location of stratigraphic logs, and lines of the correlation diagrams, both in the Star Point Sandstone. (B) Zoomed-in on the upper rectangle from (A), enlarges the Huntington Canyon area, after (Hampson et al., 2011, Hwang and Heller, 2002) in (Forzoni et al., in prep.) , (C) Zoom-in on the lower rectangle from (A), magnifying the Ferron area, after (Dubiel et al., 2000, Hampson et al., 2011) in (Forzoni et al., in prep.))

.

3.1 New data

Based on available, and new data, new interpretations on the Panther Tongue's Ksp040 parasequence are introduced by Forzoni et al. (in prep.). The new interpretation, figure 3.4, proposes that a connection exists between the Ksp040 parasequence in southern part of the Wasatch Plateau, and the Panther Tongue parasequence in the northern part of the Wasatch Plateau. Their connection implies that the systems are correlated. Both parasequences are bounded by a maximum flooding surface, and maximum regressive surface, (Forzoni et al., in prep.), and can subsequently be subdivided into four bedsets. Bedsets are defined as relatively conformable successions of genetically related beds bounded by surfaces of erosion, non-deposition, or correlative conformities, as in (Van Wagoner et al., 1990). The observed bedsets can be correlated across the whole Wasatch Plateau. They consist of minor coarsening, and thickening upward packages. For the wave-dominated shoreface succession of the Ksp040 parasequence in the south the stacking of the bedsets is progradational (BS 1-2) followed by aggradational (BS 3-4). The bedset in the Panther Tongue parasequence in the northern part of the Wasatch Plateau are progradational, (Forzoni et al., in prep.).

The focus of this study is on the Ksp040 parasequence which reflects the wave-dominated shoreface along the southern Wasatch Plateau. The associated Panther Tongue to the north is considered as the dominant sediment source for the Ksp040 parasequence. As a result of the complex 3D nature of the individual Panther Tongue lobes it is infeasible to correlate it to a 2D simulation of 2Dstratsim.

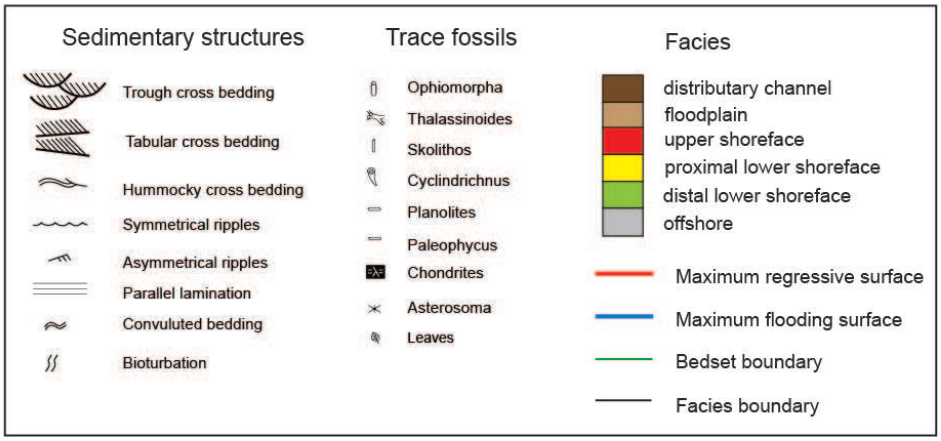

Figure 3.3: Legend for the figures 3.4, 3.5, and 3.6, after (Forzoni et al., in prep.).

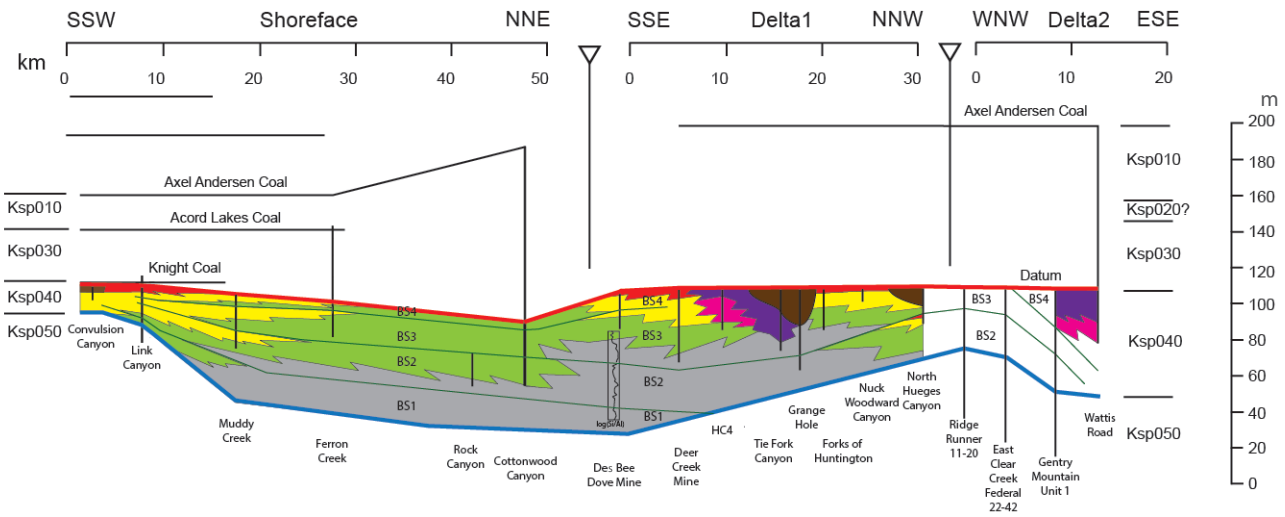

Figure 3.4: Profile of the Ksp040 parasequence following the correlation panel lines presented in figure 3.2. The vertical scale is exaggerated to illustrate the along-strike correlation between the dip-oriented Shoreface, Delta1, and Delta2, after (Forzoni et al., in prep.). The parasequence is subdivided in the bedsets 1 through 4, (BS 1 to 4), and bounded by a maximum flooding surface, and maximum regressive surface. The coal layers used to identify the different parasequences are marked in black. The logs on which the profile is based are illustrated as vertical black lines in the stratigraphy above their respective names.

The new Ksp040 profiles are used as a reference to test the 2Dstratsim model. The purpose of the new Ksp040 profiles is to compare them to the simulated 2Dstratsim profiles. A comparison between the profiles can ensue from a visual match of similar bedset geometries or from similarities in the coarsening upward trends at specific log locations. The first one is qualitatively based on the users judgment while the latter is calculated in the model to quantify its similarity. To streamline the correlation procedure minor modifications are inserted in the Ksp040 profile. The main modification relates to the initial bathymetry in the Ksp040 profile. It is chosen to attune the bathymetry of the Ksp040 profile to the model's profile. Because the model shows numeric errors when generating a stratigraphy on such a non-linear profile. An attempt to attune the model to the bathymetry of the Ksp040 profile enclosed in appendix C. Adding to this is the fact that the shape of bedset 1 (BS1) over the correlation panel is uncertain due to the fact that BS1 is only completely penetrated by the log at Link Canyon. Therefore, the exact shape of the maximum flooding surface acting as the base of BS1 is also questionable. Hence, attuning the Ksp040 profile to the model's profile is adequate for testing the model. Attuning the initial bathymetry of the Ksp040 to the model involves the introduction of a linear line as shown in figure 3.5. This modification preserves the general coarsening upward trends found in the upper part of bedset 2 (BS2) because they are equally cut off by this surface. Data below the initial surface is not considered when correlating the results. The modified Ksp040 correlation panel in figure 3.5, and associated logs in figure 3.6 represent the 'truth' to which the simulated 2Dstratsim profile is compared.

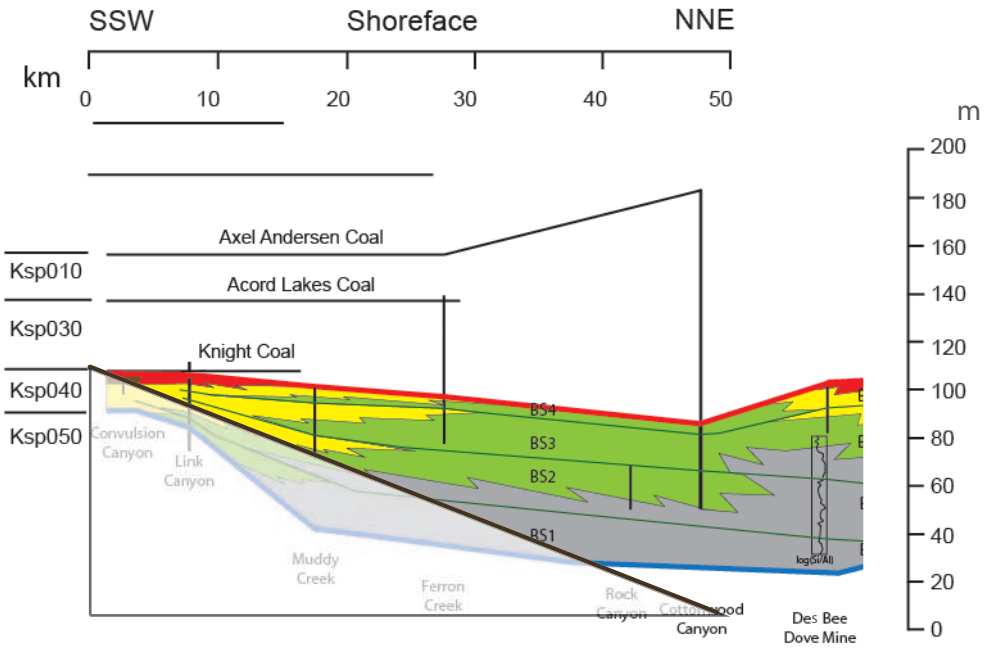

Figure 3.5: The extracted shoreface log correlation profile from figure 3.4 modified to match the dimensions of a simulated model profile. The paleo-shore is on the left of the diagram, and the sea on the right. The brown line represents the base surface used in 2Dstratsim, modified after (Forzoni et al., in prep.).

.

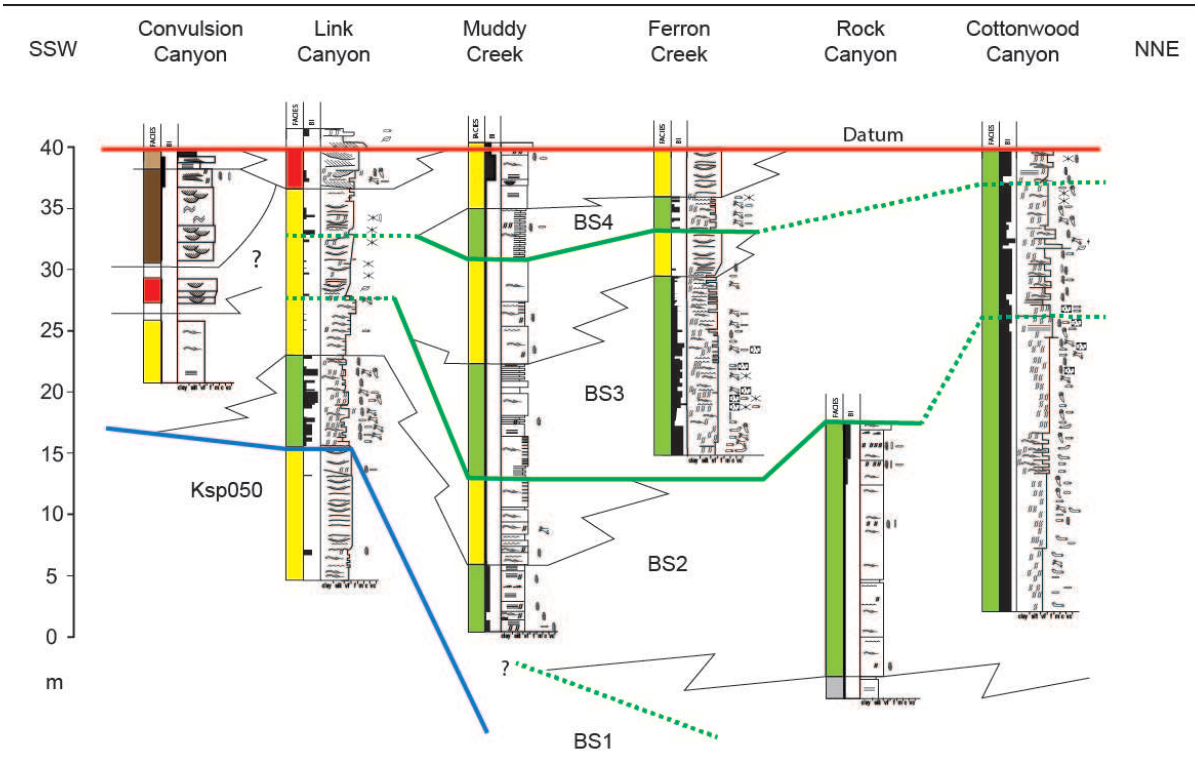

Figure 3.6: Logs fundamental to the cross-sectional diagram of the shoreface, figure 3.5. The logs give a correlation between the average grain-size, and depth. The facies are interpreted based on grain-size, and fossil content. Their boundaries are indicated in black. The bedset boundaries are indicated in green. The landward dip of bedset boundaries in the NNE (seaward) locations is an artifact, which is caused by considering the maximum regressive surface as horizontal, and likely enhanced by differential compaction during diagenesis, (Forzoni et al., in prep.).

In the offshore deposits of the Panther Tongue rock samples are collected with a vertical resolution of 1m over a distance of 48m. The selected site for sampling, Des Bee Dove Mine, is chosen because it is located between the fluvial dominated deltaic deposits, and the wave-dominated shoreface deposits, figure 3.4. Hence, it is a key location to investigate the connection between the two sedimentary environments. First, all samples are analysed with X-ray Fluorescence (XRF), which provides relative element abundances. Next, five samples are selected for further analysis with CT-scans, and thin sections, in order to characterise rock mineralogy, to calculate grain-size fractions, and average particle diameter. Finally, the calculated grain-size fractions, and the average particle diameter of the five selected samples are used to calibrate the results obtained with the XRF analysis, visualised as log ratios between the major elements. With this approach the signal from the XRF is translated to an average grain-size signal that can be used as an input for 2Dstratsim.

3.1.1 Logs

2Dstratsim is able to use the average grain-size to depth logs to quantify the correlation of a measure correlation panel, as in figure 3.5, to a simulated cross-section profile. Yet, because 2Dstratsim cannot correlate the measured logs in its current version, the logs are digitised for manual comparison only.
The image processing tool (CurveSnap) is used to digitise the logs from figure 3.5. This program is able to overlay the image of the log with a linear Cartesian coordinate axis. Subsequently, the processing tool makes use of imaging techniques to recognise the data points, or curves.

The logs from figure 3.5 describe the average grain-size over the length of the log. This average grain-size is defined according to the grain-size classification proposed by Blair and McPherson (1999), figure 3.7.

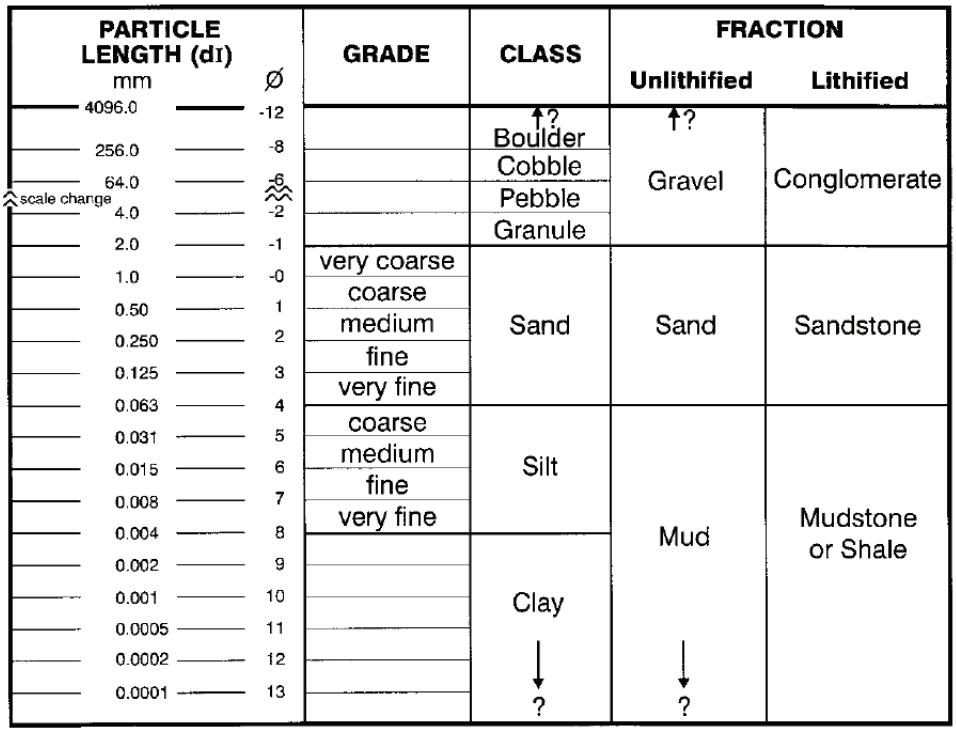

Figure 3.7: Grain-size classification proposed in Blair and McPherson (1999) is used for sand and mud description, and categorisation. The classes and subclasses originate from Udden (1914), and is modified by Folk (1954, 1974) and Folk et al. (1970).

The 2Dstratsim requires numeric values for the average grain-size, and is thereby not directly compatible with the grain-size classification system proposed by Blair and McPherson (1999). The field data is converted from a grain-size class to a metric format by using a step by step approach.
First, the processing tool translates the grain-size classification to a Cartesian grid. Then, the Cartesian log data is adjusted to the non-linear scale used by the grain-size classification system. This is done by using a quadratic regression that fits the boundary values of the grain-size classification table, figure 3.7. To create this regression line, first the numeric values of the class boundary points from figure 3.7 are inserted manually. Then, Matlab's build-in interpolation tool is used to connect these points with the regression line. Finally, the tool identified the regression line to take the from of a quadratic equation;

$$X_{g-s} = 4.4448*10^{-23}x_{ini}^{8} - 1.3202*10^{-19}x_{ini}^{7} + 6.5818*10^{-17}x_{ini}^{6} + 1.0332*10^{-13}x_{ini}^{5}. \quad (3.1)$$

Equation 3.1 is then used to transpose data points from its Cartesian initial value x_{ini} to its grain-size classification scale value X_{g-s}.

The fit of equation 3.1 to the boundary values of the grain-size classification is shown in figure 3.8. We observe that the regression line can overestimate, and underestimate the value at a given class boundary value. Thereby the use of a regression line introduces an error in the grain-size log data. This error is largest at an initial value of 1350μm at this initial value equation 3.1 gives a X_{g-s} value of 273μm, where it should be the grain-size boundary value of 250μm. Thus, the absolute maximum error introduced by using the regression line is $\sim$23μm. Whereas, the absolute error made at the boundary values of

64μm, and 125μm are 11μm and 4μm respectively.
Because most of the average grain-size values of the logs have a value around 125μm, the use of the regression line, and the error it introduces is acceptable.
Because the error is relatively high at smaller grain-sizes, 11μm at boundary 64μm, it is determined that the logs of Rock Canyon, and Cottonwood Canyon will provide unreliable grain-size data. Therefore, we use solely use the logs of Link Canyon, Muddy Creek, and Ferron Creek in the correlation to the simulated logs. The log at Convulsion Canyon is also neglected as falls below the introduce base line in figure 3.5.

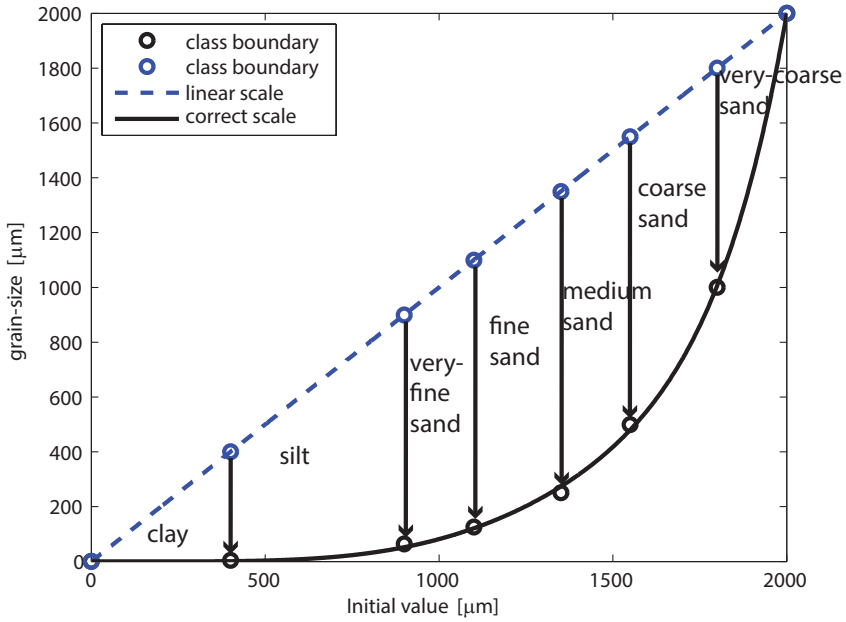

Figure 3.8: Graphic representation of the grain-size transposition from linear scale to the scale proposed by (Blair and McPherson, 1999). Arrows indicate how the class boundary is adjusted. Note that the regression line does not fit the transposed class boundaries perfectly. This will introduce a discrepancy between the grain-size from the initial log, and the final result.

The results of the digitisation process, and the conversion of units through the use of the regression line is shown in figure 3.9. on the log of Muddy Creek In the digitisation process data points are taken every ~0.05 m. At certain intervals this causes a false sense of data mismatch between the initial log, and the digitised logs due to the linear interpolation preformed by Matlab. For example the interval of 30 to 35 m in figure 3.9 shows a fluctuation which is dissimilar in shape between the logs. However, considering the model will only use the data points rather than the whole interpolated line, the model will use the log correctly.

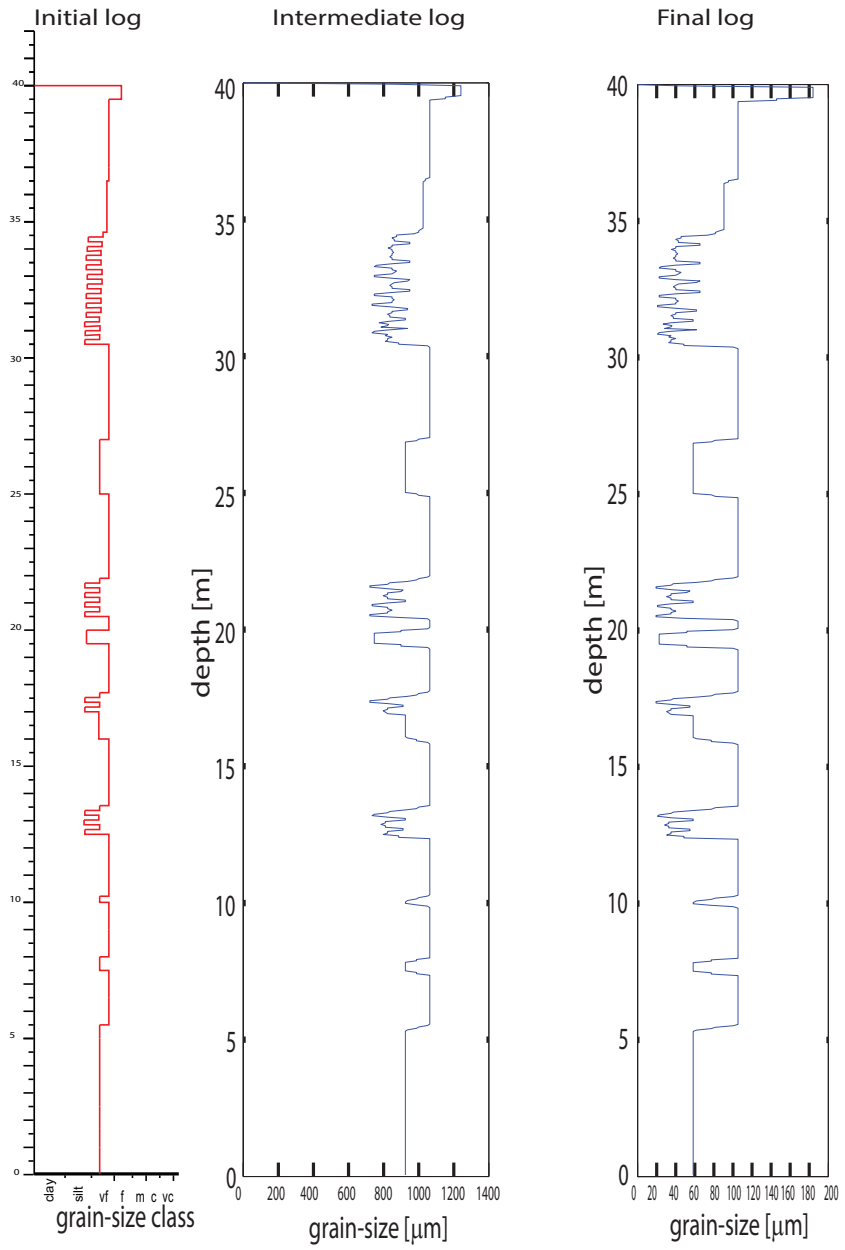

Figure 3.9: Digitisation process from left to right on the Muddy Creek log. On the left the raw image of the log is disassembled to a grain-size depth log from figure 3.4. The middle log shows the result after the digitisation process. On the right is the final result, after the grain-size correction with equation 3.1 is preformed.

The equation that quantifies the correlation between the measured log, and the simulated logs requires that the measured logs describe a similar vertical length. In addition the measured logs are required to possess a continuous signal over this length. In figure 3.5 it is observed that the Link Canyon log, and the Ferron Creek log do not meet this requirement. Therefore, the log of Link Canyon is cut at 26m, as in figure 3.6, and everything below it is neglected as it falls below the introduced initial surface, in figure 3.5. Additionally, the log of Ferron Creek is extended by 36m with artificial data so that it covers the whole vertical length of the profile from the top of the maximum regressive surface down to the introduced initial profile in figure 3.5. As the original Ferron Creek log is 27m the extension of 36m makes a log of 63m total, of which 4/7th of log data is artificial. The artificial data is based on the observation in the lowest measured point of the Ferron Creek log, which implies a decrease in grain-size downsection with in BS2 a coarsening upward sequence as observed in the off shore facies of the Rock Canyon log. The result of this extension is shown in figure 3.10.

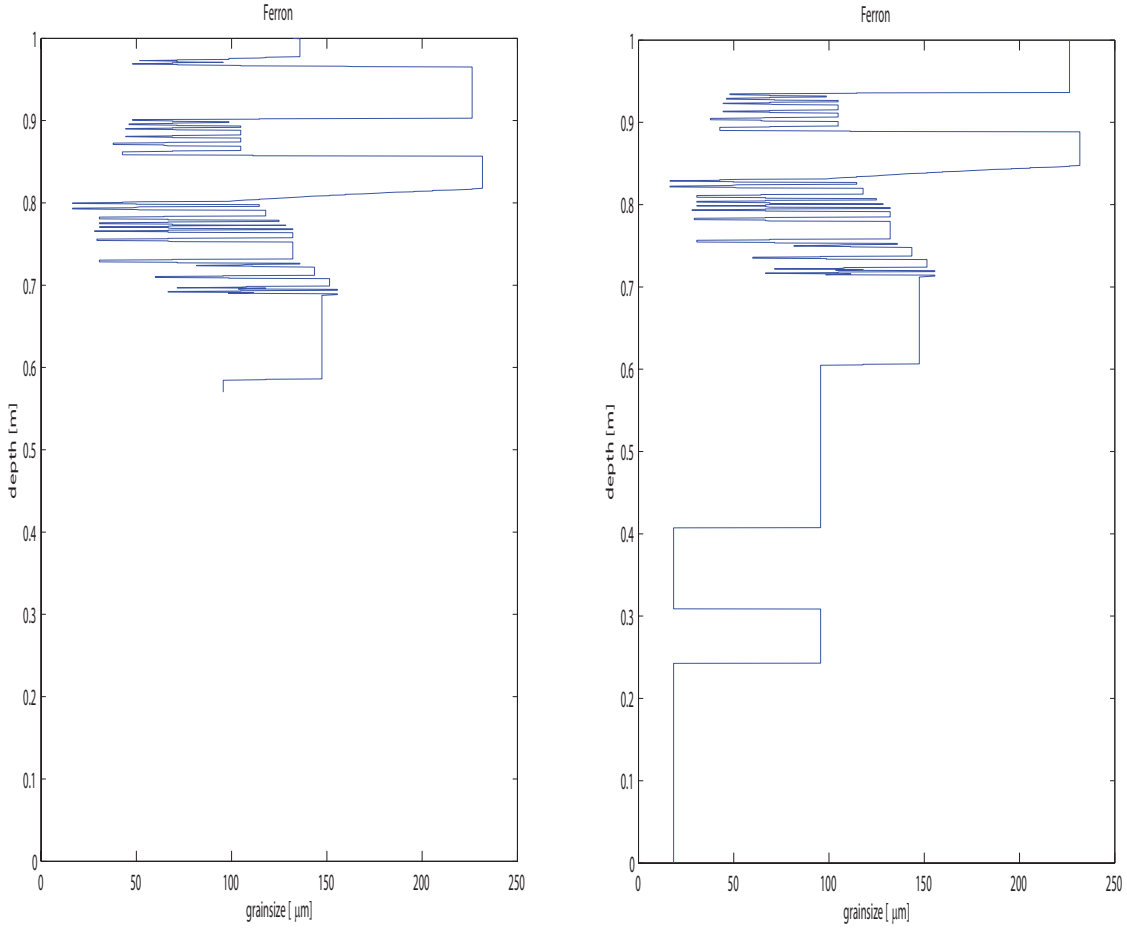

Figure 3.10: Artificial data extension on the normalised Ferron Creek log. The logs are normalised to the vertical length between the top of the maximum regressive surface down to the introduced initial profile of the profile in figure 3.5, at the location of the Ferron Creek log. On the left is the digitised image of the original Ferron Creek log. On the right is the final result, after the artificial data is implemented at the bottom of the Ferron Creek log.

3.1.2 Sample analysis

The samples acquired at the Des Bee Dove mine are investigated to obtain a first order estimation of the average grain-size to depth relation at this location. The Des Bee Dove mine is located in the middle of the delta, and shoreface, and thereby connects the Ksp040 parasequence over these systems. This location is therefore equally influenced by signals from both environments. Thus, it can be used in the 2Dstratsim model to analyse the relation of between the simulated environments as well.

Multiple steps are preformed to obtain an average grain-size to depth log from the samples. First, XRF measurements are taken every meter to acquire relative element abundances. The results of the major elements are then plotted as log ratios. Additionally, five samples are selected at the depths of 5, 14, 23, 30, and 40 m. These five samples are analysed on average grain-size of the fraction $> 4\mu m$, and mineral content based on pictures of thin sections, and CT scans of corresponding samples. An original total thin section is ∼25x∼25x0.03mm, and the used image covers an area of 1.47x1.13mm from the thin section. The cylindric cores used in the CT scans have a diameter of 2.56mm, and a height of 0.8mm. The CT scanner takes 800 photos equally distributed, every 1μ, over the core's length, this gives cross sections of the core perpendicular to its height. From these 800 photos 50 are analysed as a bulk to represent the average grain-size properties of the core sample. The ratios of the element abundance measured by the XRF can be correlated to the mineralogy measured in the samples. Thus, the combined results of the average grain-size of the samples, and their mineralogy can be to calibrate the XRF log. Thereby, the XRF can be used to give an first order estimate of the average grain-size between the samples along the vertical profile the samples are acquired from.

Per rock sample from the five depths, 2 thin sections are made (10 total), and a core (5 total). We quantitatively analyse the thin sections, and CT-scan photos of the samples with image processing software, ImageJ.

The thin sections are processed as follows; first, they are transformed in 8-bit images to enable image processing methods as erosion, and dilation. The erosion process removes the outer pixels from a cluster/particle, while the dilation process expands it again with a layer of pixels, (Voncken et al., 2004). These processes are used to erode pixel clusters 4 times, then dilate them 4 times. The consecutive erosion cycles remove particles with a maximum width smaller than 4 μm which represents the clay fraction (Blair and McPherson, 1999).

An example of an examined raw thin section image is shown in figure 3.11a, and its processed counterpart is viewed in figure 3.11b. The large bright white, and grayish particles found in the image are quartz minerals. Less abundant identifiable particles, larger than clay (4 μm), are identified as calcite, and dolomite grains. The matrix is composed of clay minerals, organic material, autigenic calcite cement, and iron oxides, (Forzoni et al., in prep.).

The result in figure 3.11 is determined to be sufficient for further use as improvements on the quality of the processing will not significantly contribute to the outcome compared to field measurements.

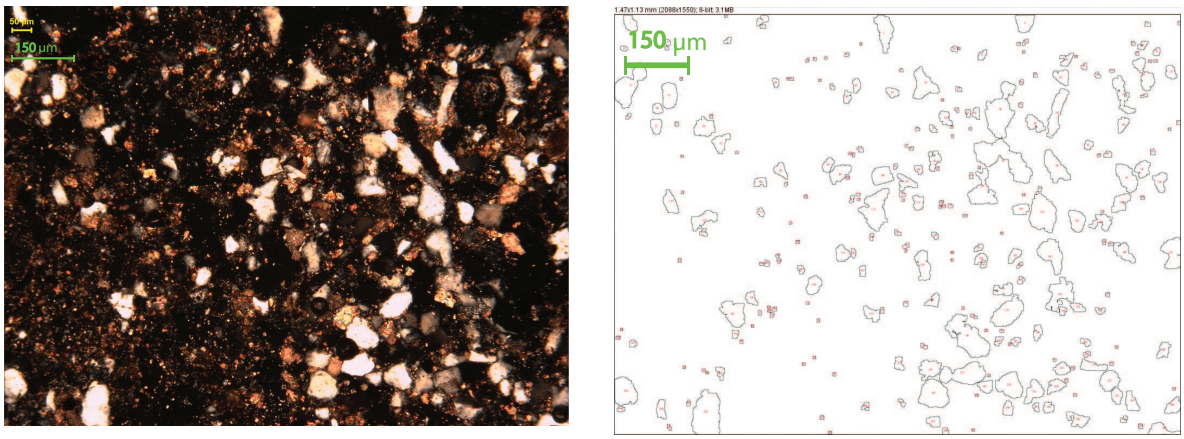

(a) example thin section, raw image

(b) example thin section, after processing

Figure 3.11: Thin section 5.2; before, and after processing with ImageJ. The image covers an area of 1.47x1.13 mm from the original thin section. This image is taken from a sample from 5m depth.

The CT-scan uses X-ray imaging techniques to chart density differences in the core sample. The sequence of photos represent the volume of the core.
The CT-scan images charts density differences, it interpreted by Forzoni et al. (in prep.) that it differentiates Fe-dolomite with a high density as white spots, quartz and carbonate grains in the light gray areas, and the clayey matrix are associated with the dark gray areas. An example image is show in figure 3.12, the raw image is figure 3.12a, and its processed counterpart in figure 3.12b.
The CT-scan image sequences are processed as a bulk with methods similar to the individual thin section images. First, every image in the sequence is turned to 8-bit followed by 4 times erosion to erase the particles with a width, $< 4\mu m$, followed by 4 times dilation to reconstruct the remaining particles to their original size. Then, the image sequence is evaluated for the average grain-size of the remaining fraction.
In figure 3.12 it is observed that the sum of the amount of light gray particles surpasses the amount of dark gray, and white particles combined. Based on the interpretations of Forzoni et al. (in prep.) it is therefore concluded that the core mostly consists of quartz, and carbonates. This result is similar to the conclusion on the composition determined in figure 3.11.

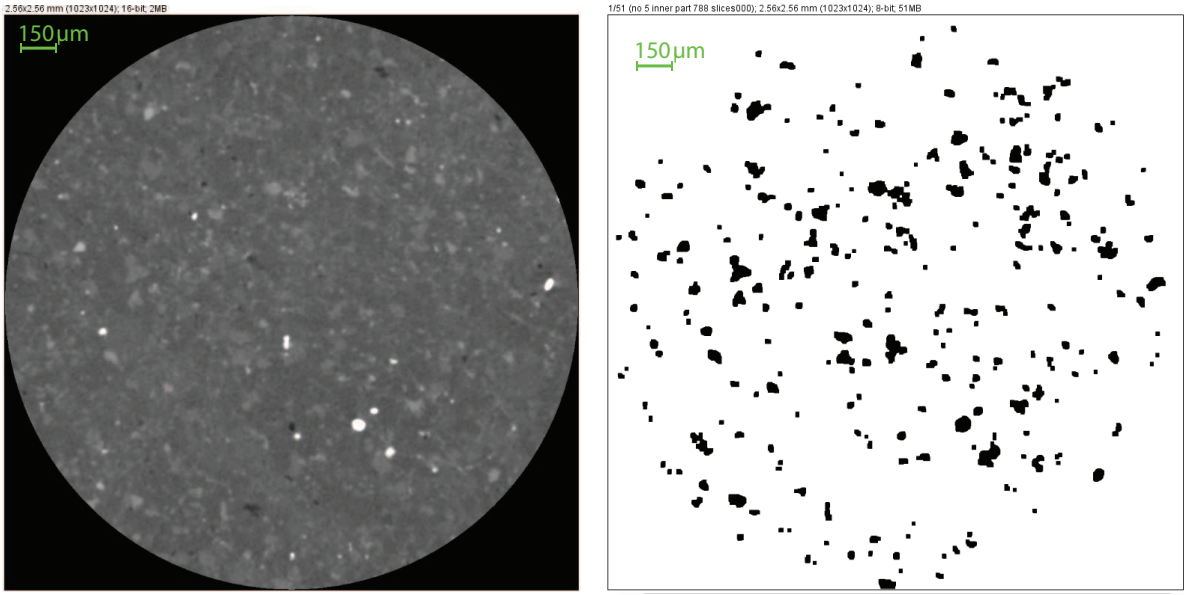

(a) example CT image, raw picture

(b) example CT image, after processing

Figure 3.12: CT scan 5; before and after processing. The image represents the cross section of a cylindric core perpendicular to its height. The diameter of this core is 2.56 mm. This image is taken from a sample at 5m depth, like the thin section image in figure 3.11.

The XRF identifies the relative abundances of elements present in a sample, this method is applied at the Dee Bee Dove mine location with a measurement every meter. In the thin sections, and CT-scans it is observed that the largest grain-size fraction, $> 4\mu m$, generally consists of quartz and calcite, and that clay minerals are mostly smaller than $< 4\mu m$. Therefore, the element abundances of silica, and carbonate measured in the XRF are used to chart the (Si/Ca) ratio. This ratio is used to approximate presence of quartz over carbonate minerals, as calcite, and dolomite, (Forzoni et al., in prep.). Because calcium is softer than quartz (Klein, 1989), and is consequently more prone to grinding, we expect the quartz grains to be larger than calcium containing minerals. Thus we expect that a high silica content corresponds to a sample with quartz grains larger than clay, figure 3.7, increasing the average grain-size of the sample. Following this logic a high calcium reading should indicate a sample with a small average grain-size.

The results of the average grain-size diameter acquired through image processing of the thin section, and CT-scan images are presented in figure 3.13. The figure shows a scatter of data originating from using the different images at similar depth. Our results in figure 3.13 are presented in combination with the results of the analysis preformed by Forzoni et al. (in prep.).
The scatter in our data at a given depth in figure 3.13a is the result from using 2 different thin section images. These thin sections are analysed by using the same processing routines. To improve the data density our results are then complemented with data from Forzoni et al. (in prep.). In figure 3.13b, the scatter is a result solely from complementing our data with the data from Forzoni et al. (in prep.) who used two different processing methods to analyse the samples.

The Si/Ca ratio based on the XRF measurements is used in figure 3.13 as a trend line for the average grain-size to the vertical depth, calibrated to the observations made in the images of the samples.

In figure 3.13 we observe more scatter between the results coming from the thin section images, see figure 3.13a, compared to the CT-scan results in figure 3.13b. We conclude that this is inherent to the fact that an image of a thin section is solely a 2D representation of a sample which is different from the sequence of CT-scan images, that can be interpreted as a pseudo volume. Hereby the sequence of images theoretically reduces the influence of small scale inconsistencies, and inhomogeneity of the sample. This theory agrees with the concept of the representative elementary volume (REV), introduced by (Harrison and Hudson, 2000). This theory states that properties tend to average as the scale of a sample is enlarged (in any direction), what implies that larger samples, like cores, represent the bulk of the rock better than thin sections which are smaller, and 2D.
From the scatter in results at a similar depth we conclude that it is hard to find a sample that closely represents the rock body at a small scale. However, a reduction in data scatter is observed as a result from increasing the sampled area, from a thin section to a CT-scan of a core. Lastly, we conclude that the Si/Ca trend can be used to as a first order approximation in interpolating the average grain-size over depth. However, the trend is not consistent between the thin section, and CT-scan data see figure 3.13. Therefore, we suggest using the CT-scan data because of the improved REV of the sample.

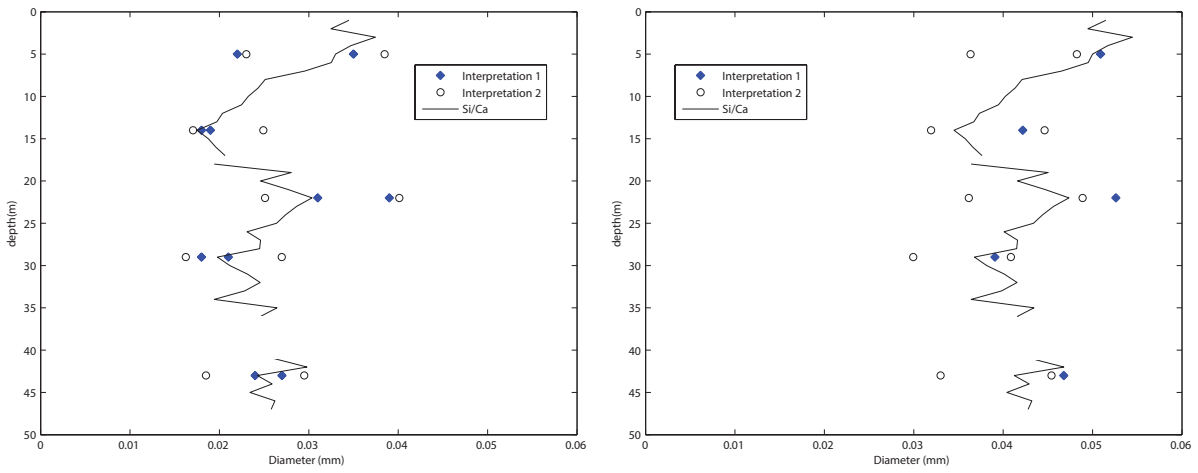

(a) Thin section data

(b) CT scan data

Figure 3.13: Interpretation results; blue diamonds indicate my own analysis (interpretation 1). The circles represent the measurements by Forzoni et al. (in prep.). The combination of the interpretations is set is fitted with Si/Ca log data based on the XRF measurements.

4. Model

The 2Dstratsim model can simulate a delta, and shoreface environment, figure 4.1. The floodplain is not considered in this thesis, and thereby sediment is directly implemented in the delta module, which contains the lower course of a river. The delta, and shoreface environments are reduced to simulated model profiles which are perpendicular to the shoreline of the environment. Consequently, a separate cross-sectional profile per environment is generated by the model. Between these environments sediment is transported from the delta to the shoreface. Additionally, the environments are subjected to an identical sea level change signal.
From these simulated profiles the shoreface environment is compared to the Ksp040 shoreface correlation panel in figure 3.5, to test the 2Dstratsim model.
Changes in the 2Dstratsim model are made on the last version of 2Dstratsim left by de Jager et al. (in prep.), further referred to as the previous model.

The model discretises the simulated profiles down dip with grid-cells of a given size. The initial surface therefore makes a stepwise decent perpendicular to the shoreline. On a given cell on this discretised profile the model takes the third dimension into account by analytically calculating the sediment volume. This allows the user to implement input signals in realistic units, while the model remains computationally fast. Subsequently, the volumetric output is averaged to the cells on the discretised profile at the end of the calculations. For this reason, the model is not suited to evaluate lateral heterogeneities within an environment but finds its application in evaluating differences in stratigraphic record between environments, influenced by common input signals. Additionally it is used to evaluate vertical heterogeneities.

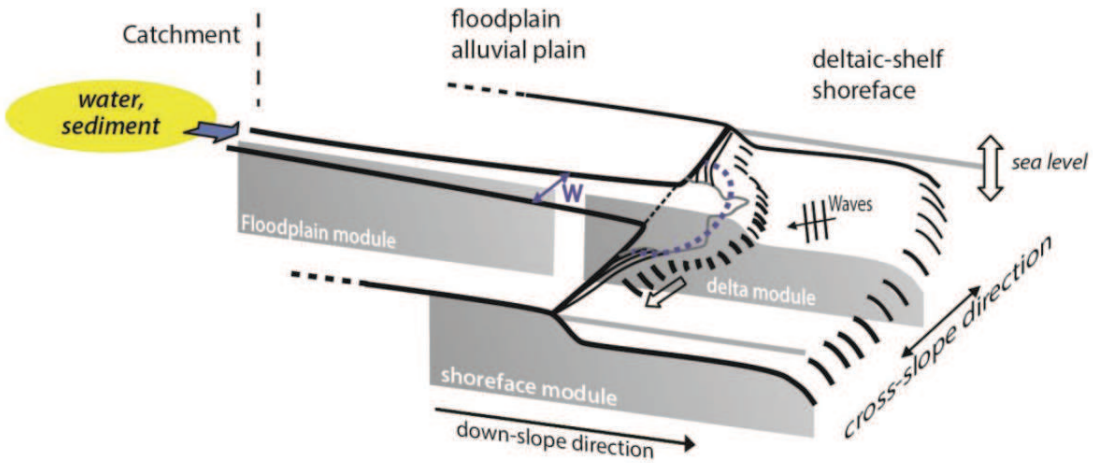

Figure 4.1: Conceptual model of 2Dstratsim showing the source where water, and sediment discharge is generated, which is subsequently deposited in one of the three environments: floodplain, delta, and shoreface. The figure is adapted from, (de Jager et al., in prep.). Note that the floodplain is not considered in this thesis. Therefore, water, and sediment is directly introduced into the delta environment. Gray areas show the different cross-sectional profiles of the model generated in the different modules.

The model simulates these environments in a forward or an inversion routine. The forward routine uses parameterised equations together with user implemented data to generate stratigraphy on simulated profiles. This routine is primarily used to investigate the causal relation between input signals, and the simulated stratigraphic output. The flowchart of this routine is described in detail in section 4.1.
The inversion routine is essentially an optimisation routine. This routine runs the forward routine multiple times, and adjusts the input signals every iteration using statistical functions. The new input signals are accepted if they improve the calculated match between simulated logs, and implemented geologic data. The inversion concept is described in more detail in section 4.2.

Parameterised equations in the forward routine describe the physical processes simulated by the model. They use the data implemented by the user to generate a simulated stratigraphy on a simulated profile. The data is inserted into the model via a configuration file, which contains the numeric properties of the profile, and geologic data in the form of static parameters, input signals, and logs. Static parameters are place, and time independent. They are used in the parameterised equations to account for various tuning factors, e.g. a wave depth over wave height ratio or a control factor to adjust the amount of fluvial erosion. The input signals in the configuration file describe the sea level change, river discharge fluctuations, and change in sediment concentration over a given time. After these signals are processed by the model the resulting simulated profile is compared to the Ksp040 profiles, and the logs.

The governing equation in 2Dstratsim is equation 4.1. It describes how the principle of mass conservation is used in the model. The derivative of elevation H over time is given as a function of the spatial derivative of sediment flux F at a location x added to the rate

of subsidence T. This subsidence rate is considered low enough to be neglected, (de Jager et al., in prep.).

$$\frac{\delta H}{\delta t} = -\frac{\delta F}{\delta x} + T \tag{4.1}$$

The sediment flux is defined as the difference between sedimentation, and erosion, as in equation 4.2. In this equation S is the location, and time dependent rate of sedimentation, and E is the location, and time dependent rate of erosion, (de Jager et al., in prep.)

$$\frac{\delta F}{\delta x} = E(x,t) - S(x,t) \tag{4.2}$$

Whereas in reality erosion and sedimentation occur simultaneously, in 2Dstratsim these processes are separated, (de Jager et al., in prep.). Additionally, erosion is separated for fluvial erosion, and wave induced erosion, and is defined as the process of making sediments available for subsequent transport. The distance sediment is transported is named travel distance, and is calculated in the sedimentation function. The implementation of the erosion, and sedimentation equations into the 2Dstratsim model is explained in detail in Charvin (2008), de Jager et al. (in prep.), Storms (2003), Storms et al. (2002).

To compare the results of the model based on average grain-size logs the user can insert the measured average grain-size log data at a given location in both the delta, and shoreface simulated environment. Additionally, these logs are inserted with an absolute measurement error. This correlation between the measured log, and the simulated log that is extracted from the simulated stratigraphy is expressed in a likelihood. The likelihood, in equation 4.3, is defined as the integral over the depth D of the squared difference between the measured x_m, and simulated x_s average grain-size values of the layers, divided by the measurement error e.

$$Likelihood = \int \frac{(x_m - x_s)^2}{e} dD \tag{4.3}$$

The integral is evaluated only for the overlapping depth ranges defined by the measured data and the simulated data. For a graphic illustration of the likelihood calculation, see figure 4.2. When no measurement error is implemented or a zero measurement error is used, the model replaces the zero value by a small value to avoid division by zero.
A zero likelihood indicates a perfect match. In order to achieve a best match between the measured and simulated wells the inversion routine in 2Dstratsim calculates the cumulative likelihood of all the wells. Subsequently, it adjusts the input signals to improve this match, which theoretically results in a cumulative likelihood that should approximate zero.

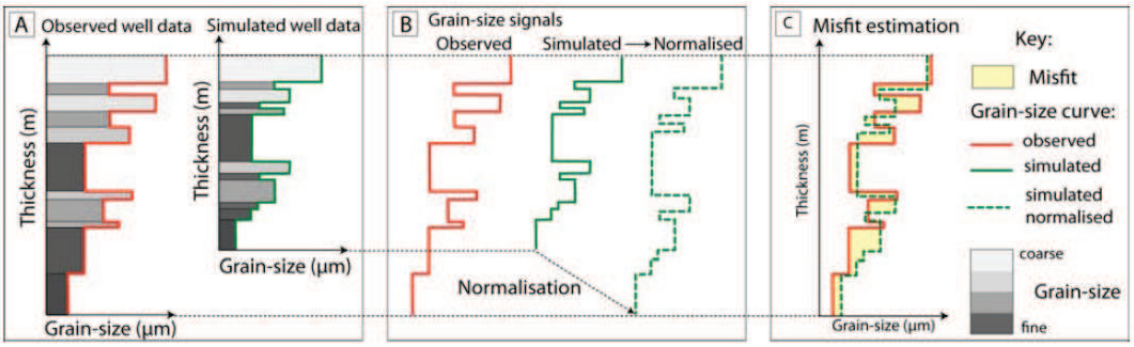

Figure 4.2: Likekihood function design for quantitatively estimating the mismatch between between the simulated, and observed average grain-size distributions at each well log. In the first step (A), the simulated and observed grain-size curves are extracted from each well. In a second step (B), the thickness of the simulated grain-size curve is normalised to the thickness of the observed grain-size curve to avoid repeating the thickness mismatch effect already evaluated. In the final step (C), the mismatch between the normalised simulated and observed grain-size curves is evaluated using the least-square distance criterion. The figure, and caption are adopted from Charvin (2008).

4.1 Forward routine

The forward routine as used in 2Dstratsim is schematically explained in figure 4.3. Rectangles represent the different function modules, and ellipsoids symbolise the switches. When a switch is turned off, the following functions are not called, forcing the model to write the data. Lastly the diamonds pass along information the model requires to advance to subsequent functions.
The flowchart starts at the top diamond, with $t = 0$. This information allows the model to generate an initial surface based on data provided by the user for the delta environment, if the shoreface is active a surface is generated for this environment as well.
Subsequently, the sediment influx is calculated based on the discharge of the river, and the sediment concentration it transports.
Next, boundary locations are determined on the simulated profile. This previously was done separately in the erosion and sedimentation functions. This resulted in a discrepancy between the locations used in these two functions. To resolve this, a single function to calculate the boundary locations is introduced, the details of this function are described in subsection 4.3.1.
Thereafter, the width of the delta is calculated. This function is revised, and is described in detail in subsection 4.3.2.
Subsequently, the model calls functions to simulate geologic events; starting with fluvial erosion, followed by the sedimentation of the fluvial material and pelagic fallout, then end with bioturbation. These functions describing geologic events handle the whole cross-section at once, then proceed to the next.

Waves are not necessarily activated, therefore the model can either write the data, and resume with a next time step, or proceed with wave erosion. The wave erosion brings sediment in suspension. This wave induced suspension is deposited in the following sedimentation function. After which the geologic simulation cycle ends with bioturbation. At

the end of the delta module the model confirms whether the user activated the shoreface in order to continue. Notice that the shoreface module can only come available when waves action is allowed in the delta as well. Because sediment is assumed transported by alongshore currents, and wave action. If this shoreface switch is off the model will write the data, and continue with a next time step.

Alternatively, when the shoreface switch is on, the model will send a user determined fraction of the delta sediment to the shoreface.
Boundary locations are determined individually for the shoreface routine. The location function is followed by the simulated geologic function sequence; wave erosion, sedimentation, and finally bioturbation. In the end all the data is written for output, and the model will proceed with a next time step. The model will remain in this loop until it reaches $t = t_{end}$.

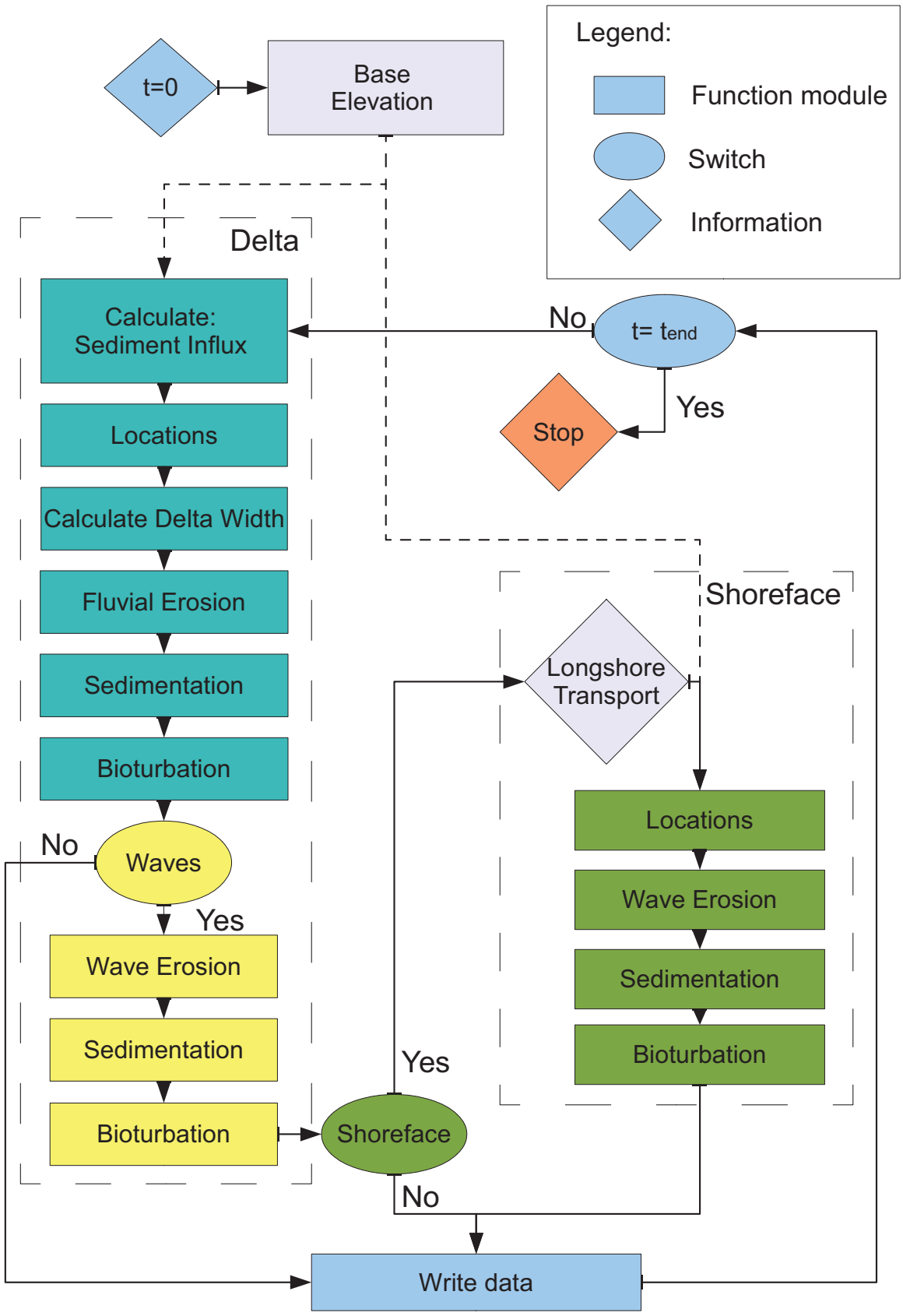

Figure 4.3: Diagram of the forward routine in 2Dstratsim. The wide spaced dashed lines encompass the different environmental routines in the model. The narrow spaced dashed line accentuates the one time generation of the initial base surface.

4.2 Inverse routine

The inversion routine is based on work from (Charvin, 2008), and its implementation to 2Dstratsim is outsourced to an expert programmer. In order to explain this routine a flowchart is shown in figure 4.4, which is based on the 2Dstratsim source code. An illustration is added in figure 4.5 to graphically explain the process behind the different sub-routines present in the inversion.
As shown in figure 4.5, two main processes are distinguished in the inversion routine: the burn-in, and the sampling process. During the burn-in routine the input signals are tempered with, using a simulated tempering algorithm, (Charvin, 2008), to improve the likelihood. The burn-in process includes a steady iteration counter, which counts the amount of consecutive iterations the cumulative likelihood is not changed significantly. When the required amount of steady iterations are made the model enters the sampling period. From the last burn-in run the input signals are used to create a probability function, (Charvin, 2008). During the sampling period the model samples the posterior probability function to create new input signals using a (Reversible Jump) Markov Chain Monte Carlo (RJ)MCMC sampling algorithm, (Charvin, 2008). When the likelihood improves by more than 10% the sampling routine restarts, whereas if the likelihood does not improve significantly the model will end after a user determined amount of sampling iterations.

The burn-in, and sampling processes can be broken down into more detail, as is done in the flowchart shown in figure 4.4. The flowchart, and the model start at the top by loading the initial parameters. These parameters amongst others include the amount iterations the burn-in routine has to make, and how many consecutive iterations have to be steady in order to move to the sampling process. The amount of iterations required to complete the sampling is predetermined here as well. Additionally, the parameters used in the parameterised equations of the first forward run are set here as well. When the first forward is completed the likelihood is calculated.
When the first forward run is completed the model enters the burn-in process. The initially calculated likelihood is saved as the maximum likelihood. Then, after automated tempering on the input signals a new forward model is run, and a next likelihood is calculated. This new likelihood is compared to the maximum likelihood. When the likelihood has improved, the new likelihood replaces the old maximum likelihood, whereas if it did not improve the model enters the steady iteration process.
In the steady iteration process, the tempered parameters are reset to the parameters leading to the maximum likelihood, and are randomly tempered again. The model remains in this loop until the likelihood improves, or the user determined amount of steady iterations is reached. To illustrate this process graphically an example is shown in figure 4.5. In figure 4.5 the likelihood has had two intervals in the burn-in routine where the likelihood did not improve. In the first interval the likelihood increased before the maximum amount of steady iterations was reached, and the burn-in routine continued. In the second interval the maximum amount of steady iterations is reached, and the model continues with the sampling process.
From the input of the last steady iteration a probability distribution is made, (Charvin, 2008). The sampling process is used to sample this posterior probability distribution, (Charvin, 2008). Given this distribution, it is then straightforward to extract individual models (e.g. the best or expected model), to construct probability distributions for in-

dividual model parameters, and to examine correlations between parameters, (Charvin, 2008). The best model is the one having the highest posterior probability. Depending on the nature of the prior function, this may or may not be the same as the model that maximizes the data likelihood, (Charvin, 2008).
During the sampling process a forward scenario can be created that produces a likelihood larger than the maximum likelihood. When the absolute difference between the two is larger than 10% of the absolute value of the maximum likelihood. The sampling procedure restarts with this new likelihood as the new maximum likelihood. Alternatively, when the user determined maximum amount of sampling iterations is achieved without breaking the previous criterion, the inversion is completed.

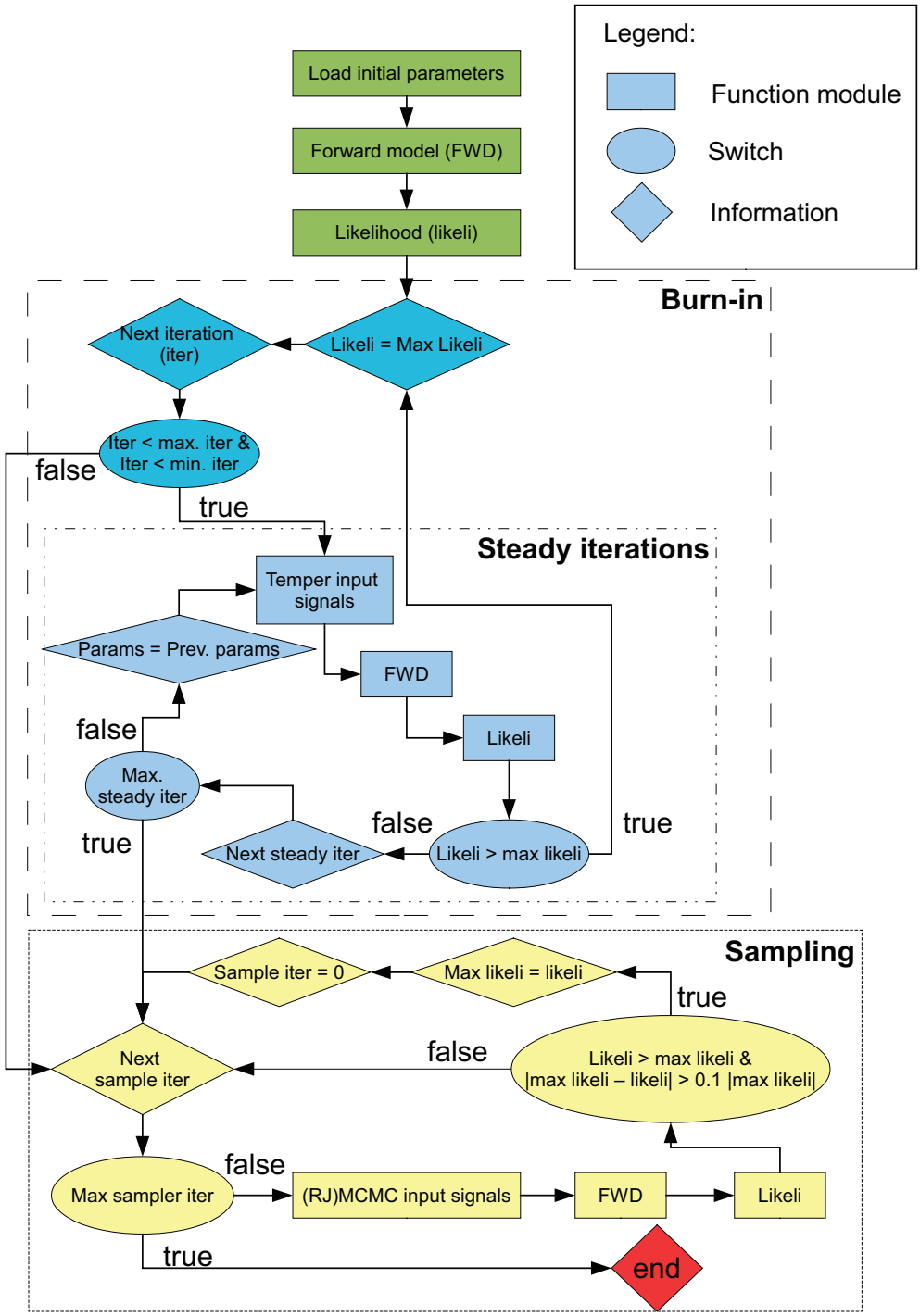

Figure 4.4: Diagram of the inverse routine implemented in 2Dstratsim, base on Charvin (2008). The forward routine described in section 4.1 is represented here as a single function module. The wide spaced dashed lines encompasses the burn-in period. Within this box is the alternated dashed dotted box, which includes the routine that counts the amount of steady iterations (where likelihood does not increase). The narrow dotted box at the bottom encompasses the sampling routine, which samples the likelihood of the burn-in period. The likelihood function module the model calculates the cumulative likelihood between corresponding measured, and simulated wells.

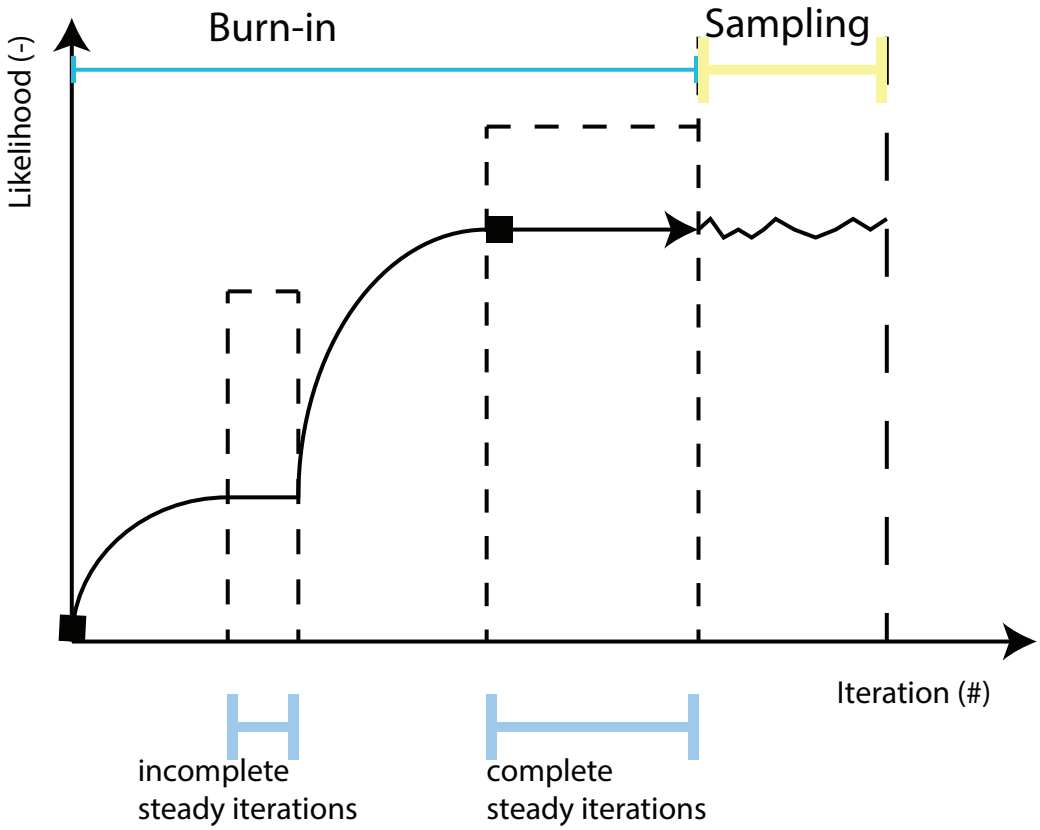

Figure 4.5: The inversion routine improves the likelihood of the simulated wells matching the measured wells. The routine is subdivided into two main routines, the burn-in, and the sampling procedure. Additionally, the steady iterations process count the amount of consecutive iterations the likelihood does not improve significantly in the burn-in procedure. In the burn-in, and steady iterations process the likelihood will fluctuate. The smooth lines used to describe the likelihood improvement in this figure are therefore somewhat misleading.

4.3 Revised modules

From the previous model it was observed that various functions in the forward routine generated erratic output. Which resulted in unrealistic simulated profiles. Therefore, the functions had to be debugged or rewritten before the model could be tested. The first lead to correct these malfunctions is from the function that calculates the model width, Storms (priv. comm.), see section 4.1. After rewriting this function it is observed that the previous model sets crucial boundary locations on the simulated profiles at different locations independently in various functions. This results in numeric instabilities within the simulated stratigraphy. Furthermore, it is observed from using the previous model that the travel distance of grain-size fractions is computed incorrectly, and that sediment is deposited above sea level in too large quantities.
The ensuing subsections will describe the modifications to the functions of the previous model in detail. The order of the subsections follows the order the functions are called in the model, section 4.1.

4.3.1 Locations

The locations function sets boundary locations based on the presence of 'dry' cells on the simulated profiles above sea level, and 'wet' cells below sea level. The locations of the transitions from dry to wet cells, boundary locations, on the simulated profile which the location file identifies are required by most functions in the model. These boundaries give information to next functions on what sub-environment they are working. The different sub-environments we can distinguish in the model are a river, lagoon, and foreshore. It is critical to know what cell is in what sub-environment, because there is a difference in how geologic processes like erosion, and sedimentation work per sub-environment, (Reading, 1996). Functions that are location independent are the bioturbation function, and the sediment influx calculation.

In the previous model a location was determined inside the function that required it. Hence, the sub-environment determined for the erosion, and sedimentation function could change for certain cells. This discrepancy would result in an artificial numeric instability in the simulated stratigraphy. Therefore, in order to approximate the realistic simultaneous nature of these events this new location function is introduced. It determines the sub-environment of the cells a single time at the start of the delta, and shoreface routine.

The model can distinguish three different sub-environments. The locations function is used to determine three different boundary locations on the profile to separate these sub-environments, figure 4.6. Firstly, the location locates the "mainland" cell where mainland ('dry') transitions to sea ('wet') in figure 4.6a, or when it exists, a lagoon (also 'wet') as in figure 4.6b. Secondly, the function determines the "foreshore" cell that points the first foreshore grid cell next to mainland as in figure 4.6a, or when it exits a back-barrier like in figure 4.6b. Thirdly, it sets the position of the last wet cell in a lagoon, called the "back-barrier wet" cell as shown in figure 4.6b.
The names of these locations differ from the ones used in the model's code because these names explain their purpose, and location more intuitively. The difference in names is shown in table 4.1

Difference in cell name usage		
Thesis name	Model name	Alternative model name
Mainland	coastLoc	coast
foreshore	firstwetLoc	firstwet
Back-barrier wet	BBwetLoc	bbwet
End of table 4.1		

Table 4.1: Difference between the cell names used in the thesis, and the model.

The 2Dstratsim model can evaluate the simulated profiles either from the left (the dry cells) or from the right (the wet cells), figure 4.6.
The mainland cell is determined by evaluating the simulated profile's grid cells from left to right, figure 4.6. The location function stops the evaluation when the elevation of the next cell drops below sea level. Therefore, the last cell the function evaluated is the last dry cell of the simulated profile.
This is different from the foreshore cell that gets determined by evaluating the simulated

profile from right (wet) to left (dry). During this analysis of the simulated profile the location function terminates at the point where the last evaluated grid cell has an elevation below sea level. The reason for evaluating the profile from right to left for this location is best explained by figure 4.6b in which we note that sea level is already above the elevation of the simulated profile in the lagoon part. Therefore, an evaluation from left to right on this profile would considerably complicate the determination of the location of the foreshore cell at right side of the back-barrier. During analysis of simulated results it was noted that the foreshore position could shift rapidly. This resulted in a coastline instability caused by numeric errors. To prevent the rapid shifting of this boundary location the position is determined by averaging the wet cell with the dry grid cell adjacent to it.
The back-barrier cell is found by evaluating the simulated profile from left to right again. However, in order to terminate the location function at the proper cell, it requires a double criterion. Namely, the current cell evaluated is wet while the next adjacent cell is dry. This criterion together with the proposed evaluation direction this will force the location function to terminate at the wet cell before the back barrier itself, see figure 4.6b.

Whether a back-barrier can form depends on the rate of sea level rise, and the amount of sediment influx. In the model a low rate of sea level rise combined with a significant amount of sediment influx will generally cause a back-barrier to form.
In such a scenario, generally a transgressive period, as illustrated in figure 4.6, a shoreface system can potentially form barrier bars. Thereby, a more pronounced distinction between the shoreface, and delta system is made as to where a certain boundary location are found. In the delta environment we want to eliminate the possibility of a back-barrier. Because it is uncommon for a fluvial dominated transgressive delta to develop a back-barrier, due to the force of the currents caused by the fluvial influx. Therefore, in our models the mainland location is always next to the foreshore cell.
In the shoreface environment during a transgressive period the mainland borders a lagoon, which is sheltered by a back-barrier from wave activity, as in figure 4.6b.

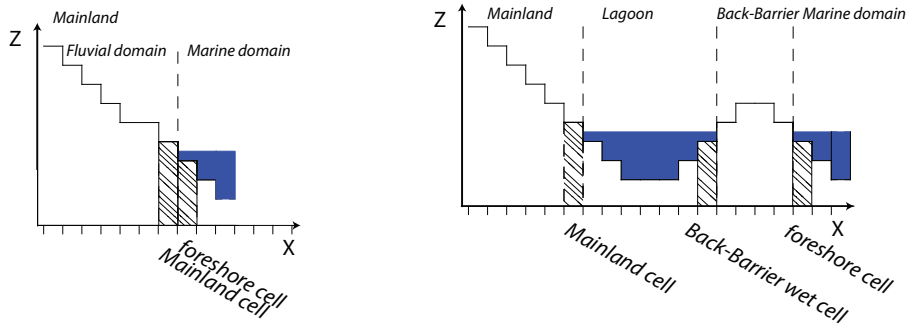

(a) Discretised simulated delta profile

(b) Discretised simulated shoreface profile

Figure 4.6: Discretised schematic cross-section highlighting the boundary locations in a delta, and shoreface environment. Whereby the shoreface is captured in a transgressive period to illustrate the location of the boundary locations with back-barrier formation.

4.3.2 Delta Width

The 2Dstratsim model takes the third dimension into account by calculating pseudo-volumes, chapter 2. The extent of the model in the third dimension is not straightforward

to calculate in the delta environment, figure 4.7. The river that introduces sediment to the delta, chapter 4, acts as a point source for sediment distribution in the marine domain. Therefore, radial dispersion of sediment will occur as soon as the fluvial domain transitions to the marine domain. The function 'model width' calculates the radial extension of a given grid-cell within the delta environment. This width calculation is not required for the shoreface environment. Because there the sediment is supplied via along shore currents, and its width is preset by the user via the configuration file. In the model the shoreface's dimensions therefore inhabits a rectangular shape if one regarded it from directly above.

The width calculation includes the distinction between the fluvial domain, and marine domain, determined by using the boundary locations as in subsection 4.3.1. To illustrate the concept of the width calculation figure 4.7 is included for a top view, and 3D representation is shown in figure 4.8. Note that the width is described as a semi-circle in the fluvial domain, whereas it has it is described by an ellipsoid in the marine domain. There are two reasons to use a semi-circle in the fluvial domain, and the half-ellipsoid in the marine part, (de Jager et al., in prep.). Firstly, further below sea level there is generally reduced progradation. Therefore, the major axis of the ellipsoid lengthens as the elevation drops. Secondly, an increased width of deposition is generally observed along the shelf slope, (de Jager et al., in prep.). Therefore, the length of ellipse's major axis along the y-axis increases by a set angle d along the x-axis, see figure 4.7.

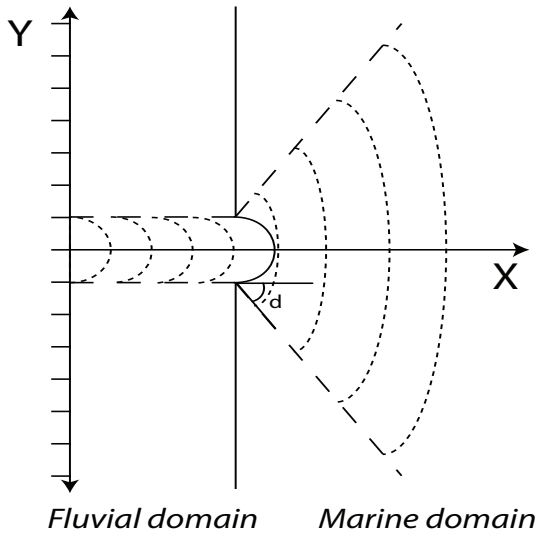

Figure 4.7: Top view of a prograding delta, illustrating the extent of the delta profile in the third dimension. Radial dispersion of sediment is observed in the fluvial domain, and is approximated with an ellipse in the marine domain. Angle d marks the start of the dispersion at the boundary between fluvial and marine domain. This angle sets the length of the ellipse's major axis.

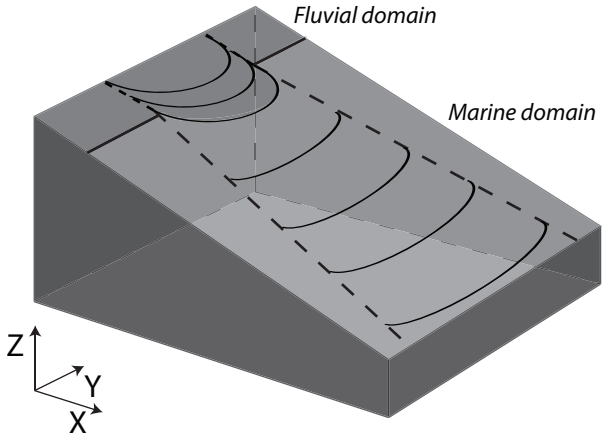

Figure 4.8: Schematic 3D view of a delta as seen in figure 4.7.

The malfunctioning of this function was observed by analysing the delta width values, which were in the order of 10^6 to 10^7 m. These values are observed at the point where the fluvial domain makes a transition to the marine domain. The values observed at the marine end of the fluvial domain are generally in the order of 10^3-10^4 m. Because a step increase in delta width values is not expected at the transition from fluvial to marine domain, it is concluded that the width calculation function malfunctions. Therefore, it is revised in this thesis by using a new approach. The new method still makes use of the semi-circle and half-ellipsoid. However, to calculate the width of the ellipsoid an analytical approximation is used instead of a derivation of the width from volumetric calculations proposed by de Jager et al. (in prep.).

To visualise the parameters that are used in the new approach to calculate the width of the delta the parameters are illustrated on a schematic of a simulated profile in figure 4.9. The schematic cross-section presented in figure 4.9 follows the x-axis of figure 4.7. This implies that the coastline in figure 4.9 is located a bit further land inward when we would move our cross-section in the y direction.

The parameters used in the calculation of the delta width are different between the fluvial, and marine domain, and so are the figures. Figure 4.9a shows the parameters in the fluvial domain, and figure 4.9b in the marine domain. In the figures of 4.9 any location of x can be used inside its corresponding domain. This cell x has an elevation $Z(x)$ on elevation line $t > 0$. Parameter $rmin$ is the first cell where the elevation $t = 0$ is below $Z(x)$ at our cell x.
For the fluvial width calculation the lateral distance between $rmin$, and x is called P, and represents the radius of the fluvial semi-circle. These parameter change as our cell of interest x changes. In the fluvial domain equation 4.4,

$$Wd(x) = \pi P \tag{4.4}$$

is used to calculate the width $Wd(x)$ of the delta. Which follows directly from the formula of the circumference of half a circle.

The width in the marine domain follows the perimeter of an half-ellipsoid, which requires more parameters to define. For the graphic representation of these parameters, see

figure 4.9b. Parameter P follows from the fluvial calculations. It represents the lateral distance between the last dry cell of elevation $t > 0$, and the first wet cell on elevation $t = 0$. The definition of $rmin$ remains the same. We introduce S as the first wet cell on elevation $t = 0$. $Xe(x)$ is the distance between x and S, and $R(x)$ the distance between $rmin$, and S.

To calculate the width of the marine part a minor, and major axis of the ellipse are defined. The minor axis follows the x-axis, and the major axis the y-axis, as in figure 4.7. Firstly, the minor axis $a(x)$

$$a(x) = Xe(x) - R(x), \tag{4.5}$$

of the ellipse is calculated.
The major axis $b(x)$ is defined as,

$$b(x) = P + R(x)\tan(d). \tag{4.6}$$

with d as the user-implemented angle as illustrated in figure 4.7.

In equation 4.7, $h(x)$ is a combination of $a(x)$ and $b(x)$, and is defined as

$$h(x) = \frac{(a(x) - b(x))^2}{(a(x) + b(x))^2}, \tag{4.7}$$

which is used in the approximating the width $Wd(x)$ of the ellipsoid in the marine domain. The width is approximated as

$$Wd(x) = \frac{\pi}{2}(a(x) + b(x))(1 + \frac{3h(x)}{10 + \sqrt{4 - 3h(x)}}), \tag{4.8}$$

because the perimeter of an ellipse, unlike its area, is not that straight forward to calculate. Equation 4.8 is modified after Ramanujan (1914) to calculate half the width of an ellipsoid. An approximation is required here because as of this date it is only solved by the use of infinite series.

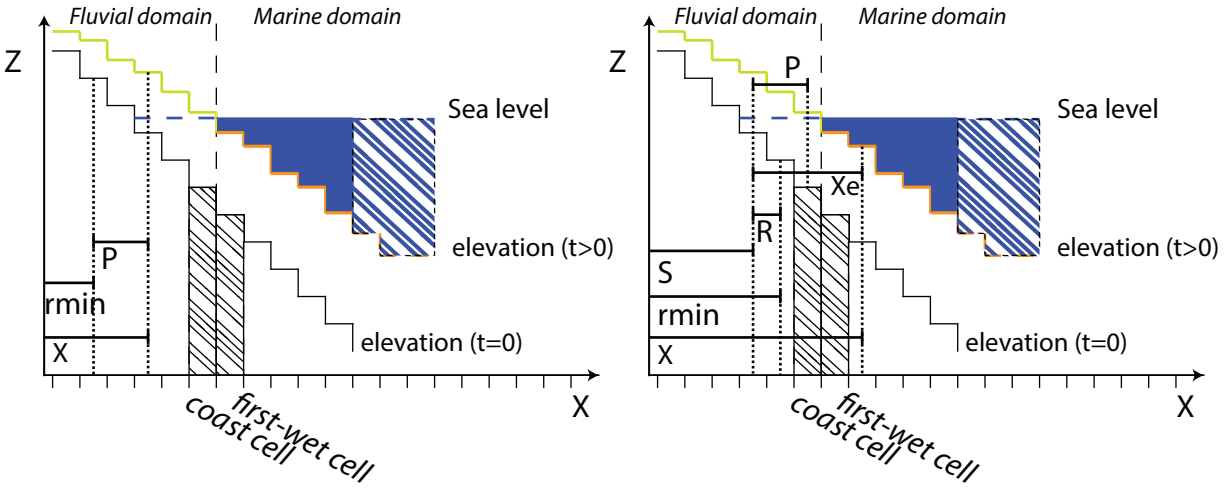

(a) parameters in the fluvial domain

(b) parameters in the marine domain

Figure 4.9: Discretised schematic side views with parameters to calculate the delta width

Finally, an analogue for this function is a scenario where a triangular carpet is used to clothe a staircase. The edges of this carpet represent the major axis of the ellipsoid at a given step/grid-cell. The tip of the triangle, upstairs, makes an angle of $2d$, figure 4.7.

4.3.3 Sedimentation

The sedimentation function is used to calculate the amount of sediment entering both the profile of the delta, and the shoreface. Using travel distance calculations for the grain-size fractions it also determines the volume of sediment that will deposit on a given grid-cell. The average grain-size of this volume is determined by averaging the grain-size fractions, (e.g.) a volume of 10% 400μm, 40% 150μm, and 50% 20μm grain-size results in an average of 110μm.

The problems encountered in the calculation of the sediment volumes are as follows. Firstly, the sediment influx signal is implemented by the user via the configuration file in $[m^3/s]$, per grain fraction. However, to acquire a realistic, and insightful model the sediment influx can be directly related to the discharge of the river as a concentration $[mg/L]$. The relation of sediment load to the discharge of a river is charted by (Milliman and Meade, 1983) for rivers all over the world, see figure 4.10.
Secondly, the travel distance calculations of the grain-size fractions in the model is erratic, as the user has to significantly compensate the distance by using manually implemented factors.
Thirdly, sedimentation in the marine domain is allowed to stack indefinitely above sea level.

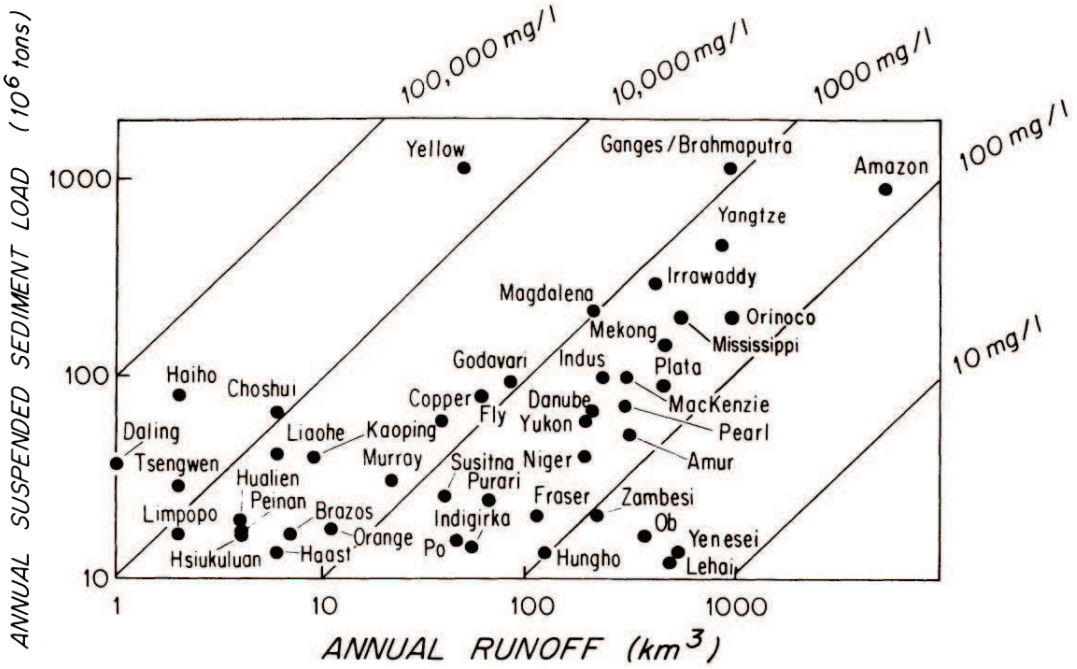

Figure 4.10: Variation of annual suspended sediment load with runoff, modified after (Milliman and Meade, 1983).

Sediment enters the model in the delta profile via a river, the discharge signal of this river is shaped by the user via a configuration file. Previously, sediment could enter the system while the river was dry. Hence, the sediment flux was completely disconnected from the amount of discharge. To establish a relation between sediment influx, and discharge it is opted to implement sediment as a concentration instead.
This implementation needs an assumption as the rest of the model remains to work with $[m^3/s]$ units. Thus, in order to translate concentration to flux, the average density of the transported sediment grains is required. The sediment entering the system possesses a high quartz content, based on the thin section analysis in subsection 3.1.2, and (Forzoni et al., in prep.). Therefore, the average sediment density is estimated to inhabit the density of quartz, 2650 kg/m^3.
The new method prevents sediment from entering the system when the river runs dry, and additionally it prevents the volume of sediment to run out of proportion compared to the volume of discharge. Additionally, the total amount of suspended sediment now has an adjustable limit that can be based on figure 4.10. When the total amount of sediment in suspension exceeds this limit a warning is displayed. In the scenarios described in chapter 5 we opted for a maximum concentration of 1000 mg/L.

The distance a grain can travel dependents on its size, further referred to as travel distance. The 2Dstratsim model adopted the equations relating grain-size to travel distance from Storms (2003). However, during the implementation process in the 2Dstratsim model these formulas were wrongly applied. The solid line in figure 4.11 draws the correlation between grain-size, and travel distance as it was originally proposed, whereas the dotted line represents the way it was implemented. This error directly resulted in an over estimation of the travel distance for grains larger smaller than 125 μm, D_{ref}. The user can scale the travel distance manually via correction factors in the configuration file.

However, this was done to such an extent that the proposed correlation as in figure 4.11 was largely disturbed.

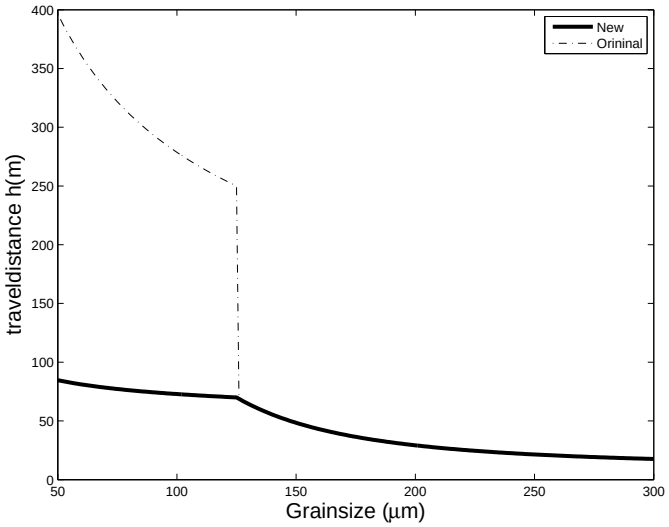

Figure 4.11: Travel distance to grain-size. The solid line is the proposed correlation by Storms (2003), and the dotted line show the correlation implemented in 2Dstratsim. The travel distance of grain-sizes is calculated from the foreshore location.

Deposition of sediment above average sea level can occur by wave action, and tidal action. However, in the model the observation was made that sediment could deposit above sea level indefinitely. This phenomenon takes place on the foreshore grid-cell, which always borders a dry cell. Therefore, we restrict sediment deposition in the marine domain to 1 m above sea level in the sedimentation function, and the extra sediment volume that was supposed to deposit on the cell is transported to the next sea-inward-cell until the sediment volume on the grid cell remains below 1 m above sea level.

4.4 Visualisation

To enhance the visualisation of the model's output data of the forward routine. Additional tools, and improvements are made in the existing visualisation script. This existing script serves to visualise simulated data from the forward routine. The script consists of multiple switches. These switches serve to enable the plotting of the average grain-size per layer, time lines, the evolution of the coast line, average grain-size to depth logs at given locations. In a separate figure the 'yearlydata' is plotted. This consists of data on the evolution of sea level, river discharge, deposition, erosion, and wave action over time. The figures in this section serve as an example to illustrate the newly implemented tools.

Previously when the user changed a value in the configuration file the value had to be changed separately in the visualisation script. Therefore, an additional script is written that can extract the required value from the configuration file automatically, and implement it in the visualisation script.
Additionally, improvements are made to the visualisation script, which include red lines to indicate the locations the included logs originate from, and time lines that represent

the paleo-morphology of the environment. Furthermore the horizontal scale of the graph is adjusted from grid position to [km], figure 4.12.

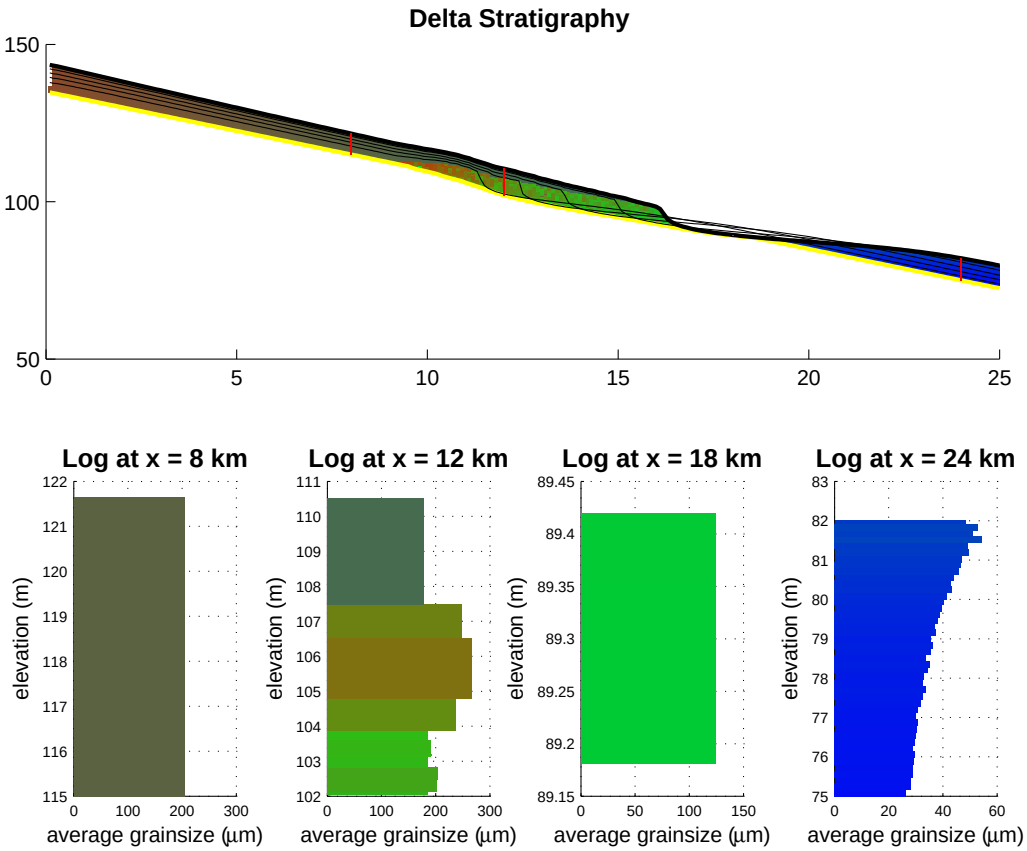

Figure 4.12: Delta stratigraphy example. Red lines indicate the position of the logs, black lines represent the paleo-morphology. The lateral distance is given in [km], and vertical scale is in [m]. Note that between 15-20 km most of the sediment has eroded due to wave activity while the morphology lines remain.

Running the visualisation script can be time consuming, up to 5 hours, when one requires to visualise the average grain-size per layer. Therefore, the visualisation is often plotted without the average grain-size per layer. However, to evaluate the stratigraphy properly one requires the average grain-size per depth date from the logs instead. But the visualisation script can only plot up to four logs at the time, see figure 4.12. To circumvent running the visualisation script multiple times a new script is written to generate additional logs.

The evolution of the coastline through time could already be added on the cross-section profile of both environments. However, this line overlies the stratigraphy, and can significantly reduce the visibility of other details. Therefore, an additional switch is implemented to the visualisation script to plot the coast line evolution in a different figure, see figure 4.13. This figure shows the location of the mainland, and foreshore locations, subsection 4.3.1, per simulated environment as they evolve through time.

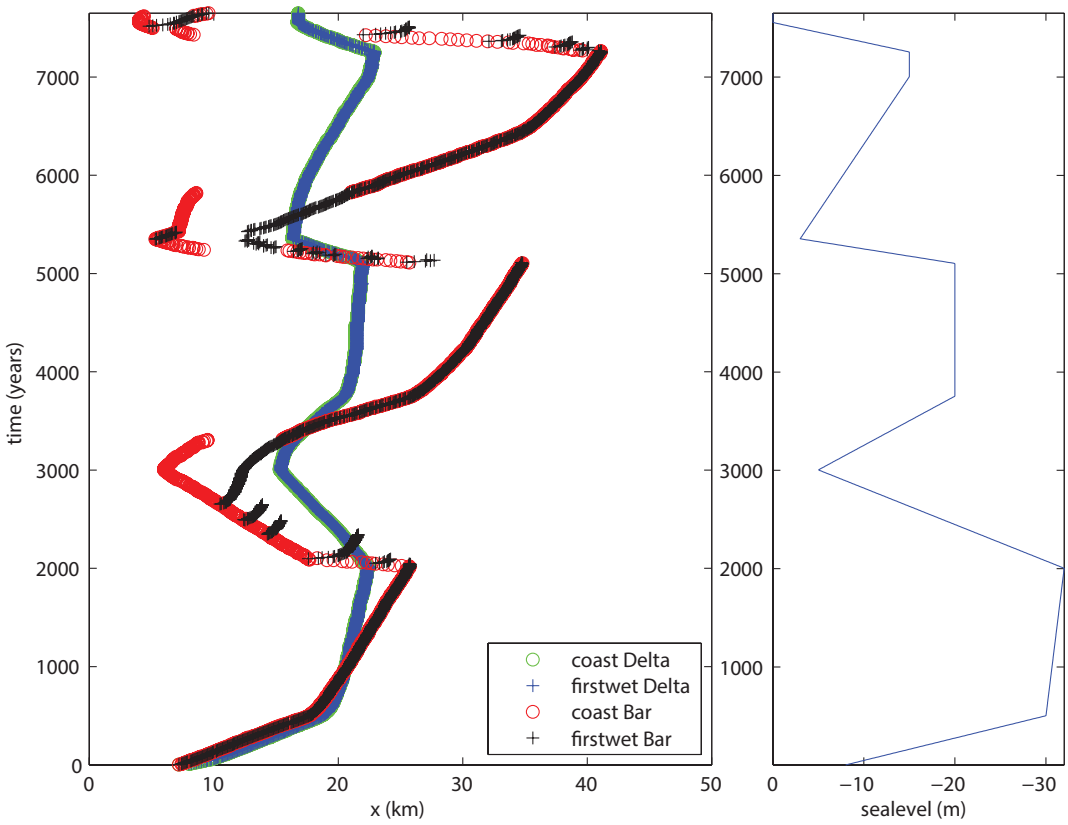

Figure 4.13: On the left an example figure of the evolution of mainland, and foreshore locations, in the delta, and shoreface(/bar) environment. The right side presents the sea level signal through time. Where the locations overlap represents a situation as in figure 4.6a, whereas when the locations diverge the simulated cross-section represents a situation with back-barrier formation as in figure 4.6b.

The yearlydata script is also improved so that it only visualises the data of requested profiles. Previously it would also plot data of profiles that were not currently active.

Visualisation scripts for the data concerning the inversion was present for one scenario, without any explanation. Therefore, new scripts are written that can analyse the data from different scenarios. This includes a figure to analise the development of the likelihood in the burn-in period, together with the fluctuations of the tempering factor, see figure 4.14.

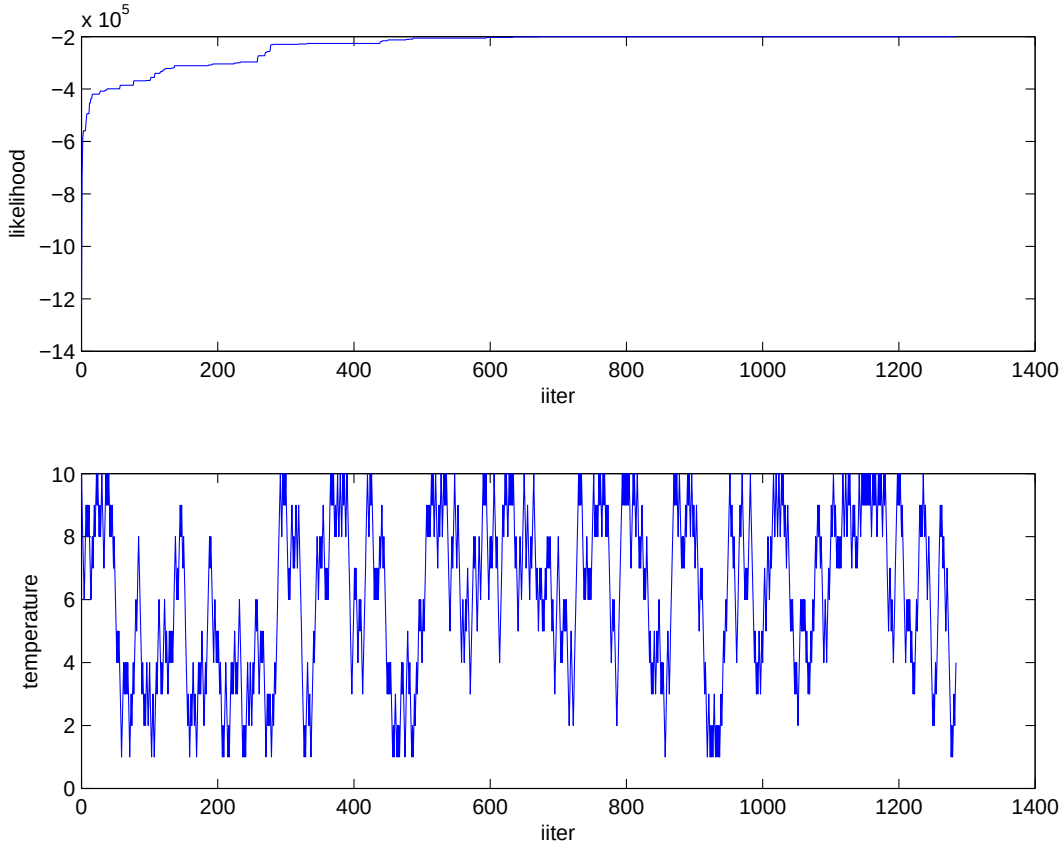

Figure 4.14: Example of the likelihood evolution, and variation of the tempering factor at given iterations in the burn-in period.

The evaluation of the likelihood in the sampling period is plotted in a separate figure. However, this plot can be combined with the likelihood data from the previous plot with a switch at the start of the script, see figure 4.15.

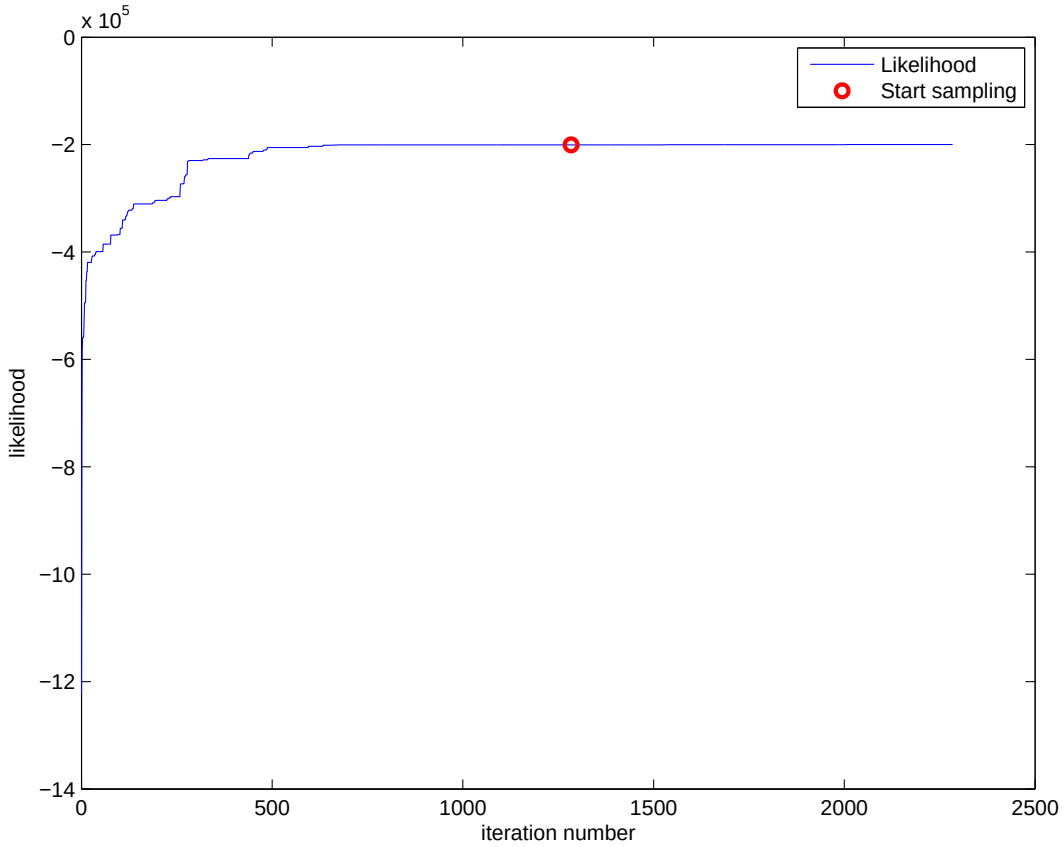

Figure 4.15: Example of the likelihood evolution in the burn-in, and sampling period against iteration number. The red circle indicates the transition from burn-in to sampling period.

Additionally, the top view of a 3D figure is added to plot a combination of a density data, its respective confidence zone, and the initial input signal, see figure 4.16. The histogram values are based on the amount of times data points are used by the model to manipulate the input signal.
The confidence zone is based on these data points. It represent the 95% confidence zone, and also includes the mean value. The extent of the confidence zone is given by the min, and max lines. The confidence zone, and the histogram can be plotted in combination with the 'truth'. The truth line represents the signal used to create the first forward scenario of the inversion, section 4.2.

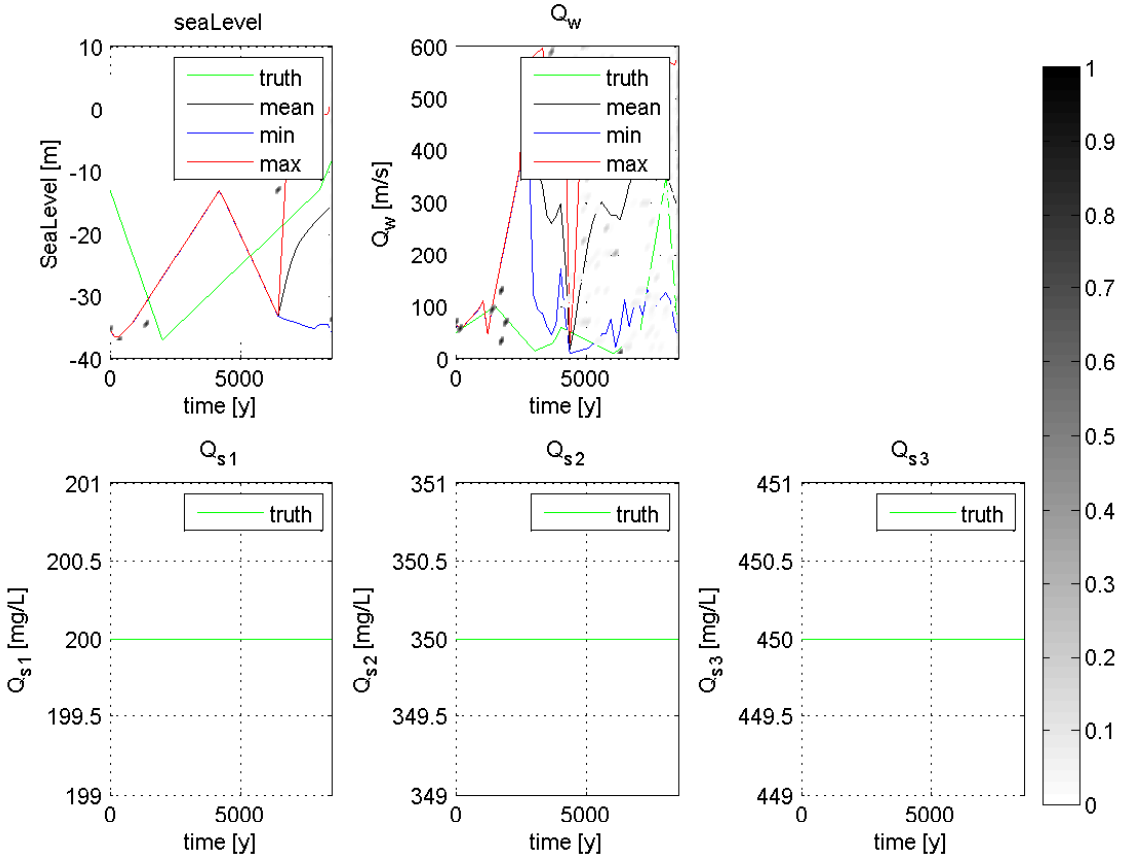

Figure 4.16: Example of the results of the inversion routine, the dots, seen in the upper two plots, represent the points which the model used to manipulate the input signal. Their histogram value is made dimensionless with respect to the most occurring parameter in their respective plot. They are coloured according to the colourbar on the right. The min, and max line are the borders of the confidence zone.

5. Application

To disentangle the forcing signals of the measured shoreface profile of figure 3.5, first the forward routine is used in an attempt to match observed coarsening upward packages in the bedsets visually by using 'extreme' scenarios. These scenarios are limited in the fact that they should still resemble the observed aggradational, and progradational trends in the measured shoreface profile of figure 3.5. The maximum, and minimum limits of the parameters used in the forward scenarios are then applied to constrain the search area of the statistic inversion algorithm. Subsequently, the inversion method is applied in combination with the limits obtained from the forward scenarios. The inversion is utilised to acquire a most likely scenario based on the computed correlation between the measure logs, and the simulated logs.

5.1 Forward scenarios

In the application of the forward routine two different geologic settings are used in simulating the shoreface. In the first setting back-barriers formation is enabled. While in the second setting the back-barrier formation is disabled. The two different settings are used because no evidence of back-barrier formation was found in the field. However, absence of evidence is no evidence of absence, and therefore the geologic setting with enabled back-barrier formation is included.
Both of the settings are used in recreating the shoreface by using the forward routing in two extreme scenarios. The different scenarios attempt to define the extreme limits of the geologic setting between which other scenarios are possible.

In order to build the extreme scenarios a step by step approach is followed to increase the efficiency, and speed of the correlation procedure.
Firstly, the bathymetry of the measured profile is slightly modified to streamline the visual comparison of the measured profile to the simulated profile in section 3.1.
Secondly, grain-size classes are assigned to the different facies, see subsection 3.1.1.
Thirdly, figure 3.5 is subdivided into intervals, bedsets observed, and defined by Forzoni et al. (in prep.).

In a given geologic setting, the first scenario 'sea level scenario' uses only a changing sea level, and a stationary river discharge to replicate the measured profile. Hence, the sediment influx to the system is also stationary as it is directly related to the discharge of the river. Therefore, an interval comprises a period of sea level fall, followed by a rise. The second scenario of a given geologic setting is the 'mixed scenario', which will replicate the measured profile by using a fluctuating discharge. Sea level change in this scenario depends on the geologic setting. In the setting where back-barriers are allowed the sea

level signal consists of a single fall, and rise. While in the setting without back-barrier formation the sea level signal consists of a single rise in the sea level. The single fall, and rise of the sea level is based on the hypothesis on the Panther Tongue formation proposed by Hwang and Heller (2002). However, their interpretation on when specific bedsets are formed over this signal is disregarded.
For the names of the different forward scenarios in this thesis, see table 5.1.

Forward scenarios			
Setting	Scenario	Scenario name	Configuration file
Back-Barrier	Sea level scenario	scenario 1	table 5.2
	Mixed scenario	scenario 2	table 5.3
No Back-Barrier	Sea level scenario	scenario 3	table 5.4
	Mixed scenario	scenario 4	table 5.5
End of table 5.1			

Table 5.1: Different scenarios created with the forward routine, their name in this thesis, and the respective table number of their configuration files.

5.1.1 Input

In order to replicate the measured profile from Forzoni et al. (in prep.), the 2Dstratsim model requires input. This input is implemented in the model by using a configuration file. This file sets the static parameters, and input signals that are processed to a simulated profile by the parameterised equations, chapter 4.
Amongst others the configuration file appoints the parameters for the horizontal length of the profiles for the simulated environments, which should be the same. The length we use is based on the measured profile introduced in figure 3.5.
What grain-size fractions are used is based on the maximum, and minimum grain-size present in the logs of figure 3.6. To generate an average grain-size the 2Dstratsim model works with a combination of three grain-size fractions, (de Jager et al., in prep.). The proportion of these fractions present in a given layer is averaged to create the simulated stratigraphy. The factor that determines the rate of grain-size grinding, and what fractions are present in the bedrock are left as they were in the previous version, Storms (priv. comm.). Just as the factor for the width of the delta plume, the parameters for wave action, and for erosion.
A modern analogue of the Panther Tongue's coupled environment system is the Danube Delta, according to Forzoni et al. (in prep.). The Danube system also consists of a delta with an adjacent shoreface. The Danube river transports ∼900mg/L sediment according to Milliman and Meade (1983), based on figure 4.10. Therefore, the maximum allowed concentration of the Panther Tongue's river is set to 1000 mg/L in the model. Additionally the signals of sea level, and river discharge are implemented via the configuration file. In a forward run these signals are changed manually to optimise the correspondence between the simulated, and measure shoreface profile.

The configuration file of scenario 1 is presented in table 5.2. Then the configuration file for scenario 2, 3, and 4 are presented in tables 5.3, 5.4, and 5.5 respectively. The tables of the scenarios 1 through 4 will only present the content that changed relatively to scenario 1. Note that not all of the data from the actual configuration file is required

by the model to run a forward simulation. The irrelevant data is therefore removed from the tables 5.2 through 5.5.

Configuration file for scenario 1		
Parameter	Value	Comment
runMode	= "Forward";	# model runs the "Forward" or "Inverse" routine
FPSwitch	= false;	# floodplain, on = true
BarSwitch	= true;	# bar, on = true
WaveSwitch	= true;	# waves, on = true
addNoise	= false;	# add noise to well measurements for inversion, on = true
newElev	= false;	# create new floodplain equilibrium profile, on = true
elevDelta	= true;	# load initial delta elevation from file
elevDeltaFile	= "deltaElevFile.txt";	# name of file which contains delta elevation
incWidthFile	= "incWidth.txt";	# name of file which contains incision data
elevBar	= true;	# load initial bar elevation from file
elevBarFile	= "barElevFile.txt";	# name of file which contains bar elevation
simulationTime	= 7650.0;	# time being simulated [years]
nTimeSteps	= 1600;	# number of timesteps
nDeltaCells	= 500;	# number of delta cells
deltaCellSize	= 100.0;	# size of delta cells [m]
rivermouth	= 100.0;	# width of rivermouth, only used for marine dispersion [m]
nBarCells	= 500;	# number of bar cells
barCellSize	= 100.0;	# size of bar cells [m]
barWidth	= 30000.0;	# width of the bar [m]
dispersal	= 1.0;	# angle delta d [rad]
cg	= 0.11;	# for h calculations, used for locally different behaviour
cw	= 0.50;	# for h calculations, for different waveheight
dref	= 125.0;	# grain-size in [μm] for which larger grain-sizes are bedload, and smaller are suspended load
rivertolerance	= 1000.0;	# total allowed sediment concentration the river can transport in [mg/L]
nGrainsizeFractions	= 3;	# number of grain-size fraction

Continuation of configuration file for scenario 1		
Parameter	Value	Comment
grainSize	= [400, 150, 20];	# grain-sizes, from coarse to fine in [μm]
hMarFactDelta	= [1.0, 2.0, 3.0];	# h correction for marine domain
hMarFactBar	= [1.0, 1.0, 2.0];	# h correction for marine domain
hFluvFact	= [19.0, 19.0, 19.0];	# h correction for fluvial domain
hBBFact	= [0.5, 0.5, 0.5];	# h correction back-barrier
waveStorm	= 5.0;	# storm waveheight [m]
cc	= 7.0;	# FIX at 7! ratio of wavedepth over waveheight
ce	= 1.0;	# TUNING PARAM FOR WAVE POWER ratio of mean shoreface to local shoreface
kf	= 0.95e-5;	# control fluvial erosion in fluvial domain
km	= 8.0e-8;	# control fluvial erosion in marine domain [smaller is less erosion](i.e. caused by fluvial water movement)
barTransport	= [0.4, 0.2, 0.4];	# Amount of sediment per grain fraction which gets transported from the delta to the bar.
fallout	= [0.0, 0.0, 0.03];	# marine sediment fall out [dm/timestep]
baseGrInSubsurface	= [0.5, 0.4, 0.1];	# fraction of sediments in subsurface (bedrock)
grind	= [0.005 , 0.005 , 0.0];	# fraction of each grain-size which is grinded to a smaller grain-size per timestep
bioturbParameters	= [0.15 , 0.15];	# bioturbation occurs when a layer is thinner than minmaxThick(0) and the underlying layer is thinner that minmaxThick(1)
seaLevel.values	= [0, -8, 500, -30, 2000, -32, 3000, -5, 3750, -20, 5100, -20, 5350, -3, 7000, -15, 7250, -15, 7550, 0 , 7650, 0];	# [time , lvl, time, lvl,...] [y, m]
Qw.values	= [0, 600, 7650, 600];	# river discharge signal, [time, flux, time, flux,...] [y, m^3/s]
Qs1.values	= [0, 200, 7650, 200];	# concentration largest grain-size [y, mg/L] sum of all Qs should not exceed the river tolerance

Continuation of configuration file for scenario 1		
Parameter	Value	Comment
Qs2.values	= [0, 350, 7650, 350];	# concentration middle grain-size [y, mg/L] sum of all Qs should not exceed the river tolerance
Qs3.values	= [0, 450, 7650, 450];	# concentration smallest grain-size [y, mg/L] sum of all Qs should not exceed the river tolerance
End of Table 5.2		

Table 5.2: Configuration file of scenario 1.

The adjustments relative to scenario 1 required to create scenario 2 are presented in table 5.3. To create a match with the new input signals a significant increase in simulation time is required as well as the reduction of 1 m in average storm wave height.

Configuration file for scenario 2		
Parameter	Value	Comment
simulationTime	= 12500.0;	# time being simulated [years]
nTimeSteps	= 2500;	# number of timesteps
hMarFactBar	= [2.0, 2.0, 1.0];	# h correction for marine domain
hBBFact	= [2.0, 2.0, 1.0];	# h correction back-barrier
waveStorm	= 4.0;	# storm waveheight [m]
fallout	= [0.0, 0.0, 0.025];	# marine sediment fall out [dm/timestep]
seaLevel.values	= [0, -13, 2000, -37, 8000, -13, 9000, -3, 10500, -1, 11500, 4, 13000, 5];	# [time , lvl, time, lvl,...] [y, m]
Qw.values	= [0, 50, 1500, 100, 3000, 15, 3700, 30, 4000, 60, 6000, 10, 7000, 50, 8000, 350, 8500, 10, 10000, 500, 10500, 10, 12000, 20, 12500, 85];	# river discharge signal, [time, flux, time, flux,...] [y, m^3/s]
Qs1.values	= [0, 200, 12500, 200];	# concentration largest grain-size [y, mg/L] sum of all Qs should not exceed the river tolerance
Qs2.values	= [0, 350, 12500, 350];	# concentration middle grain-size [y, mg/L] sum of all Qs should not exceed the river tolerance

Continuation of configuration file for scenario 2		
Parameter	Value	Comment
Qs3.values	= [0, 450, 12500, 450];	# concentration smallest grain-size [y, mg/L] sum of all Qs should not exceed the river tolerance
End of Table 5.3		

Table 5.3: Configuration file of scenario 2.

Next are the scenarios in the geologic settings where no back-barrier formation is allowed in the shoreface environment. The configuration file for scenario 3 is found in table 5.4. Note that hBBFact, used to scale grain-size travel distances in the back-barrier, is redundant in this geologic setting.

Configuration file for scenario 3		
Parameter	Value	Comment
simulationTime	= 7100.0;	# time being simulated [years]
nTimeSteps	= 1420;	# number of timesteps
seaLevel.values	= [0, -8, 500, -30, 2000, -32, 2150, -5, 3150, -20, 4250, -20, 4500, -3, 6150, -15, 6400, -15, 6700, 5 , 7100, 5];	# [time , lvl, time, lvl,...] [y, m]
Qw.values	= [0, 600, 7100, 600];	# river discharge signal, [time, flux, time, flux,...] [y, m^3/s]
Qs1.values	= [0, 200, 7100, 200];	# concentration largest grain-size [y, mg/L] sum of all Qs should not exceed the river tolerance
Qs2.values	= [0, 350, 7100, 350];	# concentration middle grain-size [y, mg/L] sum of all Qs should not exceed the river tolerance
Qs3.values	= [0, 450, 7100, 450];	# concentration smallest grain-size [y, mg/L] sum of all Qs should not exceed the river tolerance
End of Table 5.4		

Table 5.4: Configuration file of scenario 3.

The table 5.5 gives the configuration file to create scenario 4. This scenario can be directly related to scenario 2, as only the geologic setting changed. However, this change in geologic setting also allows for a significant reduction in simulation time, 3000 years less. Because, scenario 4 uses a single rise in sea level an increased travel distance factor

is required to allow large grains to travel further into the basin.

Configuration file for scenario 4		
Parameter	Value	Comment
simulationTime	= 9400.0;	# time being simulated [years]
nTimeSteps	= 1880;	# number of timesteps
hMarFactBar	= [3.0, 4.0, 4.0];	# h correction for marine domain
waveStorm	= 4.0;	# storm waveheight [m]
seaLevel.values	= [0, -12, 9200, 0, 9500, 4];	# [time , lvl, time, lvl,...] [y, m]
Qw.values	= [0, 50, 500, 300, 2000, 500, 2150, 20, 2650, 20, 3000, 200, 5000, 600, 6000, 600, 6150, 20, 7000, 20, 7500, 300, 8000, 500, 8500, 500, 8600, 30, 9400, 30];	# river discharge signal, [time, flux, time, flux,...] [y, m^3/s]
Qs1.values	= [0, 200, 9400, 200];	# concentration largest grain-size [y, mg/L] sum of all Qs should not exceed the river tolerance
Qs2.values	= [0, 350, 9400, 350];	# concentration middle grain-size [y, mg/L] sum of all Qs should not exceed the river tolerance
Qs3.values	= [0, 450, 9400, 450];	# concentration smallest grain-size [y, mg/L] sum of all Qs should not exceed the river tolerance
End of Table 5.5		

Table 5.5: Configuration file of scenario 4.

5.1.2 Results

To visualise the results, the new scripts are used described in section 4.4. The first three logs in the coming simulated shoreface profiles, shown in figures 5.1 through 5.4, represent the measured logs of Link Canyon, Muddy Creek, and Ferron Creek, as seen in figure 3.6. In these figures the measured logs overlay their respective simulated counterpart as a blue line.

The result concerning the simulated shoreface of scenario 1 is found in figure 5.1.

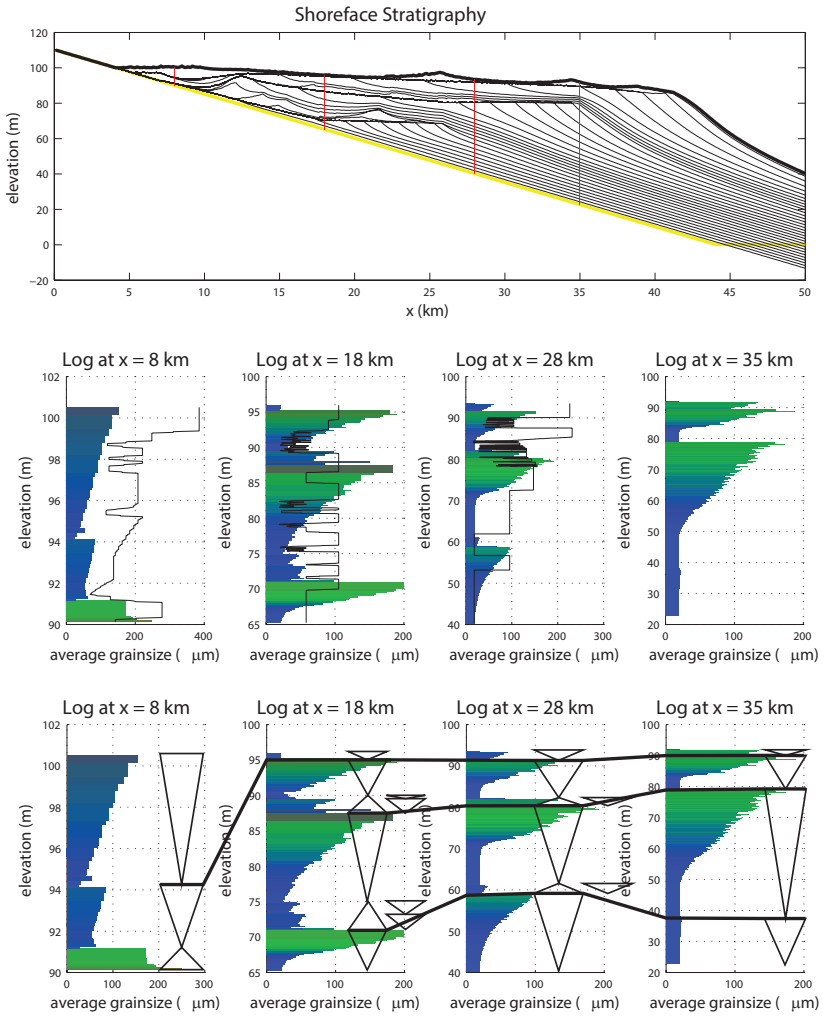

Figure 5.1: Shoreface stratigraphy in scenario 1. Black lines are plotted every 50 time steps, the time step size 'Δt' is 4.78 years. Therefore the black lines indicate the paleomorphology every 239 years. Logs of the shoreface stratigraphy are extracted, and presented below the stratigraphy. The lines over the logs show the average grain-size signal of the measured logs of Link Canyon, Muddy Creek, and Ferron Creek, at their respective position as seen in figure 3.6. In the logs at the bottom of the figure an average grain-size trend interpretation is given next to the simulated log. The thick black lines connecting the top of the coarsening upward packages, indicate the maximum regressive surfaces in the shoreface's stratigraphy.

The result concerning the simulated shoreface of scenario 2 is found in figure 5.2.

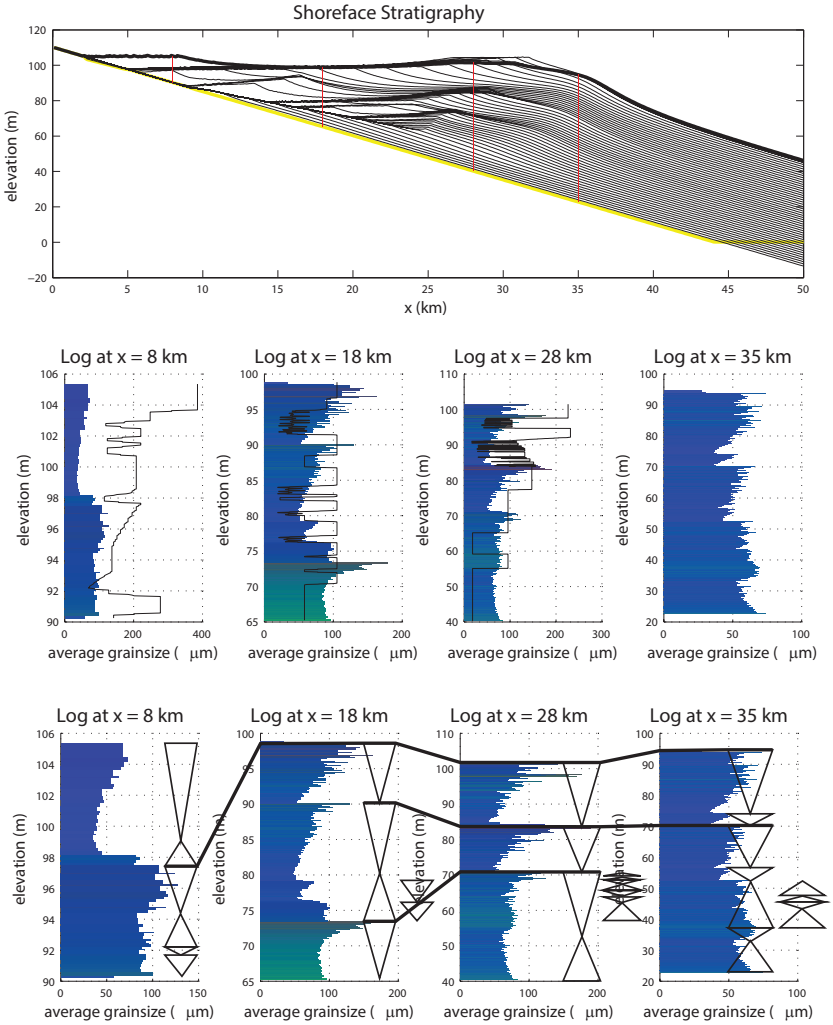

Figure 5.2: Shoreface stratigraphy in scenario 2. Black lines are plotted every 50 time steps, the Δt is 5 years. Therefore the black lines indicate the paleo-morphology every 250 years. Logs of the shoreface stratigraphy are extracted, and presented below the stratigraphy. The lines over the logs show the average grain-size signal of the measured logs of Link Canyon, Muddy Creek, and Ferron Creek, at their respective position as seen in figure 3.6. In the logs at the bottom of the figure an average grain-size trend interpretation is given next to the simulated log. The thick black lines connecting the top of the coarsening upward packages, indicate the maximum regressive surfaces in the shoreface's stratigraphy.

The result concerning the simulated shoreface of scenario 3 is found in figure 5.3.

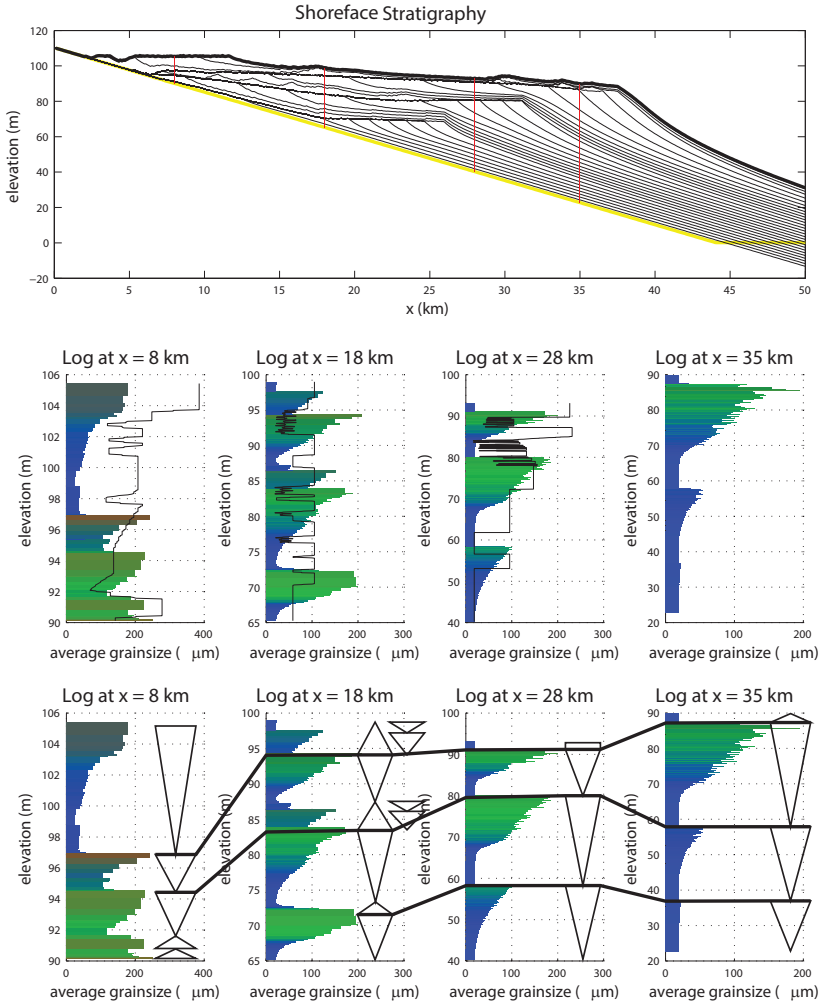

Figure 5.3: Shoreface stratigraphy in scenario 3. Black lines are plotted every 50 time steps, the Δt is 5 years. Therefore the black lines indicate the paleo-morphology every 250 years. Logs of the shoreface stratigraphy are extracted, and presented below the stratigraphy. The lines over the logs show the average grain-size signal of the measured logs of Link Canyon, Muddy Creek, and Ferron Creek, at their respective position as seen in figure 3.6. In the logs at the bottom of the figure an average grain-size trend interpretation is given next to the simulated log. The thick black lines connecting the top of the coarsening upward packages, indicate the maximum regressive surfaces in the shoreface's stratigraphy.

The result concerning the simulated shoreface of scenario 4 is found in figure 5.4.

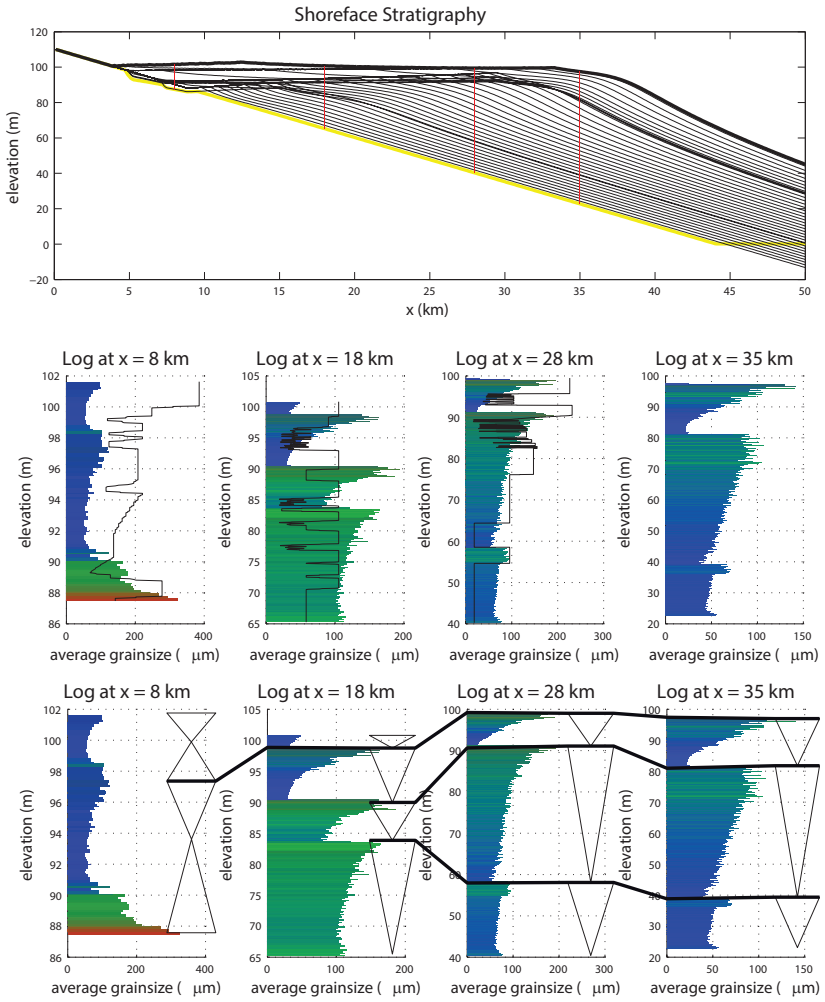

Figure 5.4: Shoreface stratigraphy in scenario 4. Black lines are plotted every 50 time steps, the Δt is 5 years. Therefore the black lines indicate the paleo-morphology every 250 years. Between 5km, and 10km in the shoreface's stratigraphy, erosion of the base surface takes place. Logs of the shoreface stratigraphy are extracted, and presented below the stratigraphy. The lines over the logs show the average grain-size signal of the measured logs of Link Canyon, Muddy Creek, and Ferron Creek, at their respective position as seen in figure 3.6. In the logs at the bottom of the figure an average grain-size trend interpretation is given next to the simulated log. The thick black lines connecting the top of the coarsening upward packages, indicate the maximum regressive surfaces in the shoreface's stratigraphy.

The evolution of the mainland, and foreshore locations during the formation of the shoreface in the different scenarios is compared in figure 5.5. Note that in figures 5.5a, and 5.5b the mainland, and foreshore location in the shoreface environment do not overlap during the periods of sea level rise, contrary to the figures 5.5c, and 5.5d. This difference is directly related to active back-barrier formation in scenarios 1, and 2.

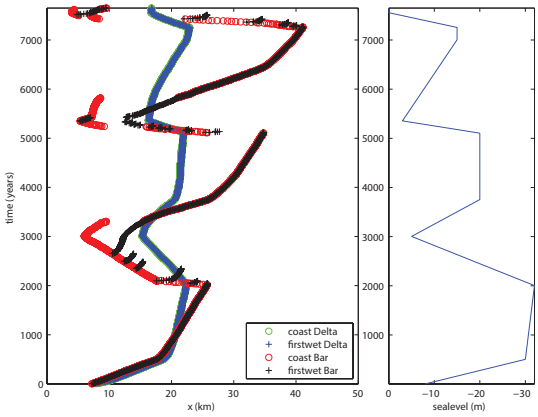

(a) Scenario 1.

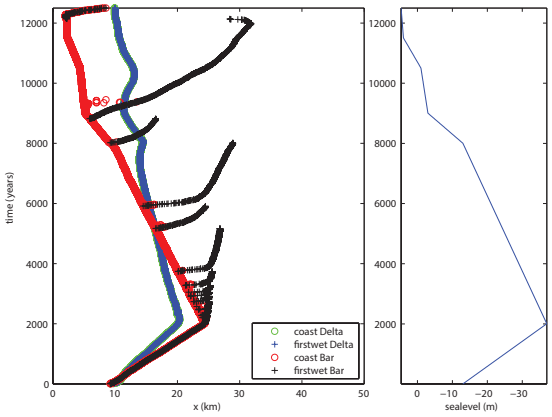

(b) Scenario 2.

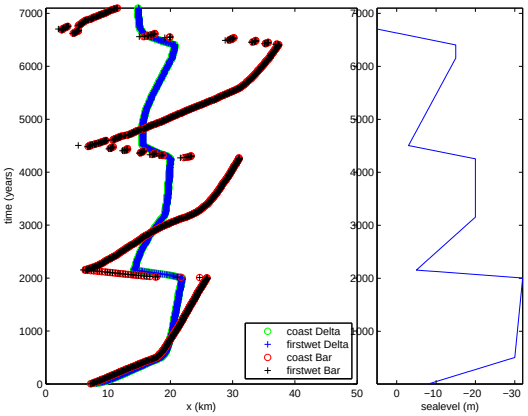

(c) Scenario 3.

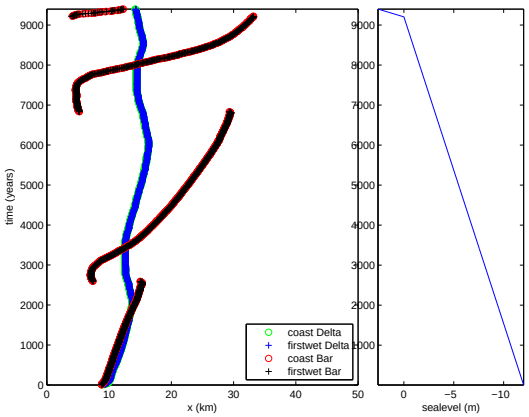

(d) Scenario 4.

Figure 5.5: Coast (mainland), and first wet (foreshore) locations as determined for the simulated shoreface and delta environment. In the geologic setting of scenario 1, and 2 back-barrier formation occurs during periods of sea level rise. Back-barrier formation is identified to take place when the mainland, and foreshore position diverge from each other.

Lastly, figure 5.6 is included to graphically compare the input signals, and the cumulative volume of sediment that deposited on the shoreface per scenario.

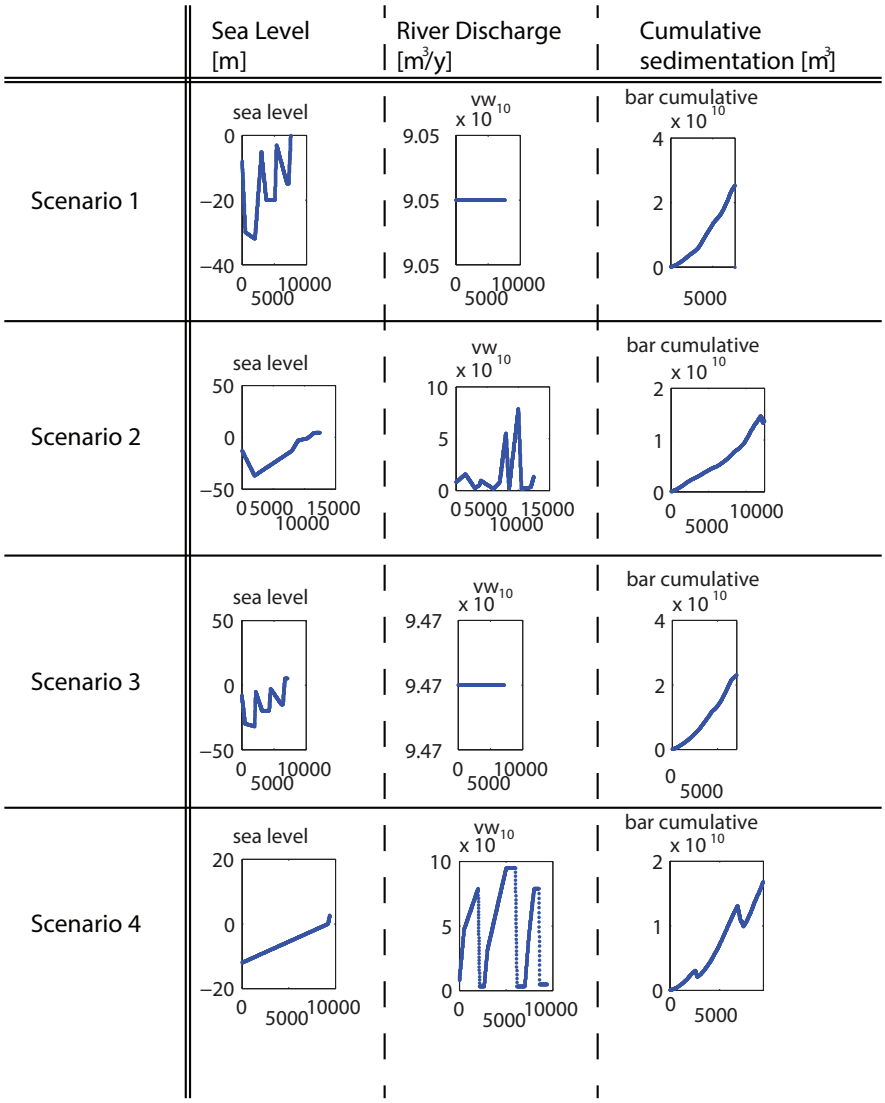

Figure 5.6: Yearly input signals of the different scenarios. The x-axis always indicates time[y], the y-axis from left to right represents the sea level signal [m], river discharge [m^3/Δt], and cumulative sedimentation on the simulated shoreface profile [m^3].

5.1.3 Analysis

First an analysis is performed per scenario. Later, in the discussion in chapter 6, the analysis is extended to their contribution to the rest of this thesis.

In scenario 1, three cycles in sea level fall, and rise take place. The sea level fall periods causes the mainland location to move basinward, which consequently allows larger grain-sizes to deposit further into the sedimentary basin. The cycles of sea level fall are linked to the three major coarsening upward packages in the logs of figure 5.1 at position 18km, and 28km. Inside the fining upward packages minor coarsening upward packages

are observed. These minor packages are caused by back-barrier formation during the periods of sea level rise, figure 5.5a. When a back-barrier forms larger grain-sizes will deposit further inside the sedimentary basin as well, forming these minor packages.
The sea level cycles fluctuate between 0m and -32m. Note that in an absolute sense the sea level rises over the whole simulation time, 7650 years.

To analyse the extent of the progradational, and retrogradational units in figure 5.1, it is analysed in combination with figure 5.5a. Figure 5.5a, shows the migration of the mainland, and foreshore location, both on the delta as on the shoreface. In the shoreface we observe progradation of the mainland, and foreshore location on the shoreface within the first 2000 years. During this period the locations migrate about 18km laterally basinward. This progradational period is followed by retrogradational period up until the year 3000. During this first retrogradation we observe five instances of back-barrier formation, of which the first four are drowned. The drowning of a back-barrier is observed through the jump in the foreshore location back to the mainland location. The last back-barrier of the first retrogradation period is closed as the sea level falls, over the years form 3000 to 3750. This period then transitions into a progradation period where the mainland, and foreshore location migrate laterally 25km basinward. At the end of this progradation, at 5100y, a new period of rapid sea level rise starts, 23m in 250y. This rapid rise in sea level causes the locations to travel land inward with a single back-barrier forming at the end of the retrogradational period. Unlike the previous back-barrier this one closes before the locations travel basin inward again caused by a falling sea level. During this last major progradational period the locations travel up to 35km basin inward. This progradational period comes to an abrupt end at 7250 years when the sea level rises 15 meters over 300 years, and the locations are forced over 35km land inward. During this transgression a back-barrier is formed five times. The scenario ends with pure progradation as sea level, and sediment influx remain constant.

Analysing the simulated logs of scenario 1 from figure 5.1 in combination with the migration of the mainland, and foreshore location in figure 5.5a. We observe that the log positions at location 8km, and 18km are aerially exposed up to three times, and the log at 28km two times, as both locations are to the right of this location. During aerial exposure of a given location no sediment will deposit or erode from this location. Progradation of the foreshore location translates to coarsening upward packages in the logs, while a period of retrogradation is marked by an overall fining upward package which is subdivided in diminishing coarsening upward packages. This is related to back-barrier formation in this geologic setting. When a back-barrier forms the foreshore location progrades basinward.
The log at 8km generally underestimates the grain-size compared to the measured grain-size but it does match the coarsening upward trends measured in the bedsets of figure 3.5. Sediment is deposited at this log location at the start, and during the transitions from sea level rise to sea level fall. Grain-size trends caused by the progradation, and retrogradation periods are hardly observed in this log as it is mostly aerially exposed.
In the simulated log at 18km we observe prograding, and retrograding trends but the grain-size correlation to the measured grain-size log is poor. In the simulated log we observe an alternation of progradational to retrogradational trends starting from the bottom with a progradational trend. This trend correlates to the first progradation of the mainland, and foreshore locations, in figure 5.5a. When tracing the location at $x = 18km$, we observe the following sequence. Progradation of the coastline in the first 500y, followed by

a period of non deposition due to aerial exposure, lasting ∼1500y. Then retrogradation of the mainland, and back-barrier forming from the years 2000 to 3000. Followed by a period of progradation, and aerial exposure to the year 5100. Thereafter, the location is exposed to a period of retrogradation followed by progradation over the years 5100 to 5350. Lastly the location is aerially exposed for 1650 years, followed by a period of rapid retrogradation, and minor progradation.
The log at location 28km is observed to posses the best correlation to its measured counterpart, when compared to the other log of this scenario. The signal observed in this log is similar to that of the log at 18km. It shows an alternation of progradational, and retrogradational trends, starting from the bottom with progradation.

Because scenario 1 has a stationary discharge we can easily preform a rough mass balance calculation to check the volume of sediment that should have deposited. To preform this calculation we split the deposited volume in a volume including transported material, calculated in equation 5.1, and the volume of pelagic sediment in equation 5.2. In equation 5.1 the volume of sediment $V_{transport}$ is calculated by multiplying the yearly discharge, Q_w [m^3/s] with the portion of the sediment concentration fraction Q_{sx} [kg/m^3] * t_{Qsx} [-] that got transported to the shoreface, times one over the average density of the sediment concentration [kg/m^3]. Finally, it is multiplied by the simulationTime [y] to acquired the sediment volume in [m^3] that got transported to the shoreface from the delta.

$$V_{transport} = Q_w(Q_{s1} * t_{Qs1} + Q_{s2} * t_{Qs2} + Q_{s3} * t_{Qs3}) * \frac{1}{\rho_{av}} * simulationTime \tag{5.1}$$

With the values from the configuration file, table 5.2, inserted in equation 5.1, we calculate a volume of $\sim 18 * 10^9\ m^3$ for the transported volume. In equation 5.2, the fallout [dm/Δt] is multiplied by the width W of the shoreface [km], and the length of the marine part L_{marine}.

$$V_{pelagic} = fallout * W * L_{marine} * nTimesteps \tag{5.2}$$

The fallout, the shoreface's width, and nTimesteps are taken from, table 5.2, the length is approximated to be 25km. This comes down to $3.6 * 10^9\ m^3$. By adding the transported, and pelagic volume in equation 5.3.

$$V_{tot} = V_{transport} + V_{pelagic} \tag{5.3}$$

We calculate that the total volume on the profile should be $\sim 21.63 * 10^9\ m^3$. Due to the approximation of the length L this is about equal to the cumulative volume of scenario 1 calculated by the model, as shown in figure 5.6.

In scenario 2, sea level starts with a fall from -8m to -37m over 2000 years, followed by a rise to 5m over the next 10500 years. During the rise of the sea level, we note that there are several occasions of back barrier formation, figure 5.5b. The river discharge fluctuates between $10m^3/s$, and $500m^3/s$ over the 12500 simulated years. We note that there are four peaks observed in the discharge signal that induce coarsening upward cycles in the

stratigraphy, figure 5.6. The first two cycles are 5 to 10 times smaller compared to the last two, see table 5.3. The second cycle of these smaller cycles starts contemporaneously with the sea level rise.

The sea level fall in the first 2000 years causes the mainland, and foreshore location on the shoreface to migrate 15km basin inward. Thereafter, the mainland is forced up to 23km land inward by the period of sea level rise. During this period of sea level rise the foreshore location progrades basinward in 12 distinguishable events. In these events back-barriers are formed, and drowned when the foreshore location jumps to the mainland location.

The simulated logs of this scenario show a poor match to the measured logs. Compared to scenario 1 the log at 28km is never aerially exposed in this scenario. Additionally, the log at 8km, and 18km are aerially exposed a single time, compared to the three times in scenario 1.

The coarsening upward sequences are less pronounced in scenario 2, compared to scenario 1. This is largely because of the constraints on the sea level fluctuation. Because of these constraints larger grain-sizes are compensated in their travel distance factors, implemented to the model by the user in table 5.3. This compensation allows the medium, and largest grain-sizes to travel further into the sedimentary basin at all times. The compensation in travel distance therefore causes an increase in average grain-size over the whole coarsening upward sequence measured in the logs of figure 5.2 compared to the logs of figure 5.1.

In scenario 3, The sea level in this scenario fluctuates between 5m and -32m over a simulated time period of 7100 years. Similar to scenario 1, the sea level signal of scenario 3 consist of three cycles of sea level rise and fall, and discharge is stationary at $600m^3/s$, figure 5.6. Additionally the travel distance factors are also similar to scenario 1, table 5.2. This results in more distinct coarsening upward sequences in the simulated logs seen in figure 5.3 compared to the logs of figure 5.2.
Because back-barrier formation is disabled in scenario 3, and 4 the foreshore location in it self is bounded to the mainland location. Note that the locations do not diverge from each other in the shoreface's environment. The difference in the locations position between scenario 1, and 3, is seen in figure 5.5a, and figure 5.5c.

During the first sea level fall in the first 2000 years the mainland, and foreshore location on the simulated shoreface migrate ∼18km basin inward. This is followed by a retrogradation of the locations about 20km land inward caused by the sea level rise between the year 2000, and 2150. Thereafter the locations prograde ∼25km basinward over the following 2100 years. This progradation is caused by the second fall in sea level, and its subsequent stationary period. The second rise in sea level causes a period of retrogradation. In this period the the locations migrate less than 25km basinward, which is less than the previous progradation. The subsequent period of progradation lasts until the year 6150y, and is caused by the longest period of sea level fall, 1650 years. Over this period the locations migrate ∼28km basinward. It is followed by the last period of retrogradation, which lasts 300 years. Over this period the locations migrate more than 30km land inward. It is followed by a period of stationary sea level of 400 years, in which

the locations prograde ∼7km basin inward.

In the simulated log at 8km in figure 5.3 shows correlation in grain-size as well as in trend size of the bedset to the measured counterpart up to ∼97m. Thereafter, the trend is still visible in a coarsening upward sequence but the grain-size is underestimated.
The simulated log at 18km in figure 5.3 an alternating sequence of progradation, and retrogradation is observed. Although the retrogradation is generally rapid in this scenario, see figure 5.5c. The first retrogradation is marked by a fining upward package after the first coarsening upward package. The second is marked after the second coarsening upward package by a fining upward package consisting of two diminishing coarsening upward packages. The third, and last retrogradation is observed after the third coarsening upward package by two diminishing coarsening upward packages, like the second retrogradation period.
In the simulated log at 28km in figure 5.3 three coarsening upward sequences can be distinguished, related to the first three prograding periods of the locations, in figure 5.5c. During the last prograding period no sediment is deposited at this location. The correlation between the measured log, and simulated log at 28km is adequate, both trend wise as in grain-size.

In scenario 4, the sea level makes a single rise from -12m to 5m, over the 9400 simulated years. The river discharge fluctuates between $10m^3/s$, and $600m^3/s$, in three cycles, as seen in figure 5.6. Analogous to scenario 2, which also is a mixed scenario, the travel distance factors are adjusted for scenario 4, see table 5.5. Hence, this also results in an overall increase in the average grain-size in the measured logs of figure 5.4, compared to the logs in figure 5.3 of scenario 3 which uses the same geologic setting.

In scenario 4, retrogradation is almost non existent, see figure 5.5d. Three cycles of progradation are observed, caused purely by sediment influx fluctuations. The minor progradation period in the last 200 years is caused purely by the lack of accommodation space compared to the low sediment influx, table 5.5. After a prograding period caused by a sediment influx pulse, the locations make a jump land inward. After such a jump of the locations land inward retrogradation is observed transitioning into aggradation, to progradation until the locations jump land inward again.

The sediment pulses cause the progradation of the locations, and therefore the coarsening upward sequences in the logs. However, in the simulated log at 8km in figure 5.4 hardly shows any correlation to the measure logs signal. Because it is aerially exposed most of the simulation time, figure 5.5d.
The simulated log at 18km does show correlation the the progradation periods of this scenario 4. But the match to its measure counterpart is poor both in trend size as well as in grain-size estimation.
The simulated log at 28km shows correlation to both the three sediment pulses of the input signal as well as a correlation to the signal of measured log.

Generally we observe that the match between average grain-size values of the simulated logs, and measured logs is poor. However, the logs at 28km in scenario 3, and 4 show a relatively good correlation to the coarsening upward trends.

5.2 Inversion scenario

Through the inversion a most likely scenario is obtained, by minimising the difference between the measured, and simulated logs. Because the model is unable to improve the likelihood when creating a scenario based on the actual measured logs, we extracted the logs from the forward scenario 3 to let the inversion create a scenario on those. Because further attempts to recreate the Panther Tongue failed, see appendix C, this will be the only scenario we discuss here.
The scenarios 1, and 2, are more sensitive to changes in input signals than scenario 3, and 4 due to the back-barrier formation. Therefore, we opted to run the inversion scenario without back-barrier formation, and minimal fallout rate.

5.2.1 Input

The parameters in the configuration file for the inversion are presented in table 5.6. Here we introduce a new set of parameters used solely in the inversion routine. These new parameters set the amount of minimum, and maximum iterations used in the burn-in period. The amount of iterations required to complete the steady iteration period, and the sampling period. Additionally the maximum tempering factor for the burn-in period, and the relative variance used in the sampling period is set. Furthermore the parameters used in the extreme forward scenarios are adapted. The simulation time is set to 8500 years in 1700 time steps, which makes a Δt of 5 years, similar to scenarios 3, and 4. The travel distance factors are increased according to observed results from the extreme scenarios. They are the average value from the values used in scenarios 3, and 4 rounded to a whole integer. A reduction in wave height is preformed in accordance to scenario 4. The fallout rate is reduced slightly to make the inversion more robust.

From the input signals the sea level, and river discharge tempered by the statistical functions of the inversion routine. The concentration of sediment is not tempered with, and held stationary as it is proportional to the river's discharge.

Configuration file for the inversion		
Parameter	Value	Comment
runMode	= "Inverse";	# model runs the "Forward" or "Inverse" routine
inversion.relVar	= 0.3;	# relative variance
inversion.minIter	= 500;	# minimum number of iterations before the burn-in is complete
inversion.maxIter	= 50000;	# maximum number of iterations before the burn-in is complete
inversion.steadyIter	= 1000;	# number of steady iterations before the burn-in is complete
inversion.sampleIter	= 1000;	# number of iterations preformed during the sampling period.
inversion.maxTemp	= 5;	# maximum tempering factor for the simulated tempering
simulationTime	= 8500.0;	# time being simulated [years]

Continuation of configuration file for the inversion		
Parameter	Value	Comment
nTimeSteps	= 1700;	# number of timesteps
hMarFactBar	= [2.0, 2.0, 3.0];	# h correction for marine domain
waveStorm	= 4.0;	# storm waveheight [m]
fallout	= [0.0, 0.0, 0.025];	# marine sediment fall out [dm/timestep]
seaLevel.fixed	= false;	# false; prone to tempering during the inversion routine
seaLevel.values	= [0, -13, 2000, -37, 8000, -13, 9000, -3];	# [time , lvl, time, lvl,...] [y, m]
seaLevel.truth	= [0, -13, 2000, -37, 8000, -13, 9000, -3, 10500, -1, 11500, 4, 13000, 5];	# [time , lvl, time, lvl,...] [y, m] initial signal used by the inversion routine
seaLevel.minvals	= [0, -37];	# lower sea level boundary in the inversion
seaLevel.maxvals	= [0, 5];	# upper sea level boundary in the inversion
seaLevel.mindim	= 2;	# minimum amount of points used in the inversion to construct a sea level signal
seaLevel.maxdim	= 50;	# maximum amount of points used in the inversion to construct a sea level signal
Qw.fixed	= false;	# false; prone to tempering during the inversion routine
Qw.values	= [0, 50, 1500, 100, 3000, 15, 3700, 30, 4000, 60, 6000, 10, 7000, 50, 8000, 350, 8500, 10];	# river discharge signal, [time, flux, time, flux,...] [y, m^3/y]
Qw.truth	= [0, 50, 1500, 100, 3000, 15, 3700, 30, 4000, 60, 6000, 10, 7000, 50, 8000, 350, 8500, 10];	# river discharge signal, [time, flux, time, flux,...] [y, m^3/y]
Qw.minvals	= [0, 10];	# lower discharge boundary in the inversion
Qw.maxvals	= [0, 600];	# upper discharge boundary in the inversion
Qw.mindim	= 2;	# minimum amount of points used in the inversion to construct a discharge signal
Qw.maxdim	= 50;	# maximum amount of points used in the inversion to construct a discharge signal

Continuation of configuration file for the inversion		
Parameter	Value	Comment
Qs1.fixed	= true;	# true; signal shall not be tempering with during the inversion routine
Qs1.values	= [0, 200, 8500, 200];	# concentration largest grain-size [y, mg/L] sum of all Qs should not exceed the river tolerance
Qs2.fixed	= true;	# true; signal shall not be tempering with during the inversion routine
Qs2.values	= [0, 350, 8500, 350];	# concentration middle grain-size [y, mg/L] sum of all Qs should not exceed the river tolerance
Qs3.fixed	= true;	# true; signal shall not be tempering with during the inversion routine
Qs3.values	= [0, 450, 8500, 450];	# concentration smallest grain-size [y, mg/L] sum of all Qs should not exceed the river tolerance
End of Table 5.6		

Table 5.6: Configuration file for the inversion.

5.2.2 Results

In figure 5.7, the evolution of the likelihood during the inversion scenario is presented. The graph of the parameters used during the sampling period are plotted in figure 5.8. From the last set of the parameters used in the sampling period an input signal is obtained. These input signals for the sea level, and discharge are then used in a forward run to graphically analyse the result. The result of the shoreface stratigraphy is shown in figure 5.9. The corresponding evolution of the mainland, and foreshore position is shown in figure 5.10.

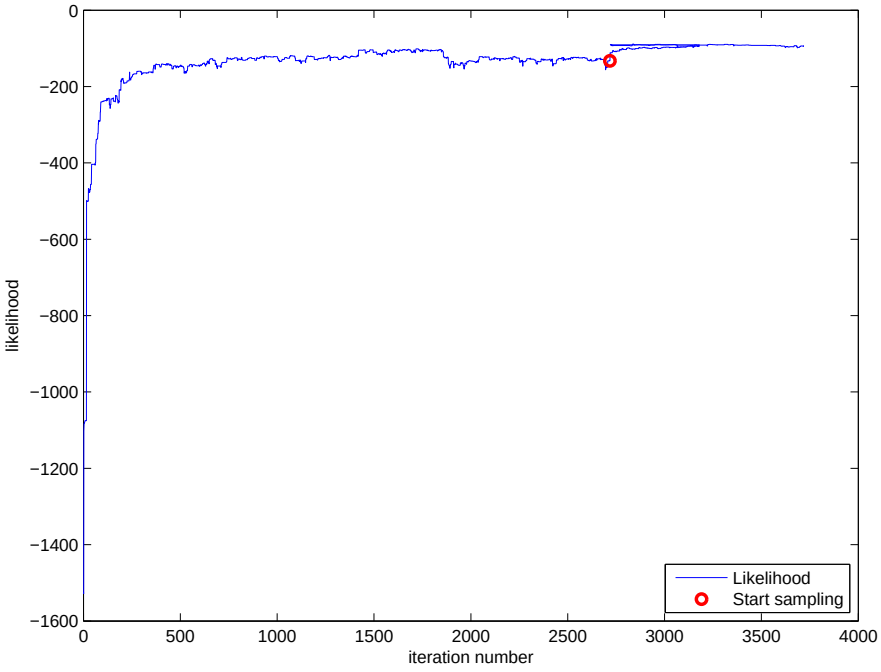

Figure 5.7: Likelihood evolution of the inversion scenario. There is a steep increase in likelihood at the start of the burn-in period, everything before the red circle 'start sampling'. During the sampling period, after the 'start sampling' circle, the iteration count is reset before the required amount of iterations is fulfilled.

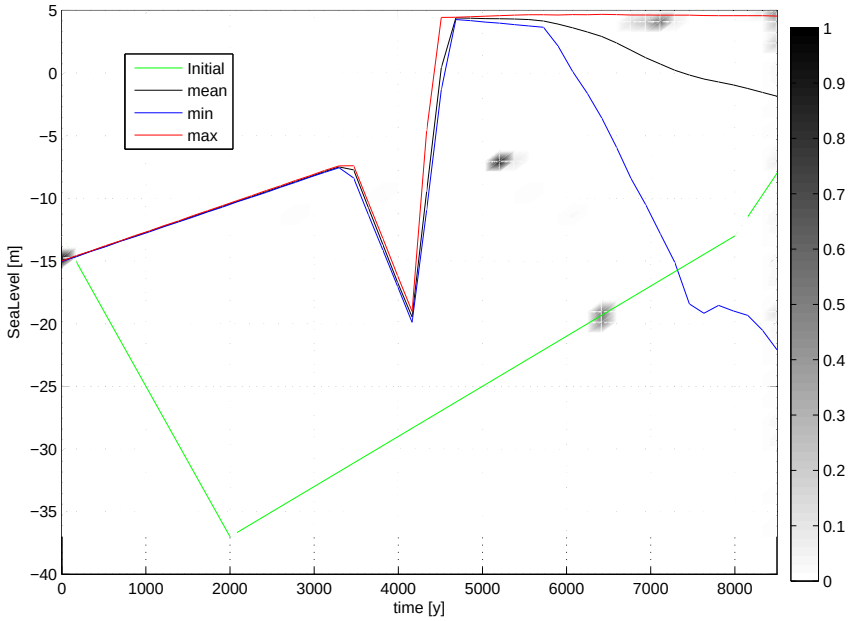

(a) Sea level in the inversion scenario.

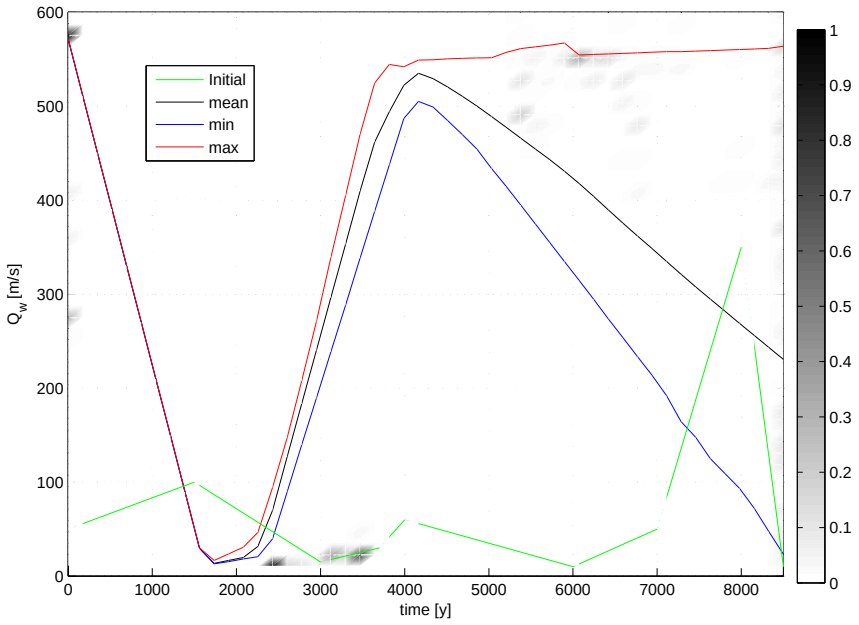

(b) Qw in the inversion scenario.

Figure 5.8: Parameter density plot in top view, shows the different coordinates used during the sampling period of the inversion as the drops. Side views of the density plot are included in appendix B. Together with the initial input signal, from scenario 3 as initial. Additionally the 95% confidence zone is plotted between the min, and max lines together with the mean line.

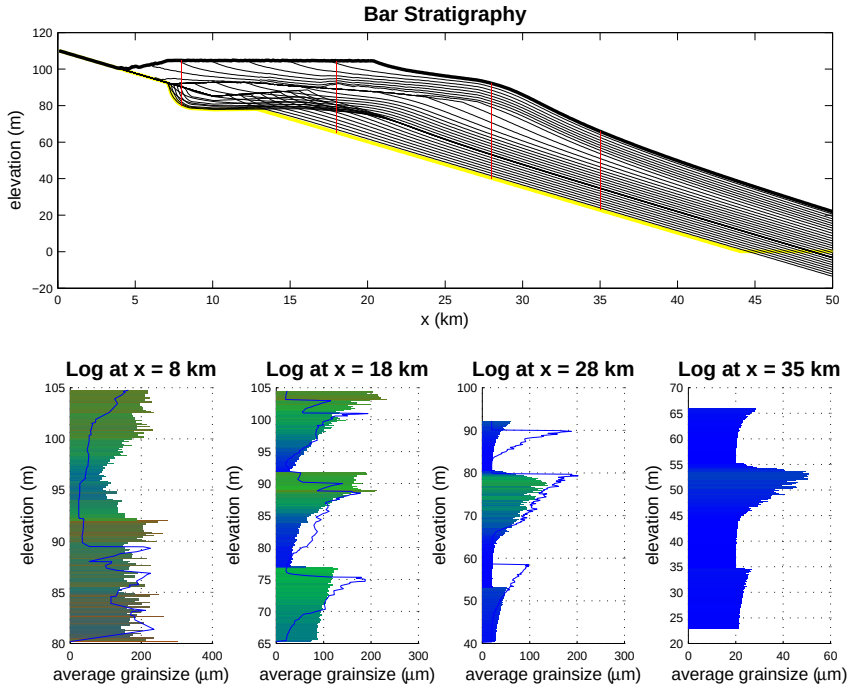

Figure 5.9: Shoreface stratigraphy from the input signals based on the last input signals used during the sampling period. Black lines are plotted every 50 time steps, the Δt is 5 years. Therefore, the black lines indicate the paleo-morphology every 250 years over 8500 years. Between 7km , and 13km the base surface is eroded. The line overlaying the simulated logs of 8km, 18km, and 28km, are the logs extracted from scenario 3. These logs are normalised then stretched over the simulated logs of the inversion.

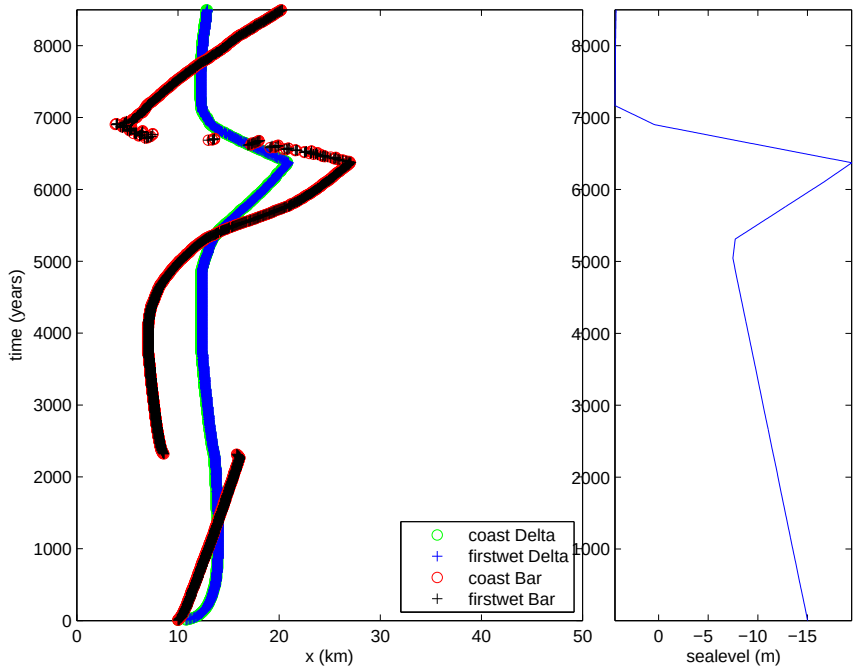

Figure 5.10: Coast (mainland), and first wet (foreshore) locations as determined for the simulated shoreface and delta environment of the inversion scenario. Note that back-barrier formation is disabled.

5.2.3 Analysis

The likelihood increases fast during the first iterations in the burn-in period, in figure 5.7. A steep increase in likelihood as in figure 5.7 is commonly observed in inversion scenarios, also see figure C.1 in appendix C. It suggests that the calculated match between measured, and simulated wells improves rapidly. Then, the likelihood stabilises until the sampling routine takes over. We observe that the iteration count of the sampling period is reset when it reaches the 460th iteration. During the sampling period the parameters used to manipulate the input signals are recorded, and plotted in the histogram of figure 5.8. It is observed that the 95% confidence zone corresponding to these parameters diverges at later simulation times. Additionally, we note that not all used parameter coordinates are located within this confidence zone. The sediment concentration of all grain-size fractions is held constant throughout the simulation, Q_{s1}, Q_{s2}, and Q_{s3} in figure 5.8.
The mean line presented in the sea level, and Qw plots in figure 5.8 are used as input signals in creating figure 5.9.
In the sea level signal we observe a rise followed by a sharp fall, continued in a sharp rise in sea level, around the year 6400. Then, it remains stationary for a period of ∼200 years, followed by a gradual fall of sea level. The discharge signal in the Qw plot, which is directly related to sediment supply starts at a relatively large value, considering its boundaries introduced in table 5.6. The discharge then drops to the lowest boundary followed by a rise to about its initial value, after which it drops back down again to $\sim 300\ m/s$.
In the evolution of the mainland position in figure 5.10 the first jump in position is due to the reduction in sediment supply, this ends the first coarsening upward sequence observed in the logs of figure 5.9. Then, as sediment supply increases again the mainland starts to

build basin inward again. The location builds outward until the sea level rises rapidly at ∼6300y. The mainland is forced land inward by this sudden sea level rise, this ends the second coarsening upward sequence in the logs of figure 5.9. Then the sea level remains relatively stationary, and the rivers discharge drops gradually. During this period we observe progradation of the coastline. This final progradation corresponds to the third, and last coarsening upward sequence clearly observed in the logs at 18km, and 28km of figure 5.9.
As in figure 5.5 the delta locations in figure 5.10 show a more stable response to the the fluctuations in sea level, and sediment supply than the shoreface locations. The logs in figure 5.9 are already quantitatively evaluated by the model through the likelihood calculation, using equation 4.3. In equation 4.3 the measurement error is introduced, and set to 10μm in the normalised grain-size signal likelihood calculation. The measurement error is set to 1m in the likelihood calculation for the length of the logs. These likelihoods are accumulated, and reduced to obtain a quantitatively acceptable scenario. However, a quantitative acceptable scenario is not directly an appropriate qualitative scenario as seen in appendix C. In this scenario the likelihood is improved to a similar value as in subsection 5.2.2. However, the final result in figure C.3 does not show the three coarsening upward sequences as in figure 5.9.

Qualitatively, in figure 5.9 three coarsening upward sequences are present in the simulated logs of the inversion, as is geologically observed from the original figure 3.5. The consistency of the simulated grain-size signal, and the signal from the logs of scenario 3 appears to be adequate as well. In the log at 28km we observe that the lower and upper coarsening upward sequences are relatively worse than other sequences. However, the biggest inconsistency is observed in the length difference between the simulated logs of the inversion, and the extracted logs from scenario 3. The inversion's log at 8km is 25m long, which was originally 15m long. Therefore, the difference 'Δx' between the logs equals $\Delta x = 10m$. The inversion's log at 18km is 40m long, which was originally 34m long. Therefore, the difference between the logs is $\Delta x = 6m$ The inversion's log at 28km is 50m long, which was originally 52m long. Therefore, the difference between the logs is $\Delta x = -2m$ The log at 35km is not used in the inversion routine to simulate the use of the measured logs.

6. Discussion

Our simulations show that 2Dstratsim can be used to recreate the sedimentary environment of the Panther Tongue's shoreface. In this thesis we were able to recreate the coarsening upward sequences observed in the bedsets presented in the modified shoreface profile in figure 3.5, after (Forzoni et al., in prep.). However, the quality between these shoreface profiles from both the forward, and inverse routine varies.

6.1 Data errors

In order to work with 2Dstratsim adjustments are required in the data, as described in section 3.1. These adjustments affect the final results in various manners.

6.1.1 Data gaps

The modified shoreface profile, in figure 3.5, introduces an error in the vertical extent of bedset 2, as interpreted by Forzoni et al. (in prep.). Additionally, the modified profile introduces a gap below the maximum flooding surface, which binds the bottom of the interpreted Ksp040 parasequence, and the introduced modified profile itself. Hence, additional sediment is required on the simulated profile to fill this gap. Alternatively, the maximum regressive surface that binds the top of the Ksp040 parasequence can be lowered as well. Resulting in a mismatch between the dimensions basinward of the measure profile, and the simulated profile.
Additionally, the logs of Link Canyon, and Ferron Creek are intersected by our proposed profile, or do not cover the complete vertical extend between the maximum regressive surface and our proposed profile. This poses a problem in implementing these logs in the 2Dstratsim model. Because the model requires logs that specifically fit the vertical extent of the modified profile without gaps in the data. Therefore, the two logs of Link Canyon, and Ferron Creek were modified to fit the shoreface profile. From the log of Link Canyon the lower part had to be removed, and in the Ferron Creek log an artificial extension of 36m is introduced. Although this is preformed in our best effort, it introduces an error when correlating the logs later in chapter 5. Especially in the Ferron Creek log at 28km as the lower 7/12th part of the log is not measured in the field.

6.1.2 Log quality

The simulated logs introduce more detail to the stratigraphy as they use more depth intervals at which they generate an average grain-size value compared to the measured logs. As is observed by comparing the quality of the correlation between the measured

part of the measured logs, and the simulated results in the shoreface profiles of chapter 5. This difference in detail is caused by the model as it is not bound to generate the average grain-size in the grain-size classes of Blair and McPherson (1999), which are used in the field.
Although these errors originate from the field measurements, we acknowledge that mapping the whole vertical length of the parasequence by using more vertical intervals, and use a more detailed method of mapping of the grain-size is often time consuming, or otherwise impossible. However, the error this introduces in the measurement of the average grain-size seems significant when we compare the results to simulated logs. Yet, because we think that more detail from field measurements is unlikely, a proper solution would be to adjust the model's comparison methods to the field data.

6.1.3 Normalisation

In the visualisation of the logs under their corresponding stratigraphy, in chapter 5.1, the normalised version of the measured logs overlays the simulated logs. The use of normalised logs also introduces an error when correlating the average grain-sizes of the logs at a specific depth. However, it finds a useful application in using them for trend recognition during the forward routine. Because a mismatch in the proportional length of the coarsening upward sequences to the other sequences is then easily recognised, and can be adjusted by modifying the input signals accordingly.

6.2 Model errors

Modifying the input signals via the configuration file is easy, and fast. However, various problems may arise here due to the stability, and sensitivity of the model.

6.2.1 Stability and Sensitivity

Stability issues cause the model to abort in both the forward, and inversion routine. The instability of the model is often directly related to the sensitivity of the model.
This sensitivity of the model is related to the effect a (slightly) changed parameter in the configuration can have on the stratigraphic output, and the stability of the model.
The stability of the model is directly related to the dimensions of the simulated environment, and the simulated time. Because the dimensions of the simulated profile dictate how much sediment the profile can theoretically accommodate. While sea level, and sediment supply signals ultimately set the available amount of volume, and the rate at which this volume is filled. However, the impact of these signals is primely confined by the simulation time. Therefore, one can argue that the model should be able to temper directly with the simulation time in addition to the input signals.

6.2.2 Dimensional limitations

The dimensions of the model limit the lateral distance over which the mainland location can migrate. This introduces a stability problem in the model, because the model terminates when the mainland location travels outside the horizontal grid of the simulated profile. The mainland location can be forced outside the horizontal grid by a seemingly small change in the configuration file. For instance when fallout rate is increased, or when sea level is constant too long at high elevations with little sedimentation. The latter causes the initial surface to erode, and possibly results in the mainland location to travel off the grid.
When working with back-barriers the model becomes increasingly sensitive. Because an minor change in input signal can cause a back-barrier not drown where it used to do. Causing the back-barrier to build toward the end of the grid, and forces the model to terminate.
Additionally, the model's dimensions are limited by the shape of the initial surface, which is required to be linear. An effort is made to run a simulation on a surface representing the shape of the maximum flooding surface based on the interpretations of Forzoni et al. (in prep.). The result, shown in appendix C, shows an erratic shape of the shoreface's stratigraphy, which should not form a back-barrier. Additionally the second coarsening upward package thins out basin inward, whereas one would expect it to thicken in the troughs rather than thin out as if the profile was linearly decreasing. Hence, the 2Dstratsim model is not ready to generate a stratigraphy on custom shaped surfaces preventing an accurate duplication of the Panther Tongue morphology.

6.3 Routine limitations

Knowing the limitations of the model, and respecting its sensitivity and stability problems both the forward routine as well as the inversion routine are used to generate promising results. However, these routines both have their respective limitations.

6.3.1 Forward limitations

Working with the forward routine is time consuming, because of the the model's sensitivity. This is observed when implementing changes to the input signals for both the sea level, and river discharge. Changes in both signals can lead to dramatic changes in the resulting stratigraphy. For instance a reduction in sediment supply may lead to the erosion of a significant part of the previous bedset. Whereby a significant portion of the respective sequence can erode completely. Which results in an unrecognisable coarsening upward sequence in the stratigraphy. Therefore, the step by step approach introduced in section 5.1 increases the time efficiency of creating a scenario with this routine significantly.
The quality of the likelihood between the coarsening upward sequences from the simulated, and measured logs in section 5.1 is generally poor. However, the forward scenarios are not created on a likelihood basis but on a visual match between the of the coarsening upward sequences. Qualitatively, this match between sequences is satisfactory in the logs at 28km in figures 5.1, 5.3, and 5.4. The goal; to set preliminary parameters for the

inversion by using extreme forward scenarios, is reached within requirements.

6.3.2 Inversion limitations

Even though preliminary parameters are set for the inversion by the forward scenarios. The inversion is not able to simulate a scenario based on the measured logs. This is partly because of the same sensitivities that are present in the forward routine. The other reason the inversion was not able to simulate a scenario based on the measured logs is because the final result of the inversion remains dependent on its input signal.
As long as the inversion solely works with the likelihood equation to quantify its result, it is prone to get stuck in a local optimum scenario. To prevent the inversion from getting stuck in a local optimum, several input signals should be tested to map the complete range of possible optimal scenarios. However, is time consuming as no automated algorithm is implemented in 2Dstratsim for this purpose. Additionally, it is not guaranteed that the inversion would find an other scenario using such an algorithm. The result of the inversion we present in section 5.2 is therefore likely to be a lucky shot at a scenario that is also geologically appropriate. However, this result does confirm that 2Dstratsim is able to use its inversion routine to generate a quantitatively, and qualitatively likely scenario within set limits.
The input signals of the inversion scenario in section 5.2 are completely reconstructed by the statistical algorithms of the inversion routine. The sea level signal shows a steep sea level rise, and fall over a significant vertical length ∼20m, in a geologically short period of time, ∼1000y. When thinking within the model's limitations this would qualify as a geologically unlikely event. However, tectonic activity is observed in the Panther Tongue making this signal geologically plausible. The river discharge signal shows changes of relatively sinuous shape, not uncommon for rivers.
To match the measured logs to the simulated logs, the inversion manipulates the input signals. The routine is allowed to use a user determined range of knickpoints. The routine correctly uses the maximum amount of knickpoints to create a best likelihood in the presented inversion scenario in section 5.2. However, the minimum nor a maximum distance between these knickpoints is assigned. Thus, they can be very close to one an other to a point that they cannot be distinguished visually from the commonly used graphs. Leading to a false belief of the model malfunctioning. However, to utilise multiple knickpoints close together in a conceptual model as 2Dstratsim is plausible.

6.4 Results

When we compare all the results from chapter 5, to the shoreface in figure 3.5. We note that at the basin inward end of the simulated scenarios the sediment looks thinner than the measured profile. However, this is caused by our surface going under the original profile. The vertical thickness of the sediment at the end of the profiles is about equal. This vertical thickness at the basin inward end can easily be increased by increasing the fallout of pelagic sediment. However, this does introduce more instability into the model, and is therefore kept low throughout the thesis.

6.4.1 Location migration

In figure 5.5, and figure 5.10 a more stable migration path of the mainland, and foreshore locations is observed in the simulated delta environment when compared to the migration path of the locations in the shoreface. This is caused by the active fluvial erosion, and sediment deposition on the aerially exposed part of the simulated delta profile. Thereby influencing the vertical thickness both above and below sea level, see appendix A for the delta stratigraphy results. Thereby generating a more uniform vertical thickness of sediment over this profile compared to the aerial part of a shoreface, which has a stair like morphology as no sediment is deposited above sea level. On the shoreface the locations that migrated basin inward can fall back to the initial profile where no sediment has deposited. This jump can be mitigated by less abrupt changes in sea level or by using a smaller time step, but this in turn results in extended computational times. Because these jumps in locations are not significant to the morphology, and bedset generation it is generally preferred to keep a time step as large as possible to minimise the computational time of the model.

6.4.2 Field observations

In the simulations of scenario 1, and 3, where the river's discharge is stationary, the discharge is kept stationary at $600m^3/y$, which is about as large as the Colorado river, Mexico, according to Milliman and Meade (1983). In scenarios 2 and 4, and the inversion this is the upper limit of the river's discharge. Hence, the latter scenarios have less sediment accumulated on the shoreface profile.

6.4.3 Bedset correlation

Observations in the field made by Forzoni et al. (in prep.) suggest that the stacking pattern in the bedsets of the wave-dominated shoreface succession of the Ksp040 parasequence in the south are progradational. At parasequence scale the trend is progradational in BS1-2, then aggradational in BS 3-4. However, in all the simulated results of chapter 5 no significant aggradational stacking patterns are observed in both the shoreface morphology as in the logs. Additionally, Forzoni et al. (in prep.), Hwang and Heller (2002) observe normal regression on the shoreface in the field. Normal regression is observed in the simulated stratigraphy of scenario 2, and 4, the mixed scenarios, as well. Only in the first bedset of scenario 2 we observe forced regression but this can be related to the use of an artificial linear initial profile. Yet, the bedsets in the simulated results of the sea level scenarios 1 and 3, and of the inversion in chapter 5 show forced regression throughout the stratigraphy of the shoreface.

7. Conclusion

2Dstratsim can be used to create sedimentary environments using the forward routine. The model is also able to use its inversion routine to automatically recreate sedimentary environments to a limited extent as no geologic constraints are considered in this routine. Therefore, there is no assurance that the final result is geologically plausible. Additionally, extensive preliminary work is required to use the inversion routine.

In some of the presented scenarios in chapter 5 the bedsets correlate at given depth intervals to the coarsening upward packages of the bedsets observed in the measured logs by Forzoni et al. (in prep.). The correlation is often limited to a single log in the presented forward, and inverse scenarios. Therefore, it cannot be concluded that the input signals of the Panther Tongue are sufficiently disentangled. Yet, the goal; to set preliminary parameters for the inversion by using extreme forward scenarios, is reached within requirements. In addition it can be concluded that the inversion can be used to replicate scenarios based on logs with sufficient detail.

Based on the results of the forward simulations we cannot discard the possibility that back-barriers did not form on the Panther Tongue's shoreface.
We observe a better match between the simulated logs and measured logs in a scenario with solely changes in sea level. Therefore, we conclude that fluctuations in the sediment supply had minor impact on the formation of the Panther Tongue's shoreface, and that sea level was the main forcing factor. However, it is observed in these simulated scenarios that the changes in the simulated sea level signals are sharp in a geologically short period of time it can be concluded that other factors as tectonics, and compaction play a significant role as well.

The difference in detail between measured logs based on the grain-size classification scale from Milliman and Meade (1983), and the metric length scale of the simulated logs is too large to calculate the likelihood properly with 2Dstratsim. The difference in grain-size detail increases the difficulty of correlating the measured logs to the simulated logs, which is directly linked to the ability of the model to properly disentangle the input signals from the simulated environment.

Logs that contain gaps in the data cannot be implemented directly into the 2Dstratsim model. Modifications are required to implement such logs in the 2Dstratsim model. These modifications introduce a bias of the user's own interpretation to the data, and therefore affect the final result.

Initial base surfaces that are not linearly decreasing over the length of the simulated profile are malfunctioning, see appendix C.

The inversion is able to completely change the initial input signals using statistical functions. However, it is observed that the final scenario remains dependent on the input signal.

In the inversion uses the proper amount of the user implemented amount of knick-points to generate a new input signal.

8. Recommendations

2Dstratsim is at a usable stage to be used as an educational tool to illustrate the effect of changes in sediment supply, and sea level change on the stratigraphy.

A step by step approach is the most time efficient method when recreating measured scenario.

To enable the 2Dstratsim model to effectively compare the simulated log to the measured logs the average grain-size values from the synthetic logs can be converted to the grain-size classes of the measured logs. This way both of the logs use the same amount of detail in mapping the average grain-size.

The sensitivity, and sensibility can be mitigated by reducing the fallout rate of pelagic material but this does compromise the final result.

Gaps in measured logs are common thus the model should be able to adopt logs with gaps. We propose to insert zeros at the borders of in depth intervals where the average grain-size is not measured, and let the model neglect the interval between these points in the likelihood calculation.

Implement a value for the minimum distance between the knickpoints used in the inversion routine.

To properly use the inversion it should be at least optional to make the simulated time automatically adjustable, possibly within a given range of values.

To correlate the amount of coarsening upward packages a geologic sub routine can be implemented in the for the inversion that measures the gradient in average grain-size change over a given interval of log.

The fluvial part of the delta shows too much sediment accumulation, and no grain-size differences. Thus it requires further investigation.

Bibliography

C. C. Bates. Rational theory of delta formation. *AAPG Bulletin*, 37(9):2119–2162, 1953.

T. C. Blair and J. G. McPherson. Grain-size and textural classification of coarse sedimentary particles. *Journal of Sedimentary Research*, 69(1), 1999.

K. Charvin. *Inverse and Forward Modelling of Shallow-Marine Stratigraphy*. PhD thesis, Imperial College London, 2008.

R. A. F. Dalman and G. J. Weltje. Simclast: An aggregated forward stratigraphic model of continental shelves. *Computers & Geosciences*, 38(1):115–126, 2012.

G. de Jager, J. E. A. Storms, and A. Forzoni. Quantifying sediment signal propagation in a fluvial-marine system using an efficient source-to-sink numerical model: 2dstratsim. in prep.

R. F. Dubiel, M. A. Kirschbaum, L. N. R. Roberts, T. J. Mercier, and A. Heinrich. Geology and coal resources of the blackhawk formation in the southern wasatch plateau, central utah. *Geologic Assessment of Coal in the Colorado Plateau: Arizona, Colorado, New Mexico, and Utah, US Geological Survey, Professional Paper*, 2000.

R. L. Folk. The distinction between grain size and mineral composition in sedimentary-rock nomenclature. *The Journal of Geology*, pages 344–359, 1954.

R. L. Folk. Petrography of sedimentary rocks. *Univ. Texas, Hemphill, Austin, Tex*, 182, 1974.

R. L. Folk, P. B. Andrews, and D. W. Lewis. Detrital sedimentary rock classification and nomenclature for use in new zealand. *New Zealand journal of geology and geophysics*, 13(4):937–968, 1970.

A. Forzoni, J. E. A. Storms, and G. J. Hampson. Architecture of shallow marine reservoirs: along-strike heterogeneities in the panther tongue delta-shoreface system, utah. in prep.

G. J. Hampson, M. R. Gani, K. E. Sharman, N. Irfan, and B. Bracken. Along-strike and down-dip variations in shallow-marine sequence stratigraphic architecture: Upper cretaceous star point sandstone, wasatch plateau, central utah, usa. *Journal of Sedimentary Research*, 81(3):159–184, 2011.

J. P. V. Hansen and E. S. Rasmussen. Structural, sedimentologic, and sea-level controls on sand distribution in a steep-clinoform asymmetric wave-influenced delta: Miocene billund sand, eastern danish north sea and jylland. *Journal of Sedimentary Research*, 78(2):130–146, 2008.

J. P. Harrison and J. A. Hudson. *Engineering rock mechanics-an introduction to the principles*. Elsevier, 2000.

W. Helland-Hansen and G. J. Hampson. Trajectory analysis: concepts and applications. *Basin Research*, 21(5):454–483, 2009.

R. M. Hoogendoorn, I. Overeem, and J. E. A. Storms. Process-response modelling of fluvio-deltaic stratigraphy. *Computers & Geosciences*, 34(10):1394–1416, 2008.

I.-G. Hwang and P. L. Heller. Anatomy of a transgressive lag: Panther tongue sandstone, star point formation, central utah. *Sedimentology*, 49(5):977–999, 2002.

D. Hydraulics. Delft3d-flow user manual, 1999.

D. J. Jerolmack and C. Paola. Shredding of environmental signals by sediment transport. *Geophysical Research Letters*, 37(19), 2010.

E. G. Kauffman and W. G. E. Caldwell. The western interior basin in space and time. *Evolution of the Western Interior Basin: Geological Association of Canada, Special Paper*, 39:1–30, 1993.

C. Klein. *Minerals and rocks: exercises in crystallography, mineralogy, and hand specimen petrology*. Wiley, 1989.

J. D. Milliman and R. H. Meade. World-wide delivery of river sediment to the oceans. *The Journal of Geology*, pages 1–21, 1983.

R. M. Mitchum Jr, P. R. Vail, and J. B. Sangree. Seismic stratigraphy and global changes of sea level: Part 6. stratigraphic interpretation of seismic reflection patterns in depositional sequences: Section 2. application of seismic reflection configuration to stratigraphic interpretation. 1977.

I. Overeem, A. Veldkamp, L. Tebbens, and S. B. Kroonenberg. Modelling holocene stratigraphy and depocentre migration of the volga delta due to caspian sea-level change. *Sedimentary Geology*, 159(3):159–175, 2003.

B. Petroleum. Bp statistical review of world energy, 2011.

M. J. Pyrcz and C. V. Deutsch. *Geostatistical reservoir modeling*. Oxford university press, 2014.

S. Ramanujan. Modular equations and approximations to π. *Quart. J. Math*, 45:350–372, 1914.

H. G. Reading. Sedimentary environments: processes, facies, and stratigraphy. 1996.

J. A. Roelvink and G. K. F. M. Van Banning. Design and development of delft3d and application to coastal morphodynamics. *Oceanographic Literature Review*, 42(11), 1995.

S. A. Schumm. Evolution and response of the fluvial system, sedimentologic implications. 1981.

J. E. A. Storms. Event-based stratigraphic simulation of wave-dominated shallow-marine environments. *Marine Geology*, 199(1):83–100, 2003.

J. E. A. Storms, G. J. Weltje, J. J. van Dijke, C. R. Geel, and S. B. Kroonenberg. Process-response modeling of wave-dominated coastal systems: simulating evolution and stratigraphy on geological timescales. *Journal of Sedimentary Research*, 72(2): 226–239, 2002.

J. P. M. Syvitski and E. W. H. Hutton. 2d sedflux 1.0 c:: an advanced process-response numerical model for the fill of marine sedimentary basins. *Computers & Geosciences*, 27(6):731–753, 2001.

D. M. Tetzlaff and J. W. Harbaugh. Simulating clastic sedimentation. 1989.

J. A. Udden. Mechanical composition of some elastic sediments. *Bull. Geol. Soc. Am.*, 25:655–744, 1914.

J. C. Van Wagoner, R. M. Mitchum, K. M. Campion, and V. D. Rahmanian. Siliciclastic sequence stratigraphy in well logs, cores, and outcrops: concepts for high-resolution correlation of time and facies. 1990.

J. H. L. Voncken, R. Ephraim, and K.-H. A. A. Wolf. Introduction to quantative image analysis. 2004.

A. Delta stratigraphy

Delta stratigraphy generated in the forward scenarios 1 through 4, and the inversion.

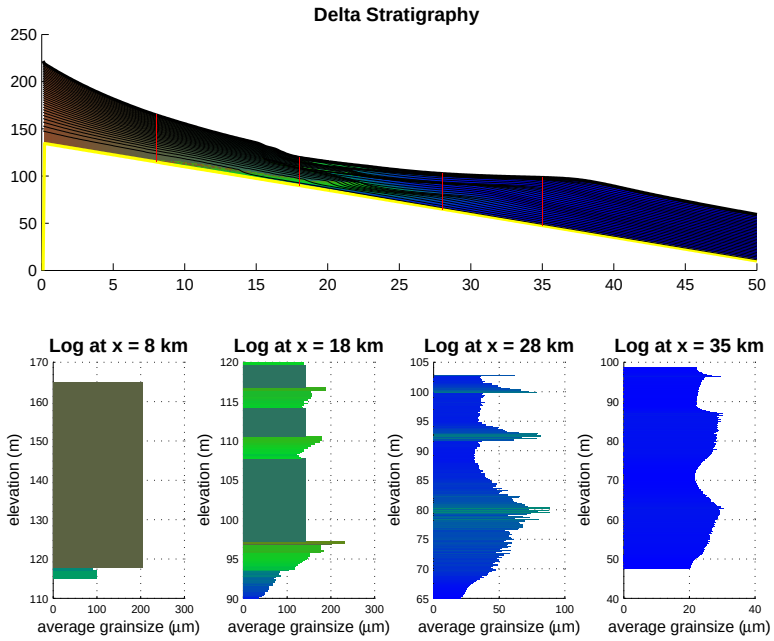

Figure A.1: Delta stratigraphy based on the input signals from scenario 1, in table 5.2.

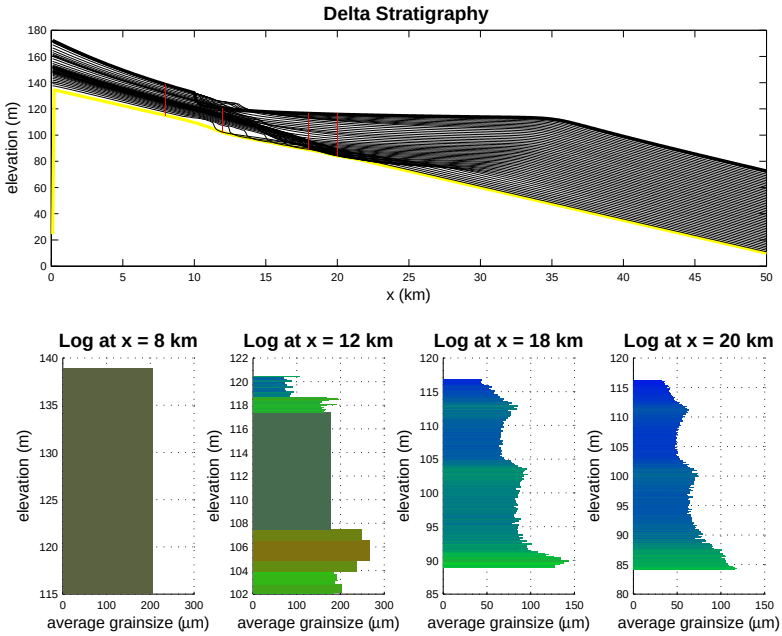

Figure A.2: Delta stratigraphy based on the input signals from scenario 2, in table 5.3.

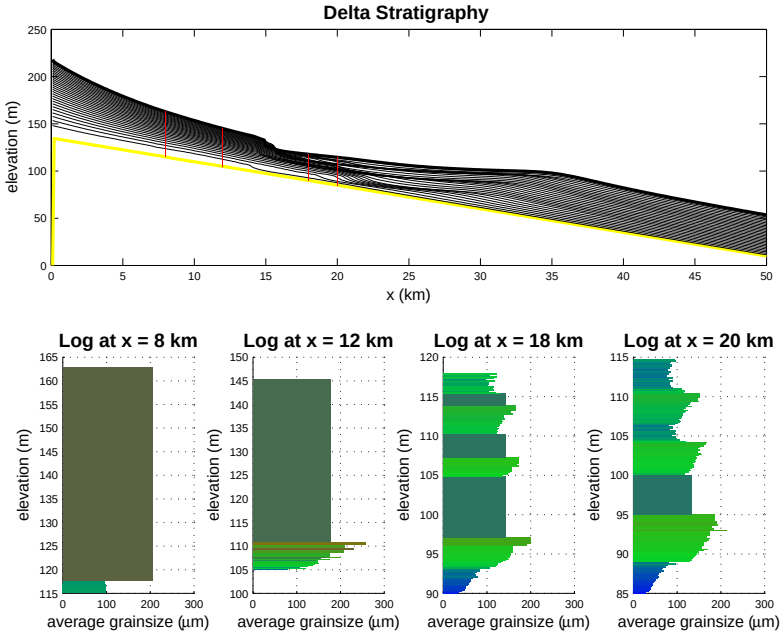

Figure A.3: Delta stratigraphy based on the input signals from scenario 3, in table 5.4.

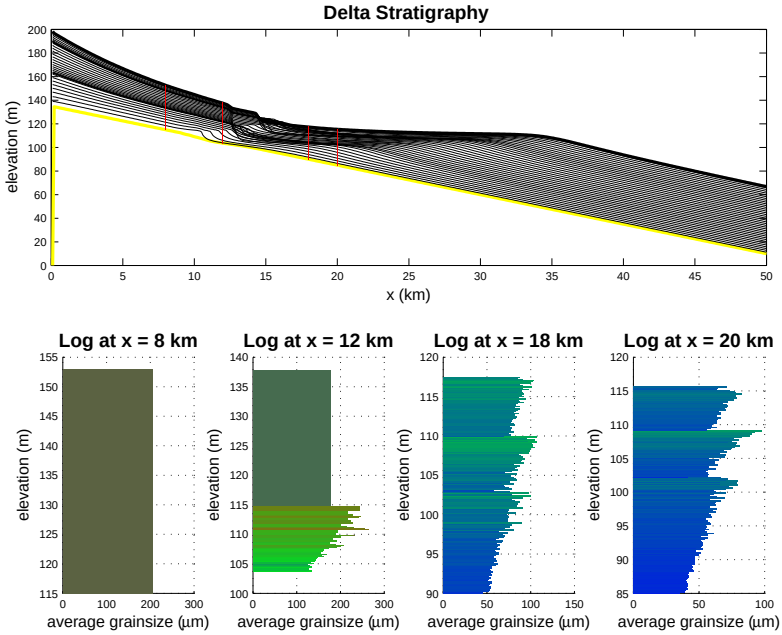

Figure A.4: Delta stratigraphy based on the input signals from scenario 4, in table 5.5.

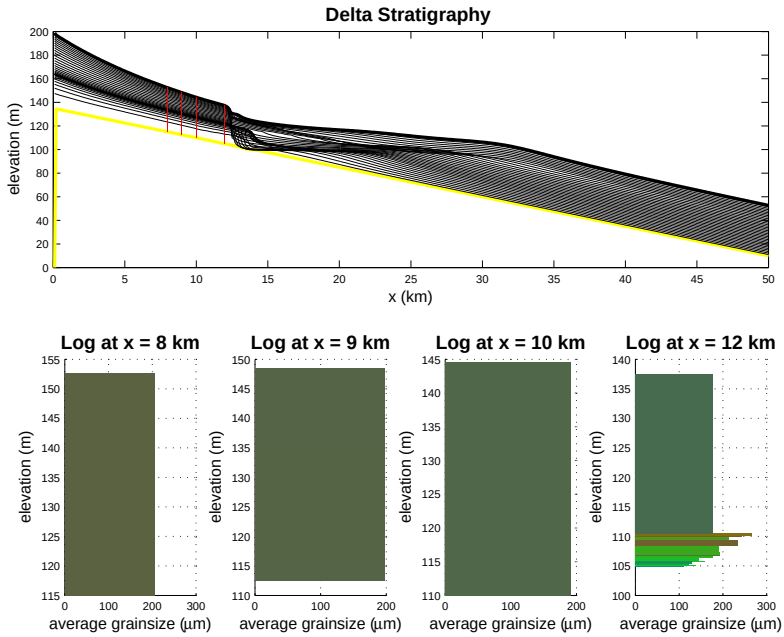

Figure A.5: Delta stratigraphy related to the inversion scenario from section 5.2, with input parameters from table 5.2.

B. Density plot inversion

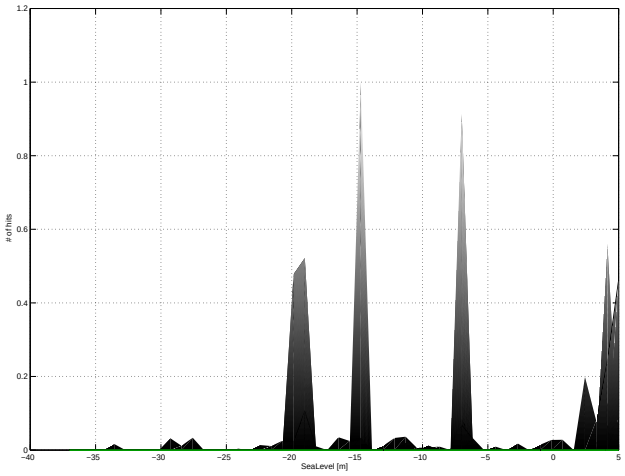

(a) Side view of figure 5.8a over the sea level axis.

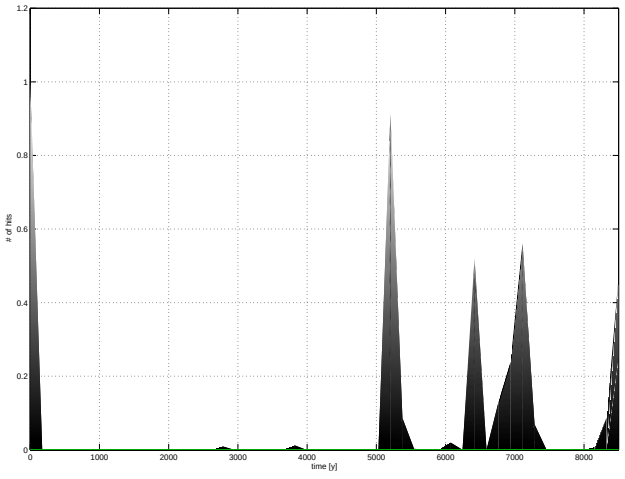

(b) Side view of figure 5.8a over the time axis.

Figure B.1: Density plots of the parameters used by the inversion routine in section 5 in constructing a sea level signal.

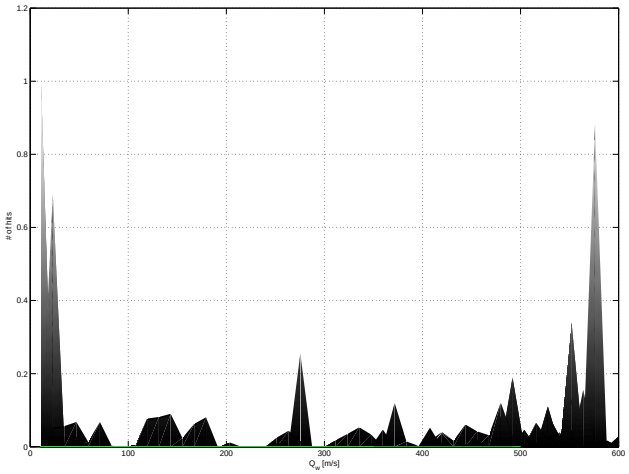

(a) Side view of figure 5.8b over the Qw axis.

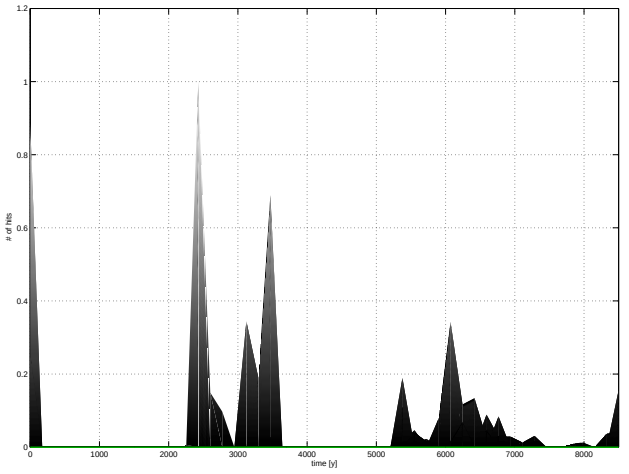

(b) Side view of figure 5.8b over the time axis.

Figure B.2: Density plots of the parameters used by the inversion routine in section 5 in constructing discharge signal.

C. Inversion on MFS

Inversion scenario, on a base surface representing the shape of the maximum flooding surface.

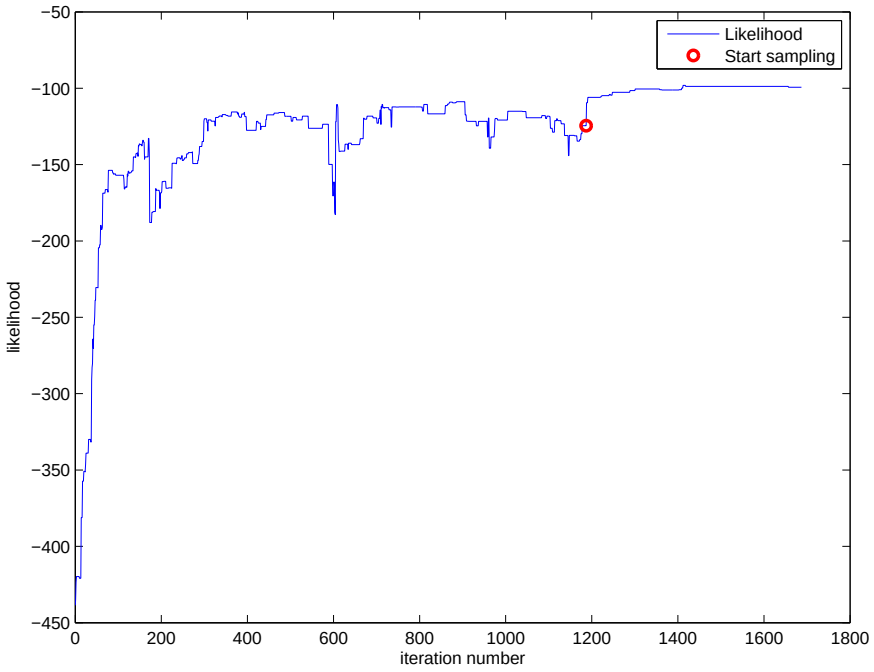

Figure C.1: Likelihood evolution of the inversion scenario. There is a steep increase in likelihood at the start of the burn-in period. During the sampling period the iteration count is reset before the required amount of iterations is fulfilled.

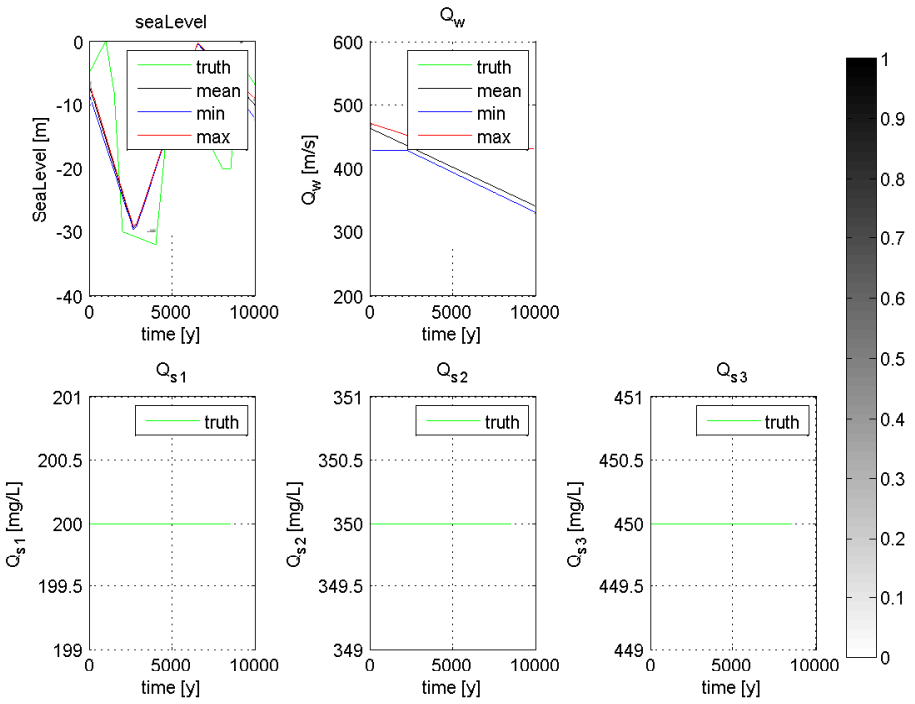

Figure C.2: Parameter histogram used in the sampling period of the inversion. Together with the initial input signal, from scenario 3. Additionally the 95% confidence zone is plotted between the min and max lines, with the mean line.

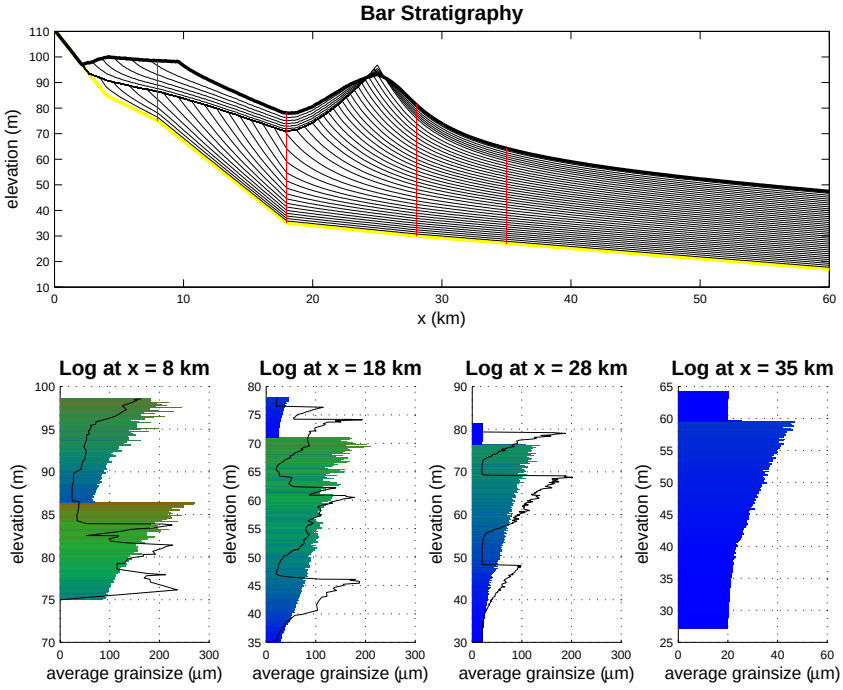

Figure C.3: Shoreface stratigraphy from the input signals based on the mean line from figure 5.8. Black lines are plotted every 50 time steps, the Δt is 5 years. Therefore, the black lines indicate the paleo-morphology every 250 years over 8500 years. The line overlaying the simulated logs of 8km, 18km, and 28km, are the 'measured' logs. These measured logs are extracted from scenario 3.

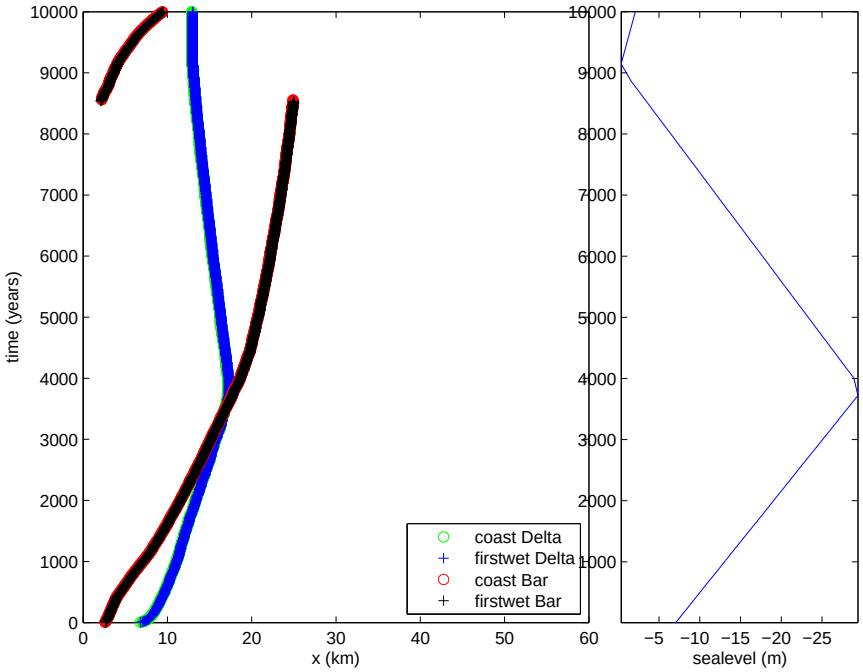

Figure C.4: Coast (mainland), and first wet (foreshore) locations as determined for the simulated shoreface and delta environment of the inversion scenario. Note that back-barrier formation is disabled.